10-4-2023

Development of a Methodology for Virtual Efficiency Evaluation of Electric Drive Modules

Luca Gonella
University of Windsor

Development of a Methodology for Virtual Efficiency Evaluation of Electric Drive Modules

By

Luca Gonella

A Thesis
Submitted to the Faculty of Graduates Studies
Through the Department of Mechanical, Automotive, & Materials Engineering
in Partial Fulfillment of the Requirements for
the Degree of Master of Applied Science
at the University of Windsor

Windsor, Ontario, Canada

2023

Development of a Methodology for Virtual Efficiency Evaluation of Electric Drive Modules

by

Luca Gonella

APPROVED BY

R. Bonavolontà
Stellantis

N. Van Engelen
Department of Civil and Environmental Engineering

J. Johrendt
Department of Mechanical, Automotive, & Materials Engineering

B. Minaker, Advisor
Department of Mechanical, Automotive, & Materials Engineering

July 19, 2023

Declaration of Originality

I hereby certify that I am the sole author of this thesis and that no part of this thesis has been published or submitted for publication.

I certify that, to the best of my knowledge, my thesis does not infringe upon anyone's copyright nor violate any proprietary rights and that any ideas, techniques, quotations, or any other material from the work of other people included in my thesis, published or otherwise, are fully acknowledged in accordance with the standard referencing practices. Furthermore, to the extent that I have included copyrighted material that surpasses the bounds of fair dealing within the meaning of the Canada Copyright Act, I certify that I have obtained a written permission from the copyright owner(s) to include such material(s) in my thesis and have included copies of such copyright clearances to my appendix.

I declare that this is a true copy of my thesis, including any final revisions, as approved by my thesis committee and the Graduate Studies office, and that this thesis has not been submitted for a higher degree to any other University or Institution.

Abstract

This study focuses on the development of a virtual methodology for the evaluation of the efficiency of an EDM (Electric Drive Module), with a focus on the mechanical characteristics, i.e, the loss that arises in the reduction unit needed to adapt the Electric Motor (EM) characteristics to the vehicle requirements that are commonly split into load losses and non-load losses, depending on their variability with the applied torque.

Two units, a test reducer and the EDM of the Fiat 500 Battery-Electric Vehicle (BEV), are modelled with different levels of complexity by using three simulation software tools available in the market (MASTA, AVL Excite and Romax). The simulations are performed in steady-state conditions to replicate the testing activity.

The project starts with a review of the analytical and theoretical loss models implemented, the modelling techniques and the testing methodology, and concludes with the simulation and comparison of results with the data coming from the laboratory tests.

The results show that analytical formulations still lack on accuracy in the prediction of non-load losses, while the models for load losses perform better in terms of percentage error.

To my family

Acknowledgements

First of all, i would like to express my sincere gratitude to my company advisor from Stellantis Europe, Raffaele Bonavolontà, whose guidance and suggestions have been fundamental throughout the development of this thesis, both regarding the experimental and the simulation phases.
I would like to extend my thanks also to Dr. Bruce Minaker from the University of Windsor, who carefully followed the progress of the work during the whole year and helped me a lot in reviewing the format of my thesis, but also to Dr. Jennifer Johrendt who assisted me especially in the initial phase of settling down at the University of Windsor.
I am deeply grateful to Stellantis, who sponsored this thesis and gave me the opportunity to take part in the Dual International Master Degree program with Politecnico di Torino and the University of Windsor.
I would also like to thank the DIMD project coordinators, Marie Mills from Stellantis, Dr. Ofelia Jianu from the University of Windsor and Dr. Maria Pia Cavatorta from Politecnico di Torino, who with their kindness helped my stay in Windsor.
I wish to show my appreciation also to Dr. Niel Van Engelen, who served of my thesis committee and assisted with the thesis Proposal and reviewed my work at the Defense.
Words cannot express my gratitude to my family, starting from my mum Raffaella, my dad Paolo and my stepdad Michele, but also to my grandparents Marisa and Stefano, who were always asking about my feelings and my plans here in Windsor and kept contact with me.
I could not have undertaken this journey without my friends. I would like to thank them all for the amazing moments spent together.
Special acknowledgements go to Piero, Luca and Giacomo, with whom I spent the first four years of University in Torino, but also to all the friends from Pista Winner where I was working on the weekend during my university career in Torino, starting from Massimiliano, Andrea, Tico, Simona, Ubaldo and the boss Massimo.
Then I wish to thank Giovanni, Natalia and Mike, who I spent this year in Canada living with them, but also Giorgio, Filippo and Riccardo that were here in the last years as students and made my year simpler thanks to their suggestions.
Special thanks to Giampiero and Ivana, who welcomed me in their restaurant and made me feel like I was at home all the time: I really hope I was helpful to them with my work in the kitchen.
Lastly, I would like to express all my love to Bryana, with whom I spent beautiful times together, but also to her family, starting from her mum Martha and her sister Marisa, who welcomed me in their home all the time.

Contents

List of Figures

List of Tables

List of Abbreviations

All abbreviations used in this work are described in this section.

Abbreviation	Meaning
ACYG	Advanced Cylindrical Gear Joint
AC	Alternating Current
EDM	Electric Drive Module
BEV	Battery-Electric Vehicle
TRB	Tapered Roller Bearing
CRB	Cylindrical Roller Bearing
FE	Finite Element
FEA	Finite Element Analysis
1D	1-Dimensional
3D	3-Dimensional
RBE	Rigid Bar Element
DOF	Degree of Freedom
NHV	Noise and Vibration Harshness
EM	Electric Machine
CAD	Computer-Aided Design
CFD	Computational Fluid Dynamics
EHD	Elasto-Hydrodynamic
EHL	Elasto-Hydrodynamic Lubrication
rpm	Revolutions per Minute
VG	Viscosity Grade
FZG	Forschungsstelle fur Zahnrader und Getriebebau (Research Center for Gears)
ISO	International Standard Organization
AGMA	American Gears Manufacturer Association

List of Symbols

Symbol	Description	Unit
ω	Angular Speed	rad/s
m	Module	mm
p	Pitch	mm
α	Pressure Angle	degree
h_a	Addendum	mm
h_f	Dedendum	mm
β	Helix Angle	degree
m_n	Normal Module	mm
p_n	Normal Pitch	mm
α_t	Transverse Pressure Angle	degree
α_n	Normal Pressure Angle	degree
a	Nominal Operating Center Distance	mm
K	Load Intensity	–
f_0	Dip Factor	–
inv	Involute Function	–
y	Center Distance Modification Coefficient	–
d	Reference Diameter	mm
d_b	Base Diameter	mm
d_w	Reference Diameter	mm
d_w	Working Pitch Diameter	mm
j_n	Normal Backlash	mm
j_t	Circumferential Backlash	mm
λ	Lubrication (Lambda) Ratio	–
μ	Friction Coefficient (Generic)	–
ϵ_α	Profile Contact Ratio	–
M	Mesh Mechanical Advantage	–
T	Torque (Generic)	Nm
R_z	Surface Roughness	μm
F	Force (Generic)	N
ρ	Density (Generic)	kg/m^3

η	Efficiency	–
η_{oil}	Viscosity	mm
ν	Dynamic Viscosity	mm
τ	Transmission Ratio	–
z	Number of teeth	–
d_a	Tip Diameter	mm
d_f	Root Diameter	mm
R_a	Mean Roughness	μm
R_z	Mean roughness depth	μm
R_t	Maximum peak to valley height	μm
e	Relative Error	[–]

Chapter 1

Introduction

This study is focused on the assessment of methods to evaluate the efficiency of an EDM (Electric Drive Module), for a wide range of operating conditions, in a simulation environment. Different loss models present in the literature will be implemented and studied. The methodology will be validated by comparing the results with experimental tests done in laboratory.

1.1 Background

Battery-Electric-Vehicles (BEVs) are gaining importance in the worldwide vehicle market share, as they contribute to the reduction of CO_2 and pollutant emissions. In many countries more stringent regulations are taking place in the transportation field to force carmakers to produce eco-friendly vehicles. In 2017, in Europe the transport sector was responsible for 27% of the total Green-House Gas (GHG) emissions, 71% of which came from road transport[1]. In 2019, the average CO_2 emitted by new passenger cars registered in Europe was 122.3 gCO_2/km. Starting from 1st January 2020, the European Union adopted Regulation (EU) 2019/631, setting a fleet-wide target of 95 gCO_2/km with a 95€ penalty per each gram of CO_2 exceeded[2], and a further 37.5% emissions reduction by 2030. In 2020, the US Corporate Average Fuel Economy (CAFE) set an average fleet-wide CO_2 emissions target of about 106 gCO_2/km [3]. European and American regulations are just two examples, since emission controls are now applied at the worldwide level. In this scenario, it is clear that BEVs, and to some extent Hybrid Electric Vehicles (HEVs), play a key role.

In this framework, the energy consumption goals could not be achieved without a detailed investigation of the efficiency of each component of the vehicle. In this context, one of the main contributors to the losses of a BEV is the Electric Drive Module. In the past, improvement of the efficiency of the internal combustion engine was the main goal, due to its sensibly lower value. Nowadays, with the high efficiency of Electric Machines (EMs), the focus on the efficiency study and improvement of the driveline is becoming an important point to be considered. In recent years, there has been a significant shift towards electrification in the automotive industry. This transition is driven by the need to reduce greenhouse gas emissions, increase energy efficiency, and address concerns related to fossil fuel dependency. As a result, the development of electric

drive modules has gained considerable attention, as they form a critical component of electric and hybrid electric vehicles (EVs and HEVs).

An Electric Drive Module (EDM) is a compact and integrated system that incorporates various components essential for the propulsion of electric vehicles. It serves as the heart of the powertrain, converting electrical energy from the battery into mechanical power to drive the vehicle's wheels. The primary objective of an EDM is to efficiently manage and control the flow of electrical power while ensuring optimal performance, range, and reliability. The EDM consists of several key components that work together harmoniously. These components typically include an electric motor, power electronics, a transmission or a direct drive system, and associated control systems. Each component plays a crucial role in the overall functionality of the EDM.

- The electric motor is the key component responsible for converting electrical energy into mechanical torque. It is usually an alternating current (AC) motor, with various types such as induction motors, permanent magnet motors, or synchronous reluctance motors. The motor's design, power rating, and efficiency are critical factors influencing the overall performance of the EDM.
- The power electronics module is responsible for managing the flow of electrical power between the battery and the electric motor. It typically consists of power converters, inverters, and controllers. The power converters enable the conversion of direct current (DC) from the battery into alternating current (AC) for the motor. The inverters ensure efficient power delivery to the motor, and the controllers govern the system's operation, including speed control, torque management, and regenerative braking.
- The transmission system, in some EDM designs, consists of gears or a multi-speed gearbox, and is also known as reducer unit since often a speed reduction/torque increase is needed to match vehicle requirements. This ensures efficient power transfer from the motor to the wheels. However, in certain applications, a direct drive system may be employed, eliminating the need for a traditional transmission.
- Since the electric motor and power electronics generate heat during operation, a cooling system is essential to dissipate this heat and maintain the components within their safe temperature limits. The cooling system, in an electric drive module, is typically controlled by a thermal management system that monitors the temperature of the components and adjusts the cooling intensity as needed. This ensures that the components operate within their safe temperature range, which maximizes efficiency, reliability, and overall performance of the electric vehicle.

The integration of an electric drive module offers numerous advantages over conventional internal combustion engines, such as reduced emissions, improved energy efficiency, and enhanced drivability. Additionally, EDMs provide the opportunity for regenerative braking, where energy is recovered during braking and fed back into the battery, further increasing efficiency. However,

challenges persist, including thermal management, system complexity, cost, and the need for effective cooling solutions to ensure consistent performance and longevity.

1.2 Motivation

Studying the efficiency of an EDM is of utmost importance for several reasons:

- Energy Conservation: The efficiency of the electric drive module directly impacts the energy consumption and overall range of an electric vehicle. Higher efficiency means less energy is wasted during the conversion of electrical energy to mechanical power. By understanding and improving the efficiency of the EDM, it becomes possible to conserve energy and extend the vehicle's driving range, which is a critical factor in the widespread adoption of electric vehicles.
- Performance Optimization: Efficiency plays a crucial role in optimizing the performance of the electric drive module. Higher efficiency means that a greater proportion of the electrical energy is effectively converted into mechanical power, resulting in improved acceleration, higher top speeds, and better overall vehicle performance. By studying and enhancing the efficiency of the EDM, engineers can achieve better power delivery and ensure a more satisfying driving experience for the vehicle owner.
- Environmental Impact: Electric vehicles are considered more environmentally friendly compared to internal combustion engine vehicles due to their lower or zero tailpipe emissions. However, the environmental benefits of electric vehicles are closely tied to the efficiency of their powertrains. A more efficient EDM reduces energy waste and the associated greenhouse gas emissions, contributing to a cleaner and greener transportation system. Studying efficiency allows researchers to identify areas of improvement and develop strategies to minimize the environmental impact of electric vehicles.
- Cost Reduction: Efficiency is directly linked to the cost-effectiveness of electric drive modules. Higher efficiency means that less energy is required to achieve the desired performance, reducing the size and weight of components such as the battery pack. This, in turn, leads to cost savings in terms of materials, manufacturing, and overall system complexity. By studying and improving efficiency, researchers can contribute to the cost reduction of electric drive modules, making electric vehicles more accessible and competitive in the market.
- System Integration and Heat Management: Efficiency studies are vital for addressing the thermal challenges associated with electric drive modules. Efficient operation generates less waste heat, reducing the thermal load on various components within the system. Understanding the efficiency characteristics helps in designing effective cooling and thermal management strategies, ensuring the reliability and longevity of the EDM.

1.3 Research Objectives

The primary objective is to develop a methodology that accurately and reliably evaluates the efficiency of the EDM in a virtual environment. By ensuring accuracy and reliability, the methodology can provide meaningful insights into the efficiency performance of the EDM. The methodology should enable accurate prediction of the EDM's efficiency under various operating conditions and driving scenarios. It should allow researchers to simulate and evaluate efficiency performance under different loads, speeds, and driving cycles. This objective helps in understanding how the EDM's efficiency varies in real-world situations and enables the identification of opportunities for efficiency improvement.

While accuracy is crucial, computational efficiency is also an objective in developing a virtual methodology. The methodology should be capable of delivering results in a reasonable time frame, allowing for efficient analysis and optimization. Optimizing computational efficiency helps researchers explore a broader range of design and operational scenarios within practical time constraints.

1.4 Methodology

Developing a virtual methodology to evaluate the efficiency of a reducer unit in an Electric Drive Module (EDM) involves several key steps:

- Component Modelling: Develop accurate and detailed virtual models of the components within the reducer unit. This includes modeling the gears, bearings, lubrication system, shafts, and any other relevant mechanical components. The models should accurately represent the geometry, material properties, and behavior of the components. Consider factors such as gear meshing, friction, and efficiency characteristics in the modelling process.
- System Integration: Integrate the reducer unit model into the broader virtual EDM system. Connect the reducer unit model to the electric motor model, power electronics model, and other relevant components within the EDM. Ensure that the interactions and dependencies between these components are properly represented in the simulation environment.
- Efficiency Calculation: Develop algorithms and methodologies to calculate the efficiency of the reducer unit within the virtual environment. Analyze the energy flow through the gears, taking into account mechanical losses, frictional losses, and other sources of energy dissipation.
- Input Data and Parameters: Gather accurate and representative input data and parameters required for the virtual efficiency evaluation. This includes gear specifications, material properties, lubrication characteristics, operating conditions, and system loads. Ensure that the input data and parameters accurately reflect the real-world behavior of the reducer unit.

- Simulation and Analysis: Perform simulations using the virtual methodology and models developed in the previous steps. Input the appropriate operating conditions and driving scenarios to evaluate the efficiency of the reducer unit. Analyze the simulation results, focusing on the efficiency metrics defined for the evaluation. Assess the performance of the reducer unit across different operating conditions and identify any areas for potential improvement.
- Validation: Validate the virtual methodology by comparing the simulation results with experimental data or reference data from reputable sources. This validation process ensures that the virtual methodology provides a realistic representation of the efficiency of the reducer unit.

1.5 Thesis Structure

In Chapter 2, the focus is on the review of the main studies reported in the literature on the efficiency of EDMs, with a focus on gear and bearing losses, as well as on the modelling techniques and the testing methodologies. In Chapter 3, there is a detailed description of the loss models implemented in the simulation software, reporting testing conditions, applicability limits and recommendations.

Chapter 4 discusses the modelling approaches, both regarding the FE discretization in Hypermesh/Optistruct and the simulation strategy in MASTA, AVL Excite and Romax.

Chapter 5 describes the first unit tested, a simple test reducer, and includes an analysis of the results of the simulation.

Chapter 6 describes the second unit tested, the EDM of the Fiat 500 BEV, and discusses the results of the simulations.

Finally, Chapter 7 includes the conclusions, the recommendations and the limitations, along with a summary of the research contributions of the present thesis.

Chapter 2

Literature Review

The purpose of this chapter is to briefly explain the theory behind this study. Since the focus is on the efficiency of a reducer unit, it starts with a description of the helical gear and the characteristics of the involute profile, and the forces that arise when they are in contact. It will then describe the main concepts of Elasto-Hydrodynamic Lubrication in bearings and gear pairs, that according to the literature is the most frequent lubrication regime, with a focus on the evaluation of the friction that arises due to this contact. It will then end with a description of the losses due to the displacement of the oil needed for the lubrication, with a focus on the dip lubrication mechanism that is adopted in the two units tested.

2.1 Gears

A gear is a rotating machine whose primary function is to transfer the torque between shafts while keeping the transmission ratio constant. There exist several types of gear, e.g., helical, spur, rack and pinion. In a spur gear, the teeth are parallel to the axis, while a helical gear has a more complex geometry and the teeth are positioned on an incline with respect to the axis. Today, helical gears are commonly used in machines to transmit high torques at high speed with low noise and vibration. This behaviour is due to the gradual engagement of the teeth during the contact cycle. Nevertheless, the efficiency of helical gears is less than spur gears of identical size. Another disadvantage is that, due to the twisting angle of the teeth, an axial force component along the shaft will arise.

2.1.1 Gear Geometry

It is useful to start with a description of how a gear tooth profile is defined. For power transmission gears, the tooth form most commonly used today is the involute profile. Involute gears can be manufactured easily, and the gearing has a feature that enables smooth meshing despite the misalignment of center distance to some degree. Figure 2.1 shows the tooth profile of a gear rack, which is the standard involute gear profile: the most important parameters are defined in Table 2.1.

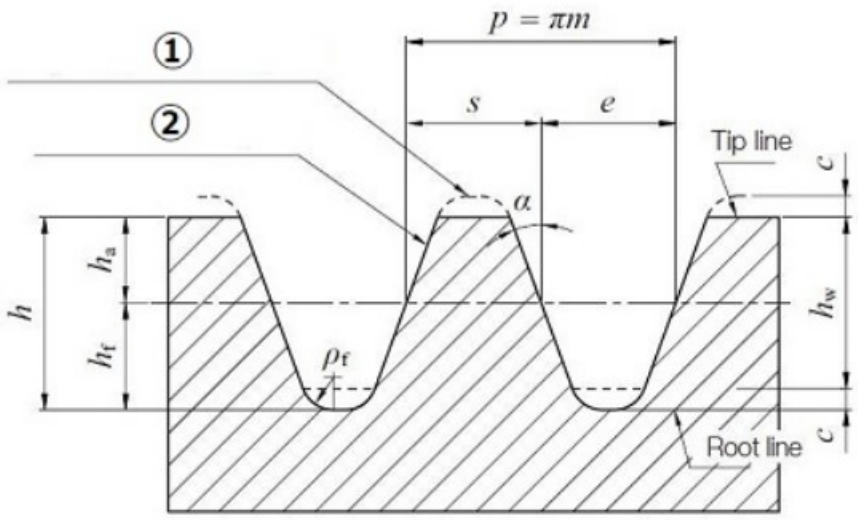

Figure 2.1: Rack used for gear cutting. Credit:[4]

Table 2.1: Spur Gear macrogeometry parameter derived from the shape of the gear rack

Parameter	Formula	Definition
Module (m)	p/π	Module is the unit size indicated in millimeters. The value is calculated from dividing the reference pitch by π.
Pitch (p)	πm	Reference Pitch is the distance between corresponding points on adjacent teeth. The value is calculated from multiplying Module by π
Pressure Angle α		The angle of a gear tooth leaning against a normal reference line
Addendum h_a		The distance between reference line and tooth tip
Dedendum h_f		The distance between reference line and tooth root

Figure 2.2 shows an element of involute curve. The definition of involute curve is the curve traced by a point on a straight line which rolls without slipping on the circle; this circle is called the base circle of the involute. In Figure 2.2, invα stands for Involute Angle (Involute α). The angle θ is called 'involute rolling angle'. The involute angle is defined as:

$$\text{inv}\alpha = \tan\alpha - \alpha \tag{2.1}$$

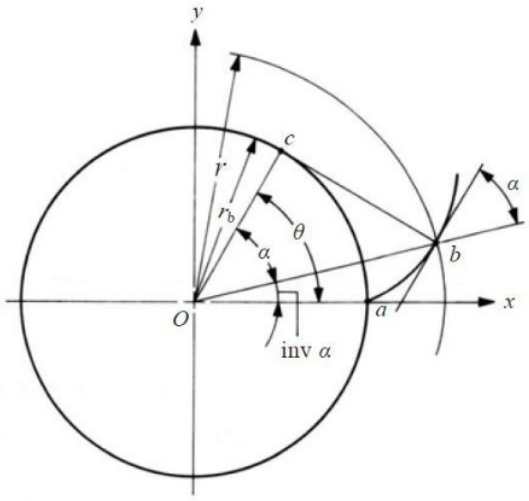

Figure 2.2: Involute Profile Shape Generation. Credit:[4]

With the center of the base circle O at the origin of a coordinate system, the involute curve can be expressed by values of x and y as follows:

$$\begin{aligned} \alpha &= \cos^{-1}\frac{r_b}{r} \\ x &= r\cos(\text{inv}\alpha) \\ y &= r\sin(\text{inv}\alpha) \end{aligned} \tag{2.2}$$

A helical gear such as the one shown in Figure 2.3, is a cylindrical gear in which the teeth flank are helicoid. The helix angle in reference cylinder is called β. The tooth profile of a helical gear is

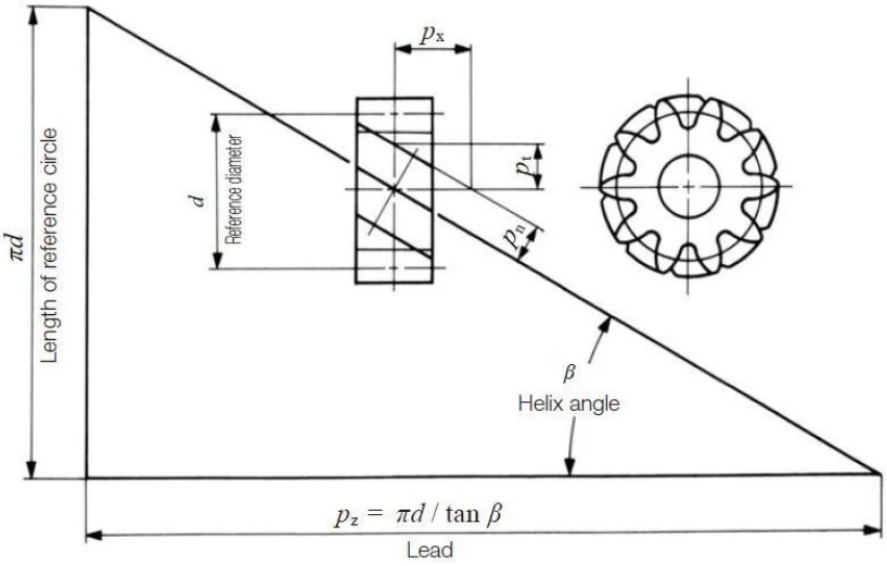

Figure 2.3: Helical Gear Main Parameters. Credit:[4]

an involute curve from an axial view, or in the plane perpendicular to the axis. The helical gear has two kind of tooth profiles: one is based on a normal system, the other is based on a transverse system.

The pitch measured perpendicular to teeth is called the normal pitch, p_n, and p_n divided by π is called normal module m_n.

$$m_n = \frac{p_n}{\pi} \tag{2.3}$$

In the axial view, the pitch on the reference is called transverse pitch, p_t, and p_t divided by π is the transverse module m_t:

$$m_t = \frac{p_t}{\pi} \tag{2.4}$$

The transverse module m_t and transverse pressure angle α_t are at the basic configuration of the transverse system helical gear. The normal system is the one that is most used regarding helical gear manufacturing, due to its simplicity: helical gears can be cut by the same gear hob if module and pressure angle are constant, no matter what the value of helix angle.

Gear teeth are sometimes shifted to prevent undercutting (cutting the root of the gear deeper than the involute curve) or to adjust the center distance between gears. In this case, the reference pitch line of the gear cutting rack is shifted radially from the position for cutting of a standard gear. The amount by which the gear cutting tool is displaced is the extra feed of gear cutter x_m, and the profile shift coefficient x is the value obtained by dividing the extra feed of gear cutter x_m by the module m.

If the profile shift coefficient is positive (e.g., x=0.5), the tooth has a positive correction, the tooth thickness increases, and the tooth is more resistant to bending. If the value is negative, the tooth will have a negative correction and the tooth thickness will decrease. In the normal system, the calculation of a profile shifted helical gear, the working pitch diameter d_w and transverse working pressure angle α_{wt} is done as in Equations 2.5. This is because meshing of the helical gears in the transverse plane is just like spur gears and the calculation is similar:

$$\begin{aligned} d_{w1} &= 2a\frac{z_1}{z_1 + z_2} \\ d_{w2} &= 2a\frac{z_2}{z_1 + z_2} \\ \alpha_{wt} &= \cos^{-1}\left(\frac{d_{b1} + d_{b2}}{2a}\right) \end{aligned} \tag{2.5}$$

For smooth rotation of meshed gears, backlash is necessary. Backlash is the amount by which a tooth space exceeds the thickness of a gear tooth engaged in mesh, as seen in Figure 2.4. Backlash can be defined in different way;, however the two most common ways will be described, with reference to Figure 2.4:

Table 2.2: Computation of the Macrogeometry parameters for an helical gear set

Parameter	Symbol	Formula
Transverse Pressure Angle	α_t	$\tan^{-1}\frac{\tan\alpha_n}{\cos\beta}$
Involute Function	$\text{inv}\alpha_{wt}$	$2\tan\alpha_n\frac{x_{n1}+x_{n2}}{z_1+z_2}+\text{inv}\alpha_t$
Center Distance Modification Coefficient	y	$\frac{z_1+z_2}{2\cos\beta}(\frac{\cos\alpha_t}{\cos\alpha_{wt}}-1)$
Reference Diameter	d	$\frac{zm_n}{\cos\beta}$
Base Diameter	d_b	$d\cos\alpha_t$
Working Pitch Diameter	d_w	$\frac{d_b}{\cos\alpha_{wt}}$
Addendum	h_{a1} h_{a2}	$(1+y-x_{n2})m_n$ $(1+y-x_{n1})m_n$

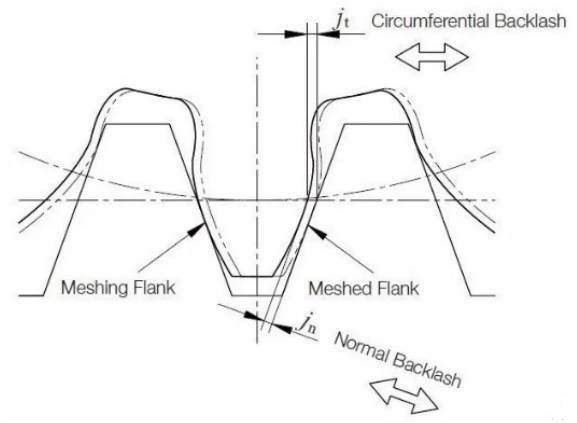

Figure 2.4: Definition of the backlash for a mating gear pair. Credit:[4]

- Circumferential Backlash j_t : Is the length of arc on the pitch circle. The length is the distance the gear is rotated until the meshed tooth flank makes contacts while the other mating gear is held stationary.
- Normal Backlash j_n : The minimum distance between each meshed tooth flank in a pair of gears, when it is set so the tooth surfaces are in contact.

2.1.2 Gear-tooth action

As Figure 2.5 shows, once two gears are interacting, Tooth Profile 1 drives Tooth Profile 2 by acting at the instantaneous point K. The common normal of the two profiles is nominated as N_1N_2 while N_1 and N_2 are the foot of the perpendicular from the center of the gears to the common normal, N_1N_2. Although, the gear profiles can have different velocities V_1 and V_2 at point K, their velocities must be constant along N_1N_2 in both magnitude and direction. Otherwise the gear pair

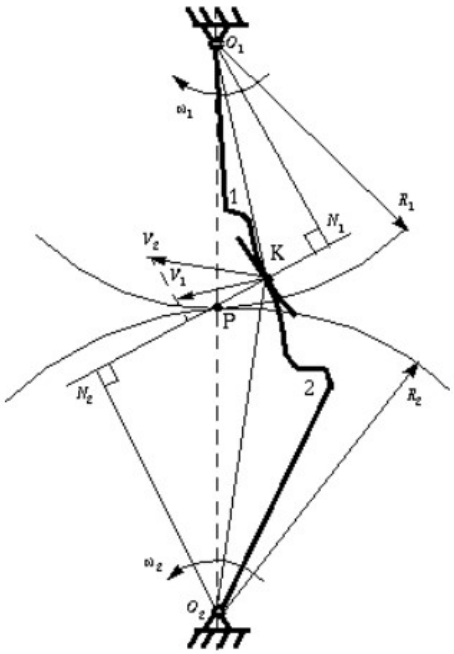

Figure 2.5: Kinematics of a mating gear pair : note the two tooth profiles 1 and 2, the two pitch radii R1 and R2 defining the pitch circles centered in O1 and O2

would be detached from each other. Thus, the angular velocities of the shafts can be derived:

$$\frac{\omega_1}{\omega_2} = \frac{O_2N_2}{O_1N_1} \tag{2.6}$$

The point P is called as pitch point and it is defined as the intersection of the tangency of N_1N_2 and the center to center line O_1O_2, and:

$$\Delta O_1N_1P = \Delta O_2N_2P \tag{2.7}$$

Equation 2.8 calculates the velocity ratio of two gears, the relationship between the angular velocities of the driving and driven gears,

$$\frac{\omega_1}{\omega_2} = \frac{O_2P}{O_1P} \tag{2.8}$$

The pitch point P is a very important point to obtain the velocity ratio of the gear pair by dividing the center to center line O_1O_2 and its position. In order to maintain constant angular velocities between a two-gear pair, the common normal, N_1N_2, to the tooth profile must always pass through the pitch point P. This principle is known as the fundamental law of gear-tooth action.

As two gears are in mesh, the number of gear teeth which are in contact varies during the meshing cycle. The contact ratio ϵ_γ is also defined as the average number of teeth in contact during the engagement cycle. The torque is continuously transmitted on the condition that the contact ratio ϵ_γ is not lower than one at all operating periods.

2.1.3 Forces in helical gears

As helical gears are in mesh, a thrust force can be due to the helix in the teeth of the gears. In order to resist the extension of the thrust forces, thrust bearings have to be placed in the direction of the thrust force. Hence, analysing and measuring the magnitude and direction of the forces acting in the helical gears during the operating period is of key importance not only for designing the helical gears but also for other mechanical components e.g., bearings. During the operating period, a resultant force F_n is acting on the tooth flank in perpendicular to the tooth surface. This approximation is caused by the assumption that the relatively small friction force can be ignored due to the slipping between the gear teeth flanks. As Figure 2.6 illustrates, due to a helical shape of the gears, the resultant forces F_n can be divided into two components, the axial component F_a and the transverse force component F_t. The transverse force component transfers the torque between two gear pair while the axial force component appears from the gear tooth twisting. It is possible

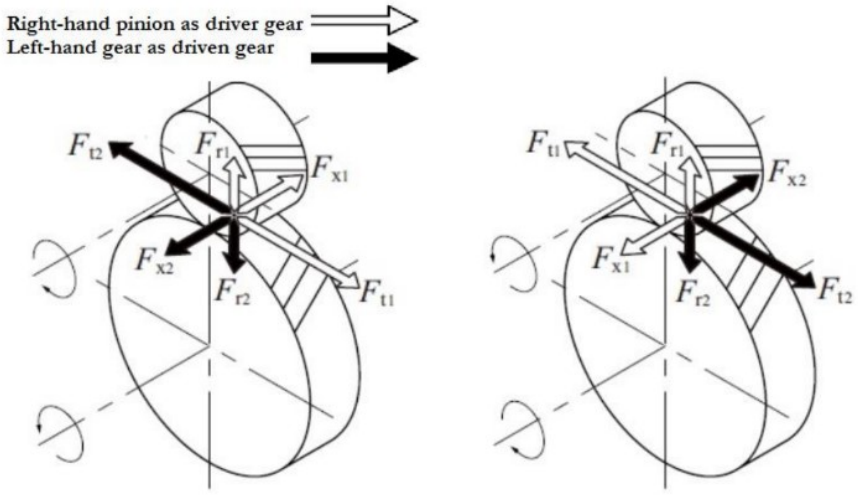

Figure 2.6: Forces acting in an mating helical gear pair. Focus on the 3 directions in a cartesian space: Normal, Tangential and Axial. Credit:[4]

to calculate the axial and transverse force components using the following: expressions:

$$F_t = F_n \cos \beta_b \tag{2.9}$$

$$F_a = F_n \sin \beta_b \tag{2.10}$$

Herein β_b is the helix angle.

According to Equations 2.9 and 2.10, if the helix angle β_b increases, the axial force component will be increased and the transverse force will be reduced. Also, the relations between the desired torque M_1 acting on the first gear and the transverse force component can be defined as:

$$F_t = \frac{M_1}{r_{b1}} \tag{2.11}$$

In addition, it is possible to combine Equations 2.9 and 2.10 to obtain the relation between the axial force and desired torque on the first gear:

$$F_a = \frac{M_1}{r_{b1}} tan\beta b \tag{2.12}$$

The resulting output torque of the second gear can be easily calculated using the gear ratio τ:

$$M_2 = M_1 \tau \tag{2.13}$$

2.2 Bearings

2.2.1 Bearing Geometry

Bearings have several geometrical parameters that define their size, shape, and configuration. These parameters are crucial in determining the bearing's performance characteristics and its compatibility with the application. Here are some of the key geometrical parameters of bearings. The inner diameter refers to the measurement of the opening or bore of the bearing. It defines the size of the shaft that will fit inside the bearing; the outer diameter represents the measurement of the outer surface of the bearing. It determines the size of the housing or structure that will accommodate the bearing; the width, also referred to as the height, corresponds to the thickness or axial dimension of the bearing. It indicates the extent to which the bearing extends in the axial direction; the contact angle is the angle formed between the rolling elements (such as balls or rollers) and a plane perpendicular to the bearing's axis. It influences the load-carrying capacity and the ability to handle axial or radial loads; the pitch diameter is the effective diameter of the rolling elements in a bearing. It is the theoretical diameter at which the rolling elements make contact with the races and is used to calculate the bearing's speed and load capacities; bearing clearance refers to the internal clearance or play between the rolling elements and the races. It affects the fit and the amount of internal movement within the bearing. The clearance can be specified as a radial clearance or an axial clearance.

2.2.2 Forces In Bearings

Bearings experience various forces during operation. These forces can be classified into three main types:

- Radial forces act perpendicular to the bearing's axis and are exerted in a radial direction. They are caused by loads that are applied perpendicular to the shaft, such as the weight of rotating components, gravitational forces, or external forces acting on the shaft. Radial forces cause the bearing to support and distribute the load, ensuring smooth rotation of the shaft.

- Axial forces, also known as thrust forces, act parallel to the bearing's axis. They are generated by axial loads applied to the bearing, such as those arising from thrust loads, preloading, or axial misalignment. Axial forces can push or pull the bearing along the shaft axis and must be properly managed to prevent excessive wear or damage to the bearing components.
- Moment or torsional forces result from torques applied to the bearing. They cause twisting or rotational movement around the bearing's axis. Torsional forces can be generated by factors like misalignment, unbalanced loads, or torque transmission through the bearing. These forces can induce additional stresses on the bearing and must be considered in bearing selection and design.

It is important to note that bearings are designed to withstand and manage these forces within their load capacity ratings. The bearing's load capacity, stiffness, and geometry play a vital role in determining its ability to handle these forces. Proper selection and installation of bearings, as well as appropriate lubrication, are critical to ensuring optimal performance and longevity while minimizing wear and damage due to excessive forces.

2.3 Lubrication

Lubrication is always implemented in gear systems, for the following reasons:

- To promote sliding between gear teeth to reduce the coefficient of friction μ
- To limit the temperature rise caused by rolling and sliding friction

Usually three gear lubrication methods are used:

- Grease lubrication
- Splash Lubrication (oil bath method)
- Forced oil circulation lubrication

At low speed, grease lubrication is a good choice. For medium and high speeds, splash lubrication and forced oil circulation are more appropriate. In the following, a brief description of the splash lubrication will be given, since it is the method adopted in the unit tested in this work. Splash Lubrication is used with an enclosed system. The rotating gears splash lubricant onto the gear system and bearings; it has several problems, two of them being oil level and temperature limitation:

- Oil level : There will be excess agitation loss if the oil level is too high. On the other hand, there will not be effective lubrication or ability to cool the gears if the level is too low. Also, the oil level during operation must be monitored, as contrasted with the static level, in that the oil level will drop when the gears are in motion. This problem may be countered by raising the static level of lubricant in an oil pan.

- Temperature limitation: The temperature of a gear system may rise because of friction loss due to gears, bearings and lubricant agitation. Rising temperature may cause one or more of the following problems, such as lower viscosity of lubricant, accelerated degradation of lubricant, deformation of housing, gears and shafts, decreased backlash.

2.3.1 Lubrication Regimes

An oil film must be formed at the contact surface of the teeth and of the rolling elements of the bearings to minimize friction and to prevent dry metal-to-metal contact. Four lubrication regimes can be identified, depending on the working conditions, and are depicted in Figure 2.7. They are usually defined making reference to the Lambda Ratio:

$$\lambda = \frac{h}{R_a} \tag{2.14}$$

The lambda ratio was originally developed to quantify the quality of lubricant operating regimes relative to bearing performance; since the 1990s, the lambda ratio has been used to define optimal lubricant regimes for gears. The lambda ratio is a measure of the lubricant film thickness relative to the roughness of two mating/contacting surfaces. The larger the lambda ratio, the greater the separation between the mating surfaces.

- Boundary Lubrication: Is associated with metal-to-metal contact between two sliding surfaces. During initial start-up or shut-down of the machines, but also under heavily loaded conditions, the metal surfaces in a lubricated system may actually come into severe contact with each other. If the oil film is not thick enough to overcome the surface roughness of the metal, a lambda value lower than one may result.

- Mixed Lubrication : Generally speaking, boundary lubrication is dramatically reduced as sliding speed increases, creating a wedge of lubricant film between the surfaces in motion. As the potential for asperity contact is reduced and film thickness is increased, the coefficient of friction drops dramatically to the condition known as mixed lubrication.

  Some metal-to-metal asperity loading is still occurring combined with loading (lift) on the lubricant. This is an intermediary condition between boundary and hydrodynamic/elasto-hydrodynamic lubrication regimes, the gray area between them. As the oil film thickness increases further, the system now moves into full film lubrication, either elasto-hydrodynamic or hydrodynamic lubrication.

- Hydrodynamic Lubrication: This lubrication regime occurs between sliding surfaces when a full film of oil supports and creates a working clearance (e.g., between a rotating shaft and journal bearing). This lubrication regime occurs after a machine has begun to rotate and the speeds and loads are such that a wedge of oil has been formed between the shaft and bearing surfaces. This wedge of oil lifts the shaft away from the bearing surface so there is

little risk of asperity contact. This is a desirable condition to avoid friction and wear. Any friction remaining is found within the lubricant itself, as the molecular structures of the oil slide past each other during operation. Lambda values are usually greater than 2.

For hydrodynamic lubrication to be effective, the oil viscosity must be such that the hydrodynamic condition will be maintained under every operating condition, such as high speed and high load, low speed and high load, low speed and low load, etc. If the operating conditions cause the working clearance to be reduced too much, metal-to-metal contact between the metal high spots or asperities could occur.

- Elasto-hydrodynamic Lubrication: This condition occurs when a rolling motion exists between the moving elements, and the contact zone has a low degree of conformity. For example, note that the curve of the roller and the race in a rolling element bearing are very dissimilar. In fact, the roller and inner race are curved in opposite directions and thus have a small contact area (almost a single point of contact). This creates high-contact pressures (hundreds of thousands of psi).As the oil enters the contact zone between a ball and raceway (by rolling action), the oil's pressure rises sharply. This high pressure in turn significantly increases the oil's viscosity and load-holding ability. This concentrated load will slightly deform (flatten) the metal of the rolling elements and race in the contact zone. The deformation only occurs in the contact zone, and the metal elastically returns to its normal form as the rotation continues.

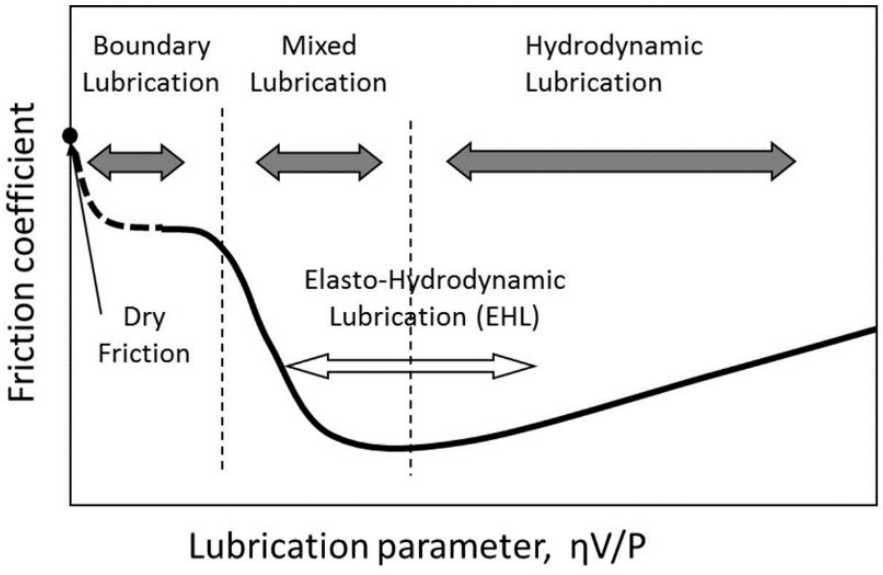

Figure 2.7: Possible Lubrication Regimens between two surfaces in contact: note the four lubrication regimes (Boundary Lubrication, Mixed Lubrication, Elasto-Hydrodynamic Lubrication and Hydrodynamic Lubrication. The friction coefficient is plotted as a function of lubrication parameter. Credit:[5]

2.3.2 Elasto-Hydrodynamic Lubrication

Most gears operate in a mixed elasto-hydrodynamic lubrication (EHL) regime, in which both hydrodynamic lubricant films and rough surface asperity contacts coexist. A good understanding of mixed EHL characteristics is vital to gear performance and efficiency improvement, design optimization, and failure prevention.
The following are some basic characteristics of gear lubrication that have presented difficulties to researchers and engineers:

- Interaction between gear teeth is carried out through non-conformal surface contacts, which are often lubricated. Non-conformal (or concentrated) contact can be classified as line contact (often found in spur, helical, and straight-bevel gears and most worm gears) and point contact (in hypoid and spiral bevel gears, helical gears with crossed axes, and circular-arc (Novikov) gears). Localized high contact pressure in the small contact zone between the gear teeth can be as high as 1–4 GPa, causing significant surface deformation and viscosity increase. Therefore, gears are typical components operating in the EHL regime.

- Commonly used machining processes for finishing gear tooth surfaces include hobbing, milling, shaping, rolling, shaving, broaching, grinding, lapping, honing, and polishing. Most processes produce tooth flank surfaces of roughness Ra a greater than 0.5–1.0 μm, while a small percentage of gears may be better finished by precise grinding, honing, or polishing to Ra = 0.15–0.4 μm or so. It is often difficult and costly to obtain significantly better tooth surface finish due to complicated gear geometry. The surface roughness, therefore, is usually of the same order as, or greater than, the possible EHL film thickness in tooth contacts. A complete separation of the tooth surfaces by a hydrodynamic lubricant film is seldom achieved. In most cases, the lubricant films and rough surface asperity contacts coexist, and neither can be ignored. When studying gear lubrication, one has to consider both simultaneously in the same system of mixed EHL.

- When a pair of gears is engaged, the contact between two teeth moves in a specific way. For a spur-driven gear, for example, the location of the tooth contact line moves from tip to root on the tooth surface, while for a helical gear it moves in a diagonal angle, as shown in Figure 2.8. In worm or hypoid gears the contact and its movement are much more complicated. During the movement the tooth load, the rolling and relative sliding velocities, and the radii of curvature of tooth surfaces are all changing constantly. The number of pairs of teeth that share the load keeps changing as well. Machining and assembly errors/misalignments and tooth geometric modifications may bring in more complexity especially at high speeds. The contact and lubrication conditions, therefore, are basically transient, influenced by gear dynamics and many other factors.

For the reasons mentioned above, the contact and lubrication mechanisms of gears, even of the simpler types such as spur and helical, are very complicated. In practice, today engineers still

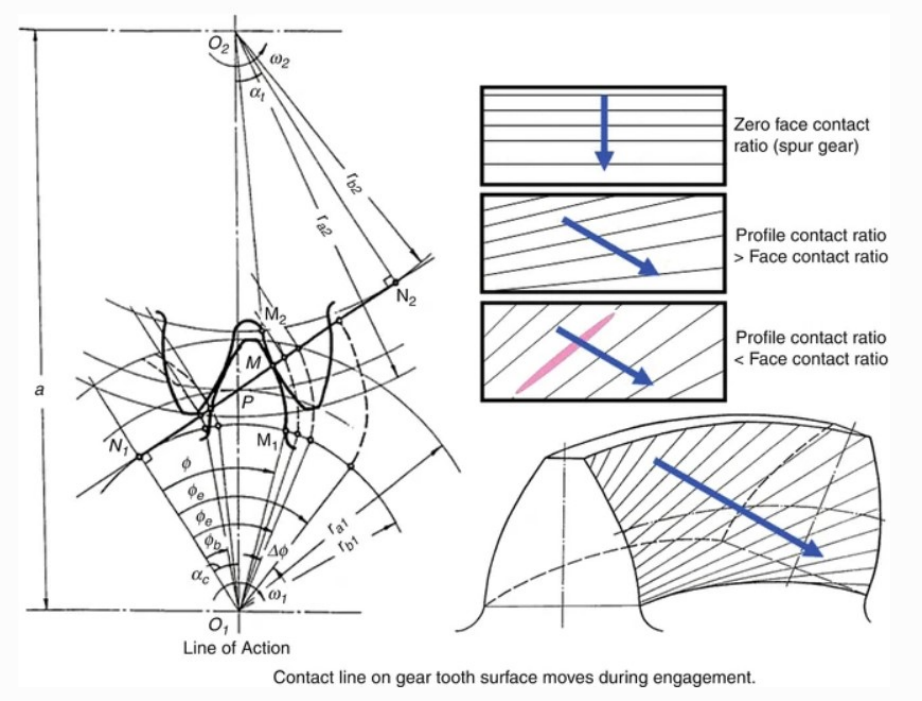

Figure 2.8: Contact line on gear tooth surface during engagement. Note the movement of the line in an helical gear pair

largely rely on empirical data and experience. Model-based comprehensive lubrication design and analysis tools simulating all the dynamic and mixed EHL mechanisms are not yet available. Simplified analyses of various types, however, can be found in the literature. One of the remarkable early efforts was by H. M. Martin[6], who published his hydrodynamic lubrication analysis for line contacts in spur gears in 1916. In his study, a pair of gear teeth was simplified to two parallel smooth rigid cylinders lubricated by an incompressible isoviscous Newtonian fluid. It was found, however, that the lubricant film thickness between gear teeth estimated by Martin's model was extremely small and disagreed with engineering observations.

Reasonable lubricant film thickness in gear tooth contacts was first predicted by Dowson and Higginson[7] based on line contact EHL theory under smooth surface, steady-state, and isothermal assumptions.

Since transient EHL models are complicated, Gu[8] proposed a criterion that can justify the use of a quasi-steady solution for analyzing gear lubrication. Estimating film thickness in gears by using steady-state EHL formulae (such as that by Dowson and Higginson[7]) at chosen critical contact locations has become a common practice since then. Predicted film thickness is found to be a good reference in gear design.

Later, Wang and Cheng[9] developed a numerical solution of EHL film thickness, friction, and surface temperature for an entire meshing cycle in spur gears, considering dynamic and thermal

effects, but surface roughness was neglected. Zhu and Cheng[10] extended the analysis to a three-dimensional (3D) one for helical gears, but dynamic effect on load distribution between pairs of teeth was ignored for simplicity.

Rapidly developing computer and information technologies have fuelled significant advancements in thin-film and mixed EHL theory and practice since the late 1990s. Deterministic solutions for mixed EHL with real machined rough surfaces using a unified numerical approach have been obtained by Zhu and Hu[11], Hu and Zhu[12], Holmes et al.[13], and others. Newly developed numerical approaches appear to be capable of simulating the entire transition from full-film and mixed EHL down to dry contact under severe operating conditions. Also, a 3D line contact mixed EHL model has been developed by Ren et al.[14]. This is of great importance to gear lubrication studies, because line contacts widely exist in various gears but machined gear tooth surface topography is usually three-dimensional. A 3D deterministic model is needed to simulate the effects of surface roughness and topography on contact and lubrication, although the macro tooth contact geometry may be simplified to two-dimensional (2D). Based on the development of mixed EHL mentioned above, Martini et al.[15] also analyzed mixed EHL frictional behavior in gears and proposed practical means for friction reduction.

2.4 Power Losses

The study of the gearbox efficiency , or more precisely the prediction of it, has always been considered a very difficult task. The combination of different types of gears, shafts arrangements, bearings seals and housing design is almost infinite. Combined with the almost infinite design possibilities, the operating conditions, namely speed and torque, as well as other environmental parameters (temperature), complicate the problem even further.

According to Michaelis et al.[16], the total power loss in a gearbox is the sum of gears, bearings, seals and auxiliary losses. Gear and bearing losses can be separated in load dependent and speed-

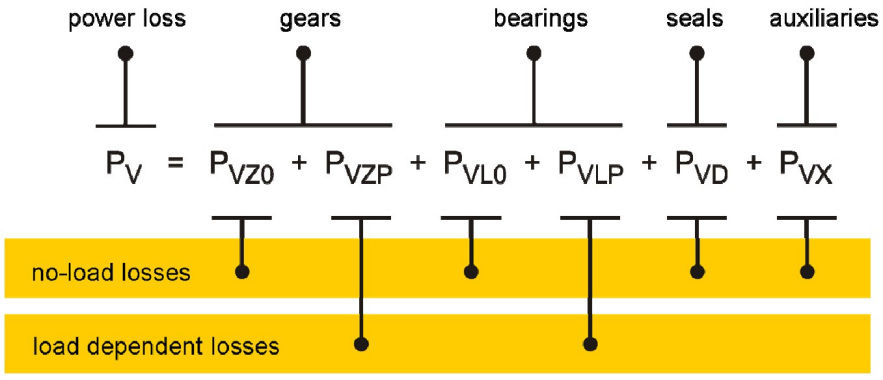

Figure 2.9: Gearbox power loss contributions, according to Hohn et al. [17]. Gears and Bearings are source of both load-dependent and speed-dependent power losses, while seals and auxiliaries losses are independent of the load.

dependent losses. Speed dependent losses occur with the rotation of the mechanical components, even without torque transmission: they are mainly related to lubricant viscosity and density as well as immersion depth of the components in a sump lubricated gearbox, but are also dependent on the operating conditions and internal design of components and gearbox housing. Load-dependent losses occur in the contact of the power transmitting components. Load losses depend on the transmitted torque, friction coefficient and sliding velocity in the contact area of the components. Usually, for nominal operating conditions, the dominant power losses of a gearbox are the load-dependent losses. When working at high speeds and with low or moderate loads, speed-dependent losses can overcome load-dependent losses.

In order to predict the efficiency, it is fundamental to understand how each component contributes to the total power loss and how the operating conditions and the lubricant formulation can influence each energy dissipation source.

2.4.1 Gear Mesh Losses

When considering losses, one of the main contributions comes from the sliding friction. Principally the instantaneous sliding friction loss is a function of the instantaneous sliding velocity and the friction force, which itself is a function of the instantaneous normal tooth load and the instantaneous coefficient of friction. Benedict et al.[18],O'Donoghue[19], Drozdov[20]and Misharin[21]

Table 2.3: Analytical formulations for the gear meshing friction coefficient proposed by early investigators.

Authors and Formulae	Applicability Ranges	Specific Units
Drozdov and Gavrikov $\mu = [0.8\sqrt{v_k}V_s + V_r\Phi + 13.4]^{-1}$ $\Phi = 0.47 - 0.13(10)^{-4}P_{max} - 0.4(10)^{-3}v_k$	$v_k \in [4, 500]$ $V_s \leq 15, V_r \in [3, 20]$ $P_{max} \in [4000, 20000]$	V_s, V_r : m/s P_{max} : kg/cm^2
O'Donoghue and Cameron $\mu = 0.6\left[\frac{S+22}{35}\right][v^{1/8}V_s^{1/3}V_r^{1/6}R^{1/2}]^{-1}$		S : μin, CLA V_s, V_r : in/s R : in
Misharin $\mu = 0.325[V_sV_rv_k]^{-0.25}$	$V_s/V_r \in [0.4, 1.3]$ $P \geq 2500$ kg/cm^2 $\mu \in [0.02, 0.08]$	V_s, V_r : m/s
Benedict and Kelley $\mu = 0.0127[\frac{50}{50-S}]\log_{10}[\frac{3.17(10)^8W'}{\nu V_sV_r^2}]$	$\frac{50}{50-S} \leq 3$	S : μin, RMS W' : lbf/in V_s, V_r : in/s

performed twin disc experiments and provided empirical formulas for the coefficient of friction

that are reported in Table 2.3, that were also analyzed and compared with exerimental data in a work by Gurd et al.[22].

Anderson et al.[23]studied the influence of the geometric parameters of a gear pair on its efficiency. They focused on module, face width, rotational speed, load, spin, bearing losses and lubricant viscosity. It was found that course-pitch gears are more efficient at low loads than finer pitched gears, while the opposite is true for highly loaded gears. It was also stated that rolling and spin are the main losses in lightly loaded gears and that rolling and spin losses dominate the efficiency losses in lightly loaded gear pairs. The model showed that increasing the rotational speed increase the overall efficiency by reducing the coefficient of friction and the sliding friction loss due to increased film thickness. Similarly, a more viscous fluid would improve efficiency under heavily loaded conditions. The effect of the face width on the gear set efficiency was shown to have greater influence at lighter loads as well. Although the accuracy of these studies was limited to the accuracy and applicable ranges of the empirical μ formula employed. These μ formulae were also limited to a certain type of lubricant, ranges of operating temperatures, speed, load and surface roughness conditions of disk specimen used.

Chase[24]studied the effect of surface roughness, coating, pitch diameter rotational speed, load, lubricant viscosity, temperature and face width. In his study he found that after 8000 rpm spin losses increase gradually with the speed, while the mechanical losses decay with speed, so the two contributions are somehow balancing each other. He found also that friction loss becomes insensitive to the input torque after a certain load value and that total and mechanical efficiency are increasing with increasing lubricant temperature. The geometric parameters that influenced the efficiency the most was the gear module, while the face width had a negligible effect. The most recent studies used EHL theory models to evaluate the friction forces between the mating teeth of spur gears, and developed models that does not require an user-define coefficient of friction.

Yang et al.[25] investigated the performance of helical gear pairs with consideration of the properties of non-Newonian lubricant and 3D topology of tooth flank, by performing numerical simulations. They found that for an increasing rotational speed film thickness becomes larger, while coefficient of friction decreases.

Clarke et al.[26] quantified the effect of measured profile deviations on the EHL lubricant film developed between helical gears, and stated that it has an effect on how the lubricant film carry the load, however they did not considered the roughness of the tooth flank.

Han et al.[27] showed that the pinion addendum will firstly enter a mixed lubrication regime and the friction coefficient in the plane of action will increase with rougher surfaces or less transmitted load, whereas the increase of pinion rotating speed will speed up the transition from a boundary lubrication regime to a mixed regime.

2.4.2 Gear Churning and Windage Losses

For dip-lubricated gears, oil churning is a major source of power loss which is related to the fluid circulation generated by rotating gears partly immersed in the air-lubricant mixture[28]. The

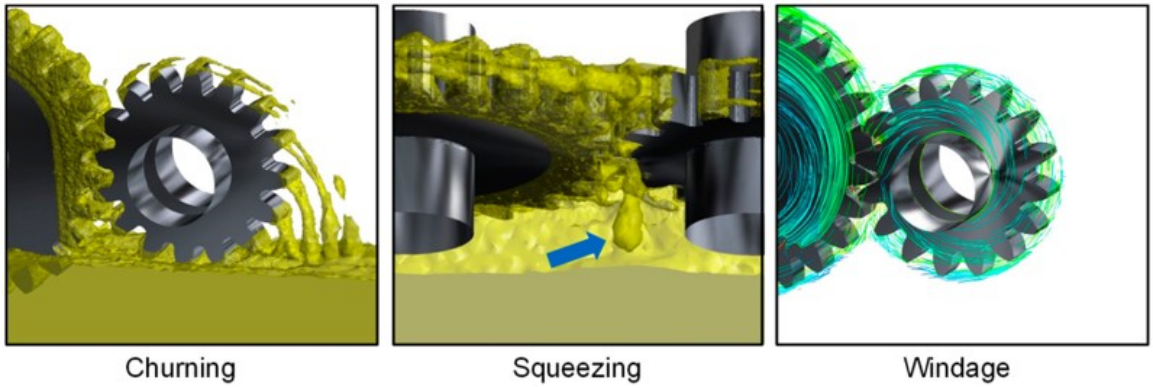

Figure 2.10: Speed Dependent Loss mechanisms in a gear pair, illustration from a CFD simulation. Churning due to oil drag, Sqeezing due to oil compression between gear teeth and Windage due to gear wheel aerodynamic drag. Credit:[29]

power loss due to dip lubrication can be subdivided in multiple components: churning, windage and squeezing. See Figure 2.10.

- The windage power losses arise due to the interaction of a mechanical component and a single phase fluid that can be either air or lubricant. These losses evolve with rotational speed and become significant only for high tangential speeds or for fluids with high viscosity grades and densities.
- The churning losses are similar to the windage losses, but involve at least two phases. These losses are the most important speed dependent losses in geared transmissions: the majority of the gearboxes, in fact, are dip lubricated and, therefore, subjected to churning losses.
- The squeezing losses are of a lower order of magnitude and arise due to the fact that the cavity between two teeth is reducing its volume during the engagement causing pressure gradients and therefore, additional fluxes.

Terekhov[30] studied the gear churning losses caused by high viscosity lubricants (200 to 2000 cSt) at low speeds and tested gears with modules ranging from 2 to 8 mm.

Changenet[31] deducted from dimensional analysis a set of equations to calculate a dimensionless gear drag torque. These equations are selected according to different flow regimes dependent on a critical Reynolds number (related to the flow nature) and a centrifugal acceleration parameter (related to fluid projection by the rotating gears). According to Changenet, the total churning power losses on the gearbox are calculated as the sum of the individual losses on each pinion/wheel. This method was demonstrated to give good results for pinion/wheels pairs rotating clockwise, as in Figure 2.11. When working in a counter-clockwise rotation, additional loss

Figure 2.11: Definition of a gear pair rotation sense, according to Changenet

mechanisms appear, making it inappropriate to estimate the churning power loss as the sum of the individual losses on each gear pair. From a physical point of view, Changenet[31] pointed out that this difference is probably due to the trapping of lubricant by meshing teeth (squeezing) and by a swell effect, see Figure 2.12, which dissipates energy and increases the immersion depth of the pinion. Factors influencing the oil churning loss are the viscosity of the oil, as this resists the

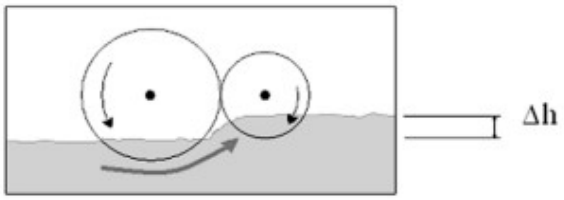

Figure 2.12: The Swell Effect: note how when the pair is rotating in a counter-clockwise manner, the gear is driving some oil to the pinion, thus increasing its actual immersion depth by a certain amount Δh, and so influencing the gear pair churning loss.

motion of the gears; peripheral velocity; operating temperature; the tooth module; the helix angle; and the submerged depth of the gears. All rotating components that are in direct contact with the lubricant, i.e. dipped into the oil, contribute to the churning losses, and the deeper the components are submerged, the higher the losses. With larger helix angles, the power losses are lower as the gear teeth slice through the lubricant rather than displacing the lubricant along the whole gear face width[32].

Guo[33] studied the influence of gear geometry parameters and operating conditions on gear pair churning losses, and found that the primary factor was the increase of rotational speed, but also the depth of oil immersion due to the collision and friction of the gear pair with the oil. The churning losses decreases as the oil temperature increased due to the effect of viscosity and the density of the oil. The factors affecting the gear pair parameters were tooth width and helix angle.

Changenet et al.[34] focused on the churning losses in gearboxes with emphasis on the contributions of enclosures, and demonstrated that the influence of radial clearance is weaker than axial clearances and that power losses can be substantially reduced by mounting flanges close to the gear lateral faces. He also stated that the pumping effect by the teeth is one of the physical mechanisms at the origin of churning loss and that obstacles deviating the lubricant flow between

the teeth can improve the system efficiency. He also reported that the losses may depend on the sense of rotation when a pinion-gear pair is considered.

Factors that influence the magnitude of the windage loss include the rotational speed of the gear because power losses rise with an increase in peripheral velocity. Other factors are the tooth module, the amount of oil mist present inside the casing and the diameter of the gears [35].

Ruzek et al.[36] performed experiments on a pinion-gear pair rotating in air and demonstrated that the air flow generated by one gear member can drive the other member to some extent thus leading to global windage losses slightly lower than those obtained by considering individual losses, especially at high rotational speeds.

Dai[37] performed a series of numerical studies on an isolated gear, and demonstrated that an increase of working temperature greatly reduces the windage losses, due to the change in the oil properties.

Dai et al.[32] focused on the influence of the geometry of the housing, and demonstrated that the the gear teeth are the main source of windage losses, and that the distance of them from the housing should be carefully evaluated. It is also demonstrated that a grooved shroud provides a considerable increase in energy efficiency of about 10% over the smooth shroud.

2.4.3 Bearing Losses

When evaluating the efficiency of bearings, several parameters are important to consider. These parameters provide insights into the performance, power losses, and overall efficiency of the bearing. Friction torque is a crucial parameter for assessing bearing efficiency. It represents the resistance to rotation caused by friction within the bearing. Lower friction torque indicates reduced power losses and improved efficiency.

Bearing clearance refers to the internal play or space between the rolling elements and the raceways. Proper clearance is crucial for smooth operation and minimizing unnecessary friction. Excessive clearance can result in increased power losses and reduced efficiency.

Proper lubrication is vital for reducing friction and enhancing bearing efficiency. Parameters related to lubrication include the type of lubricant, viscosity, lubricant film thickness, and lubrication method. Insufficient or improper lubrication can lead to increased friction and reduced efficiency.

Like churning losses in a transmission gear pair, the rotating roller elements in bearings may cause remarkable churning losses. Due to the difficulty in direct experimental testing, getting realistic estimates for churning moments in roller bearings is an extremely difficult task and the various approaches used only provide a rather gross approximation.

Gao[38] performed CFD simulations in roller bearings and demonstrated that the churning moments is linear with the fluid density and exponential to the fluid viscosity. He also stated that

the SKF model, the Palmgren model and the Parker model are reliable for their specific conditions. Results demonstrated that a numerical model agree well with Parker model for most calculated conditions, and is close to SKF model only if the bearing is fully lubricated. His results showed that churning loss on the roller cylindrical surface takes the most part of the total hydraulic losses, while the drag loss occupies a rather small portion.

During transmission, the rotating elements of the bearings (rollers in case of roller bearing and balls in case of ball bearing) rotate inside the raceway, increasing temperature because of friction between them. This temperature is a consequence of frictional losses and is cooled by lubricant continuously circulated through the bearing.

A number of operational and non-operational factors affect the bearing friction. The friction between interacting surfaces which are in relative motion always changes. Hence, it is difficult to predict exact frictional loss values. However, there are certain models available to predict losses which estimate loss values close to experimental observations.

2.4.4 Oil Seal Losses

When a shaft rotates within an oil seal, friction torque arises due to the interaction between the rotating shaft and the sealing lip of the oil seal. The friction torque is the resistance torque experienced by the shaft as it moves through the seal. The friction torque in an oil seal is primarily caused by two factors:

- Radial Lip Friction: The sealing lip of the oil seal makes contact with the rotating shaft. As the shaft rotates, the sealing lip exerts a radial force on the shaft surface. This force creates a frictional resistance, resulting in the generation of friction torque. The magnitude of the radial lip friction depends on factors such as the design and material of the sealing lip, surface finish of the shaft, and the type and quality of lubrication present.
- Lip-Lubricant Friction: Oil seals often rely on a thin film of lubricating fluid (such as oil or grease) to reduce friction between the sealing lip and the rotating shaft. However, even with lubrication, there is still some frictional resistance between the lip and the lubricant. This friction, known as lip-lubricant friction, contributes to the overall friction torque.

In most applications, seal power losses represent a minor fraction of the total power loss of a gearbox, and are almost negligible when compared to the losses of other components.

Croes et al.[39] suggested that the frictional losses in sealing elements is a problem that is yet fully understood. The contact zone is quite small and the microscopic phenomena is not easy to parametrize. Equation 2.15 is one of the simplest approaches.

$$P_{VD}^{C} = \frac{1}{2}\mu^{seal} F_R d_{sh} \omega \tag{2.15}$$

In Equation 2.15 the main problem is in obtaining the correct radial force F_R and the coefficient of friction μ^{seal} (which are interconnected). The frictional torque resulting from this radial load is only a part of the total friction loss at the seals. The type of atmosphere being sealed, pressure differential across the seal, tangential speed, ambient temperature and the lubricant and method of lubrication are just some of the parameters that influence the seals losses. Another very well known approximation suggested by Simrit (a seal manufacturer) is given in Equation 2.16.

$$P_{VD}^{S} = 7.69 * 10^{-6} d_{sh}^{2} n \tag{2.16}$$

In Equation 2.16) d_{sh} is the shaft diameter and n is the shaft rotational speed. The seal power loss is independent of the transmitted torque, the major influences being the seal design, operating speed and the shaft diameter.

More recently Bauer et al. [40] performed experimental studies on the power loss of lip seals and its influencing parameters. Bauer has concluded that in addition to the aforementioned influencing parameters shaft wear at the sealing contact also plays an important role in seal friction. According to Bauer et al., it is almost impossible to accurately predict lip seal frictional losses, not only due to the very complex nature of the problem but also because the losses can even be greatly influenced by the assembling.

2.4.5 Testing Procedure

During the test process of a gearbox, the rigid application of mathematical formulas could lead to incorrect results. This is because all of them are based on the principle of conservation of energy. The main drawback of these methods is that there exist some energy storage devices in the system, that could store energy in a first phase, thus leading to a lower efficiency than expected, and then release it later. If this energy is not considered in the calculations, one may get efficiencies higher than one.

Li[41] developed a calculation method to eliminate the interference factors from the mathematical calculations, relying on the energy conservation along the whole testing procedure.

Wei et al.[42] performed simulations on a high fixed ratio traction drive speed reducer considering the WLTC cycle as the working condition. He demonstrated that most of the energy lost in the transmission occurs in the low torque-low speed region, and that increasing the peak efficiency outside this region will have minimal effect on the overall efficiency.

Wink[43] presented an hybrid analytical-experimental method for determining overall power losses of an automotive transmission. The method consisted in the measure of load-independent losses and the prediction of the load-dependent one by using well-known mathematical models, and observed a very strong correlation in a light-duty six-speed transmission.

2.4.6 Modelling

Duan et al.[44]studied the influence of housing flexibility and shaft flexibility on the transmission error by theoretical and experimental methods and found that a condensed housing model is able to replicate in a good way its stiffness.

Draca[45] developed an analytical FE model of a double-stage helical gear reduction. He stated that gear pair position has a negligible effect on bearing forces, while the stiffness of the bearings on the force acting on them is significant if it is low.

Marques[46] studied the influence of dynamic effects on both a gear pair and a planetary gearbox. He showed that friction has a not significant effect on gear torsional dynamics, but there can be some differences (up to 3,6 %) between the quasi-static and dynamic power loss in the case of spur gears, and that helical gear sets are less affected by dynamic effects, with the gear meshing stiffness being the most influential parameter; in his work, non-linear stiffness and surface roughness effects were neglected.

Hambric et al.[47] studied the influence of gear mesh, bearing and housing stiffness on low-order shaft resonance modes, and concluded that the bearing stiffness increase the shaft resonance frequency quite significantly, and including the housing stiffness further increases some of the resonance frequencies.

Chapter 3

Loss Models

In this chapter, a description of the loss models that are implemented in the software will be given. The focus will be on the limitations, especially regarding the testing conditions that were used during their development.

Table 3.1: Analytical loss models implemented in the simulation software.

	AVL Excite M	MASTA 12	Romax 2022.2
Gear Mesh	• EHL Theory	• ISO 14179/1 • ISO 14179/2	• ISO 14179/1 • ISO 14179/2 • Anderson • VFC
Gear Drag	• None	• ISO 14179/1	• ISO 14179/1 • ISO 14179/2 • Terekhov • Changenet 2007 • Changenet 2011
Bearings	• SKF	• ISO 14179/1 • ISO 14179/2 • SKF	• ISO 14179/1 • ISO 14179/2 • SKF • Palmgren
Oil Seals	• None	• ISO 14179/1 • ISO 14179/2	• ISO 14179/1 • ISO 14179/2

3.1 Gear Mesh Loss Models

Table 3.2: Analytical loss models for gear drag loss, with focus on the loss mechanisms that are taken into account into the analytical equations.

	EHL Theory	ISO 14179/1	ISO 14179/2	Anderson
Sliding Speed	X	X	X	X
Normal Load	X	X	X	X
Viscosity	X	X	X	X
Tooth Surface Roughness	X		X	
Mixed Lubrication	X			
Lubricant Traction				
Local Coefficient of Friction	X			

3.1.1 ISO 14179/1

This loss model is derived from the calculation method based on AGMA Technical Paper 96FTM9 [48]. The gear load losses are derived from the early investigators of rolling and sliding friction who approximated gear tooth action by means of disk testers. The influence of the main parameters of load, speed, viscosity and surface roughness on the coefficient of friction were measured individually in twin disk tests and verified in gear experiments. The coefficients in the load loss equation were then developed from a multiple parameter regression analysis of experimental data from a large population of tests in typical industrial gear drives.

- Assumptions are made to give a simple equation for the coefficient of friction based on the experiments conducted, which is valid for pitch line velocity varying between 2–25 m/s and load intensity K between 1.4–14 MPa . Outside of these limits, the value must be determined by experience.
- Power loss is calculated from normal load (F) x friction coefficient (fm) x sliding velocity (v). The ISO use of mesh mechanical advantage (M) assumes linear sliding velocity along line of action and makes simplifying assumptions to calculate the average sliding velocity used in the formulas.
- Roughness is not considered in the equations.

3.1.2 ISO 14179/2

The power loss of cylindrical, bevel and hypoid and worm gears can be calculated according to theoretical and experimental investigations into those different gear types undertaken at the Technical University in Munich. The load dependent gear power loss results in the calculation of

the coefficient of mesh friction. The influence of the main parameters of load, speed, viscosity and surface roughness on the coefficient of friction were measured individually in twin disk tests and verified in gear experiments.

The applicability and limitations of the model include:

- Assumes coefficient of friction only changes slightly with the variable operating conditions on the path of contact, and assumes an average coefficient of friction can be used as an approximation.
- Includes roughness in the coefficient of friction calculation.
- Uses an approximating factor in the calculation to consider different lubricants (according to Schlenk [49])
- Coefficient of friction (μ_{MZ}) is limited for applications where the maximum tangential velocity is below 50 m/s (for velocity greater than 50 m/s, 50 m/s is used as a hard limit in the equations) and $F/b > 150$ N/mm (a hard limit of 150 N/mm is used when the tooth normal force/face width value is less than this).

3.1.3 Anderson

Anderson and Loewenthal developed an analytical model for calculating the gear mesh efficiency of spur gears over the late 1970s and early 1980s. They extended the initial formulation to handle non-standard gear profiles in 1984, and came up with methods to optimise the gear geometry for reducing gear mesh loss. In Romax, their 1983 paper[50] is implemented, which is a culmination of their previous work. Romax includes the 1986 section[51] on non-standard gear profiles, which refers back to 1984 and contains validation. The loss model was validated for the complete T56/501 gearbox (used in aerospace) in conjunction with the Harris model for bearing loss, and showed good correlation.

- The coefficient of friction model is taken from Benedict and Kelley[18] for mineral oils, based on disk machine data. This model is applicable in the EHD lubrication regime with some asperity contact ($\lambda < 2$). Lubricant type is important when using a certain model, and the Benedict and Kelley model is not applicable for all lubricants.
- The film thickness model does not consider the thermal and starvation effects that occur at high operating speeds (above 40 m/s) and is limited to conditions within this. The formulation assumes EHL conditions.
- The windage loss equations are not considered in the gear mesh loss implementation, but are implemented in the Terekhov model under gear churning loss.

3.1.4 EHL Theory

The EHL Theory approach is the implementation of the work made by Klein[52]. Based on EHL Theory, μ_{local} is calculated by:

$$\mu_{local} = 0.032(p_H)^{0.1} V_{\sum vert}^{-0.2} (s_x)^{0.05} (\lambda_z)^{-0.1} \tag{3.1}$$

- $p_h[N/mm^2]$ Hertzian pressure in the contact zone
- $V_{\sum vert}$ Summarized Velocity
- (s_x) Slip in the contact zone

λ_z is the relative oil film thickness, calculated with the actual central oil film thickness $h_0[\mu m]$ and the surface roughness $R_z[\mu m]$

$$\lambda_z = \frac{h_0}{R_z} \tag{3.2}$$

Herein the central oil thickness h_0 is estimated using the regression formula according to Ertel/-Grubin[53][54]:

$$h_0 = 1.9510^3 \rho G^{0.73} U^{0.73} W^{0.09} \tag{3.3}$$

G,U and W are tribology parameters by Taylor.

3.2 Gear Drag Loss Models

Table 3.3: Analytical Loss models for gear drag loss, with focus on the loss mechanisms that are taken into account into the analytical equations

	Changenet 2007	Changenet 2011	Terekhov	ISO 14179/1	ISO 14179/2
Diameter/Immersion Depth	X	X	X	X	X
Tooth Width	X	X	X	X	X
Lubricant Viscosity	X	X	X	X	
Immersion Volume	X	X			
Helical Gears		X		X	
Tooth Roughness				X	
Swell Effect	X	X			
Centrifugal Acceleration	X				
Windage Loss			X		

3.2.1 Changenet 2007

The results given by Changenet[55] are based on dimensional analysis and have been experimentally validated using a single gear, and a pinion-gear pair over a wide range of speeds, gear geometries, lubricants and immersion depths. The work builds on the work of previous authors and studies to provide a better model for gear churning loss (excluding windage). Previous work examined were from Terekhov[30], Lauster and Boos[56], and Boness[57]. Unlike previous models, Changenet considers the impact of gear tooth geometry on churning loss. Furthermore, Changenet takes forward Boness' normalisation of the churning torque as that is the most logical since it considers the immersed surface area of the pinion. Changenet also considers the sense of rotation in the formulation of the loss equations (into or out of mesh - swell effect due to air-lubricant trapping by the teeth).

It was found that at low-medium speeds, gear geometry is influential via the submerged surface area only, while tooth number and face width play a negligible role. At high speeds, churning losses are found to be largely independent of oil viscosity and the inertia forces become much more significant than the viscous ones. These thresholds are characterised by a critical Reynolds number, and the transitions are an important consideration when calculating churning loss.

- Experimental validation and resulting equations only consider spur gears
- Testing was conducted for rotation speeds between 1000 - 7000 rpm and for various gear geometries, lubricants, and relative immersions between 0.1 - 0.6.
- The tooth module was initially considered in the formulation but was found to have negligible effect on churning loss regardless of operating regime.
- Multiple tests conducted with different gear geometries, lubricants, relative immersion depths (between 0.4 - 0.7) and speeds (pinion speed between 500 - 1500 rpm) to quantify the swell effect.
- Model validated by more than 100 experimental measurements from a specific test rig, with particular attention paid to the influence of temperature on lubricant viscosity and that of windage on high speed measurements in order to avoid bias.

3.2.2 Changenet 2011

This formulation extends on the Changenet 2007 model [55] to dissociate speed and temperature (which are considered together in the viscosity term in the Reynolds number), so that each factor and the effect can be considered independently. This dissociation can happen in practise in transient conditions, and a number of transient measurements have been carried out to account for the transitions between fluid flow regimes which are not apparent in steady state conditions.

It was found through experiments that alongside lubricant viscosity, the gear face width contributes significantly to the loss in relation with speed. It is postulated that this is due to the

projection of lubricant by centrifugal effects and a new parameter is introduced in the 2011 paper to account for this 'centrifugal acceleration' term (denoted by gamma γ). By accounting for the influence of Reynolds number and the centrifugal acceleration term, this paper can explain a number of experimental evidence which previous literature could not account for. Thereby, the formulation has four equations for different operating regimes, rather than the two in Changenet 2007.

- Formulation has been extended to include helical gears
- Critical Reynolds number in this case is 4000, however the transition between flow regimes does not happen exactly at this point for all cases, it is chosen based on the experiments done as part of the study as a first approximation.
- In Romax, the Changenet 2011 model can be used with the inclusion of the swell effect from the 2007 model.
- Experimental rig improved compared to 2007 to measure instantaneous churning torque and its time variations to get better matching, and experiments conducted with mineral oil for temperatures between 20°–75°C

3.2.3 ISO 14179/1

The gear churning loss formulations originally appeared in work presented by Dudley[58] and have been modified to account for the effects of changes in lubricant viscosity and amount of gear submergence.

- Tooth roughness is considered in the formulation, unlike in other standards/papers.
- If the gear has a helix angle < 10°, 10° is used in the calculation of churning loss
- Uses an arrangement constant of 0.2 as a consideration of the housing influence, very simple.
- This constant was selected as a first approximation based on tests conducted by the researchers.
- The calculation is based on standard conditions of 25°C maximum ambient temperature and 95°C maximum oil sump temperature in a large indoor space, ambient air velocity less than 1.4 m/s in a large indoor space)

3.2.4 ISO 14179/2

The no-load gear system losses are determined according to Mauz[59], but further simplified for the standard. In the case of the arithmetic formulations derived by Mauz, no distinction is made between splash and squeeze losses, as, according to his investigations, the squeeze component is negligible.

- For high immersion depth, contradictory results for the influence of viscosity were found: In some cases, power loss increased with increasing viscosity, while in others, it decreased. Therefore, no account is taken of viscosity in the calculation equation.
- The calculation is for a gear pair, so the loss is split between the two gears in the results seen in Romax.
- The distance between gears and walls has to be large enough to prevent the pumping effect and cross-effects, as a large gearbox/open space is assumed.

3.2.5 Therekov

This was one of the original works[30] that tackled developing a reliable universal method for the quantitative evaluation of churning losses, founded on extensive experimental research to permit the results obtained to be generalised. It was validated with truck gearboxes, so applicability will depend on use case. It includes loss due to oil expulsion from teeth as well as disk loss from the rotation of the gears.

- Terekhov's work does not include the impact of gear tooth geometry, which is likely due to the experimental conditions under which the model was validated – high viscosity lubricants (20–2000 cSt) combined with low speeds (the input speed varied between 200–3000 rpm), which limit the quantity of lubricant between the teeth being expelled by centrifugal effects and makes the gear behaviour close to that of a disk. Gear module seem to have practically no impact on the churning loss (tested for modules between 2–8 mm) and is not included in the formulation.
- Radial and endface clearance between the gears and housing had no significant effect unless:
  - Radial clearance/pinion radius < 0.2
  - Endface clearance/pinion radius < 0.1
  - Inside these limiting values, the loss increased substantially but there is no formulation to account for this
- The reduction in the parameter Vg/Vo (submerged volume / lubricant volume) only effects the churning loss up to a specified limit, in any operating regime. This critical value is 0.04, and is used as a constant in Romax's implementation of the Terekhov method, rather than following the exact physics in the equations and leaving the ratio V_g/V_0 as a variable for the user to define.
- Windage loss is included the the implementation, taking equations from Anderson[50]. This is validated for helicopter/aerospace gearboxes in the paper. The model assumes an oil-rich gearbox atmosphere with conditions generally found in helicopter transmissions lubricated with oil jets.

3.3 Bearings Loss Models

Table 3.4: Analytical Loss models for bearing loss, with focus on the loss mechanisms that are taken into account into the analytical equations

	SKF	ISO 14179/1	ISO 14179/2	Palmgren
Geometrical Dimensions	X	X	X	X
Viscosity/Speed	X	X	X	X
Load	X	X	X	
Mixed Lubrication	X			
Misaligment				
Internal Clearance				

3.3.1 SKF Model

This model[60] was derived from more advanced computational models developed by SKF, and is also based on tabulated data by SKF, but considers more detail through updated equations and coefficients. Load-dependent loss is broken down into rolling friction (and the effect due to high-speed starvation and inlet shear heating) and sliding friction (and effect on lubricant quality). Load-independent loss due to lubricant drag is also considered.

- The model assumes lithium soap grease with mineral oil – the base oil viscosity is used in calculations, for ambient temperature 20°C or higher, so 'grease' lubrication can be considered.
- It is applicable for oil bath, oil-air and oil jet, viscosity ranging from 2–500 cSt.
- It assumes normal operating clearance (no misalignment).
- Drag loss is applicable when the oil reservoir is large and external oil agitation is minimal.
- This model considers the bearing type, load, speed, lubricant viscosity and lubrication regime.

3.3.2 ISO 14179/1

This calculation method is based on AGMA Technical Paper 96FTM9[48] and SKF general catalogue.

Bearing losses are calculated from catalogue information supplied by bearing manufacturers, which in turn can be traced back to the work of Palmgren[61]. The formulation has been verified by cross checking predicted results to experimental data for various gear drive configurations from several manufacturers. The method is split into load-independent and load-dependent loss and has been validated by extensive testing of concentric-shaft, base-mounted reducers with shafts

mounted in a horizontal orientation. Limited testing of some parallel shaft gear units has also been performed in order to spot check the adequacy (validity) of the model.

- Model validated for 25°C maximum ambient temperature and 95°C max. oil sump temperature, in large indoor space. Axially loaded cylindrical roller bearings must be operating in the elastohydrodynamic region (no metal-metal contact) and there are limitations to the axial to radial force ratio acting on the bearing.
- It only considers oil churning, based on dip factor f_0
- It considers only bearing macro design, lubricant viscosity and bearing speed.
- Coefficients are based on SKF bearings and may vary for other manufacturers.

3.3.3 ISO 14179/2

The method has the same empirical equations as ISO 14179-1, with the same coefficients for load-dependent loss. There are slight differences for some load-independent loss coefficients (f_0), depending on bearing type and lubrication method.

- Validation done under the same conditions as ISO 14179-1
- Provides different values for different types of lubrication (churning, windage, grease), unlike ISO 14179-1.

Chapter 4

Analysis Theory

This chapter will focus on both the mathematical equations used to model each component present in this unit, both regarding the mechanical and the oil properties, how the components are discretized and will end with some words about how the solution is derived.

4.1 Components Modelling

4.1.1 Gear Contact Model

The contact model implemented uses a discretization where the pinion and gear are cut into slices. The slicing is done by face-cutting along the pinion's/gear's width direction. The reference point of a particular slice defines the slice's internal node. The location of the internal nodes are defined by the positions of the original nodes, the effective face width of the gear and pinion, and the user's input for the number of slices per original nodes as outlined in Figure 4.1. During the evaluation of the joint all motion information (position and velocities) given for the original nodes are interpolated to the internal nodes. Resolution of the contact as well as the force computation in then carried out with respect to the internal nodes only. Finally, forces/moments acting on the original nodes are obtained by a distribution-algorithm based on the forces/moments at the internal nodes.

Friction forces are computed based on Coulomb's approach using the relative velocity at the current contact point measured in the tangential direction (normal to the Plane of Action), as shown in Equations 4.1 and 4.2.

$$\Delta V_{\text{tangential}} = V_{\text{tangential, Gear}} - V_{\text{tangential, Pinion}} \tag{4.1}$$

$$F_{\text{Friction},i} = \mu F_{\text{Elastic},i} \frac{\Delta V_{\text{tangential}}}{V_{\text{tangential}}} \tag{4.2}$$

Regarding the friction coefficient, several approached could be used, with different complexity.

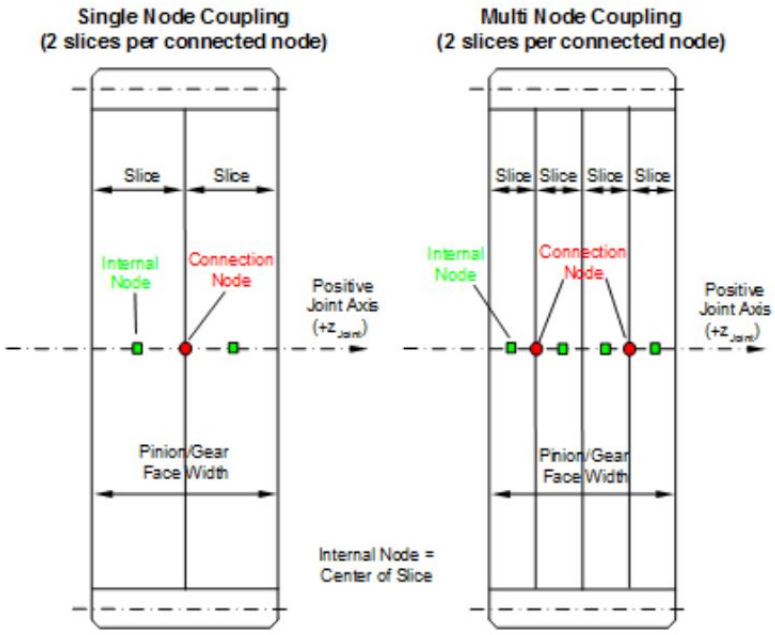

Figure 4.1: Discretization of the gear meshing with node coupling

- Average friction coefficient based on the equation in the gear meshing coefficient of friction models, with sliding velocity and normal load at each mesh point, integrated over the tooth.
- Friction coefficient calculated at each mesh point as well, using a proper film thickness calculation method instead of the standards-based model. This is then multiplied with the local sliding velocity and normal load, and integrated over the tooth surface to give the mesh loss.

4.1.2 Shafts Model

Due to their relatively simple shape, the shafts can be either modelled by using a 1D approach, by considering them as beam elements, or by considering the condensation of a FE mesh into relevant nodes. In general, the 1D approach is managed inside the simulation software, while for the external condensation, an additional software is used. In the following, a brief description of how the three softwares manage the two approaches will be discussed.

Shafts in MASTA and Romax are modelled as classic finite element Timoshenko beams. These are based on Euler-Bernoulli beams but with a further correction for shear deformation. Euler-Bernoulli assumes:

- Normal plane sections remain plane during bending.
- Normal plane sections do not stretch during bending.
- Normal plane sections remain normal during bending.

Euler-Bernoulli beam theory does not account for the effect of transverse shear strain. As a consequence, this theory underestimates deflections and overestimate natural frequencies. For thin beams, these effects are insignificant, although for thicker beams these effects can be significant. Timoshenko beam theory takes into account the effect of transverse shear strain; in effect the third assumption that normal plan sections remain normal during bending is removed.

In AVL Excite, the 1D approach is managed inside the simulation software by a tool called 'Component Modeller'. In it, it is possible to manage simple shapes by using predefined components. After the 3D shape is generated, the tool will condense the properties of the shaft into specific nodes that are decided by the user.

4.1.3 Bearing Elastic Model

The bearing representation must be understood as a pure force-displacement/velocity relationship between the connected bodies. The mass effect of involved bearing components (rings, cage, rolling elements) is not considered. As a consequence, no joint-internal iteration or integration is performed. For roller bearings, the stiffness is derived from non-linear load deflection models using Hertzian contact theory and bearing internal geometry according to Harris[61].

4.2 Lubrication Oil

According to the loss formulations found in the literature, the oil properties play a fundamental role in the evaluation of the losses.

For the oil density, according to the ISO/TR 15144-1[62], it is necessary to provide the value at 15°C. The density curve will then be evaluated according to:

$$\rho_\theta = \rho_{15}[1 - 0.7\frac{(\theta + 273) - 289}{\rho_{15}}] \tag{4.3}$$

where ρ_{15} is the oil density at 15°C while θ is the oil temperature. Regarding the oil viscosity, many formulations are present in the literature. However, the one most commonly used is the Vogel equation:

$$\eta = a \exp\left(\frac{d}{\theta - c}\right) \tag{4.4}$$

where a, c and d are parameters depending on the oil properties.

In order to determine the curve, it is necessary to provide the dynamic viscosity value at two oil temperatures, as well as a value for the c coefficient (the codes suggest a value of -95°).

Another value to be provided is the pressure viscosity coefficient, which describes how the oil density is changing when a pressure is applied on it. In this work, it will be evaluated according to the ISO/TR 15144-1[62], in which it is assumed to be variable according to the oil temperature

according to:

$$\alpha_\theta = \alpha_{38}\left(1 + 516\left(\frac{1}{\theta + 273} - \frac{1}{311}\right)\right) \tag{4.5}$$

An important condition to be studied is how to account for the oil level inside the reducer unit. Figure 4.2 displays how the simulation softwares account for it. The procedure consists in defining

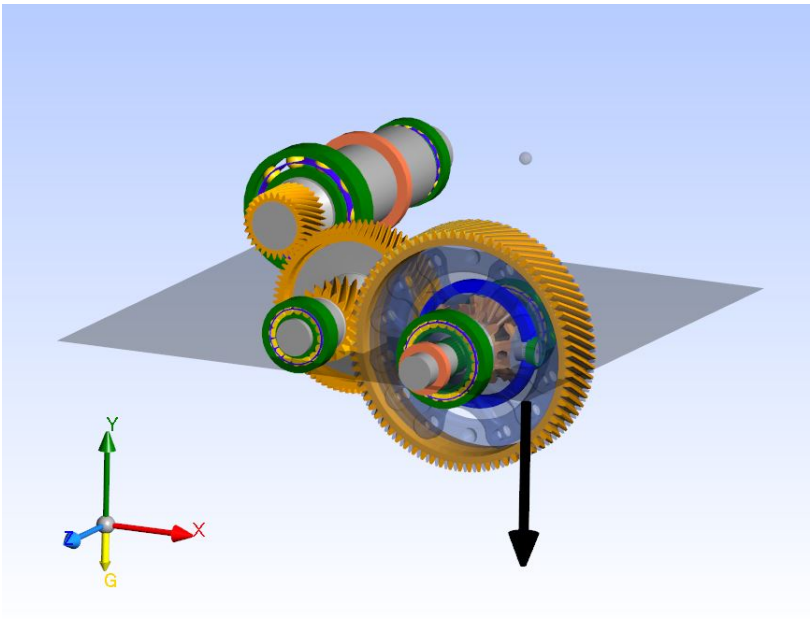

Figure 4.2: Oil level definition: will be used for the computation of the dip factors.

a gravity orientation vector, that has to be carefully chosen according to the mounting of the gearbox during the testing procedure. The next step is to define the oil level inside the unit; this is done by defining a reference point in the space, and then by defining an offset with respect to this point. In this way the oil level and orientation will be completely defined.

During simulation, this parameter will be used to determine the oil level for all the components inside the gearbox (gears and bearings), and will be used to determine the churning losses associated to that components. In practice, it is called the 'dip factor', and can vary from 0 (totally unsubmerged) to 1 (totally submerged). This parameter will be given as input to the loss formulations implemented in the softwares.

In this area, some differences are present in the simulation softwares: AVL Excite does not have a formulation to account for gear churning losses; more over, the oil level has to be set manually in each bearing, and this one will be provided as input to the SKF loss model (the only one present). In MASTA and Romax, the dip factors are automatically evaluated; however, in Romax there is the possibility to rely on the Changenet Models for the gear churning losses evaluation: in this case the formulation requires the definition of the volume of oil present inside the reducer unit.

4.3 3D Discretization

According to the mathematical formulations implemented in the simulation softwares, the losses are also function of the forces applied on the various components. The forces mainly arises due to the torques applied to the shafts, but they also cause a deformation of the components themselves, leading to misalignment in the teeth mating and of the bearing races, thus modifying the actual working conditions.

For all the reasons mentioned above, a FE discretization of the model is required to take into account all these effects, and one of the goals of this work is to understand how much this deformation affects the total efficiency.

Today, finite element methods (FEM) are very useful tools in science and technology applications and there are a various types of FEM commercial codes. FEM methods were introduced in the 1950's and, gradually with the development of computer science and technology in the 1970's, have become very popular in all engineering fields. In the beginning of releasing the computers, due to lack of technology, it was very time consuming to solve a large engineering problem by using numerical methods. In general, when it comes to numerical methods, it is very important to reduce the runtime. Although the speed of computers has been multiplied through the last decades, powerful computers are still very expensive. Hence, besides the advanced computer technology, it has been very important to simplify a complex problem to save time and money.

4.3.1 Volume Mesh

Since the problem deals with solid bodies with all the three dimensions comparable in size, the obvious choice for the discretization is to use 3D elements. There are four different 3D element types: tetras, bricks, prisms and pyramids, as shown in Figure 4.3. These four elements can be used, in various combinations, to mesh any 3D model. Tetrahedral elements are the default element adopted in Hypermesh. Tetrahedra are also known as a simplex, which simply means that any 3D volume, regardless of shape or topology, can be meshed with them. They are also the only kind of elements that can be used with adaptive mesh refinement.

The other three element types (bricks, prisms, and pyramids) should be used only when one is motivated to do so. It is first worth noting that these elements will not always be able to mesh a particular geometry. The meshing algorithm usually requires some more user input to create such a mesh.

The quadratic tetrahedral element has ten nodes with three degrees of freedom at each node. This yields a total of 30 Degrees of Freedom (DoFs). The displacement field equations (u, v, w) will contain quadratic terms in the expressions and thus strains (which are a derivative of displacements) will vary linearly through the element.

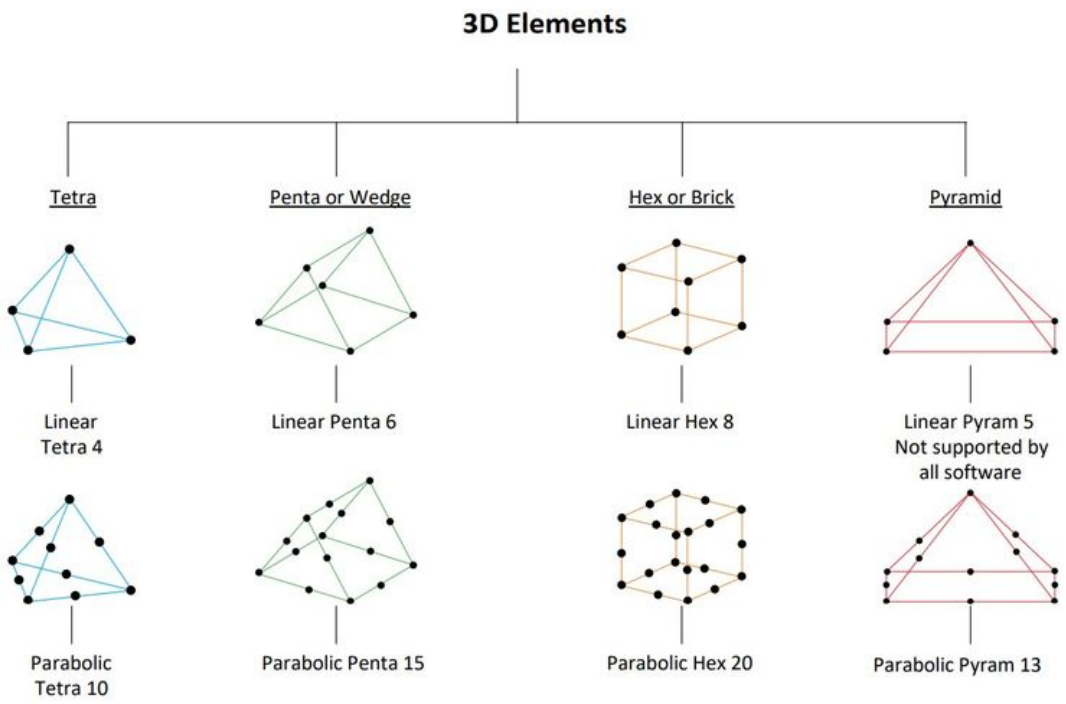

Figure 4.3: Common elements used for a volume discretization in a mechanical problem: note the number of nodes present for each element. In a linear element the edge is described by a first order equation that fits two nodes, while in the parabolic element it is described by a second order polynomial that fits three nodes. It is clear that the parabolic elements needs a much larger computer memory to be solved, considering that in space each node has 6 DoFs.

A complete quadratic polynomial in terms of spatial coordinates x, y, and z with no additional cubic or higher-order terms has exactly ten terms. Thus, the ten-node tetrahedral element employs a complete quadratic function to interpolate the displacement field across the element from the nodal values. This means that the strain tensor for the element is linear (i.e., each of the various strain components can vary as a linear polynomial over the element volume), and the element performs much better under bending types of loads. It also turns out that the element can now take on a quadratic shape. Thus, for example, the edges of the element may be curved to fit a portion of a circular arc.

4.3.2 Matrix Reduction

In this kind of problems, especially when dealing with system dynamics, the combinations of a large complex domain with detailed model and discretizing in small time step often cause to increase the simulation runtime. In order to overcome to this limitation, it is essential to simplify the dynamic problems. One idea is to use structural elements, such as beams and shells, to simulate the behaviour of the entire original problem. However, this method is not appropriate for a problem with complex geometry and boundary conditions. Another solution is to use reduction methods to

reduce the DoFs. In this mathematical method, the DoFs are divided into two categories: master, which are still available after operation, and slave DoFs.

One reduction method is the Guyan-Irons reduction method which is very suitable especially for static problems. This method also shows acceptable results for dynamic problems with low frequency or if the load is not applied suddenly. Nevertheless, this method is not proper for dynamic problems with high-frequency range because an appropriate reduction of the mass matrix must be implemented. Another reduction concept is the Craig-Bampton method, which is quite suitable for dynamic problems in the high frequency range. In this method, the structure is divided into small dynamic substructures that can be reduced independently. Afterwards, the substructures can be assembled to the original condition[63],[64].

A challenge in FEM methods is the mesh generation, especially, if it is required to have high quality mesh to obtain acceptable results. By using the reduction methods, it is feasible to hold the fine meshing for demanding domains while the rest of domain can hold a coarse mesh. The validity of the results is extensively discussed in [64] by presenting several useful examples.

The dynamic substructuring has several advantages, as below:

- It reduces the total number of DoFs from millions to tens. Thus, it is possible to study a very detailed model and reduce the runtime. Furthermore, a reduced system needs less computational resources and it is easier to be implemented and saves money.
- It simplifies the model and allows reducing the entire structure so that it gets rid of those subdomains that do not contributes to the dynamic behaviour of the model.

Finite Element Methods are widely used because any geometry of continuous system, such as a gearbox housing, can be represented by a mesh, which is a collection of simple shapes known as elements. However, more elements form a larger stiffness matrix, as shown previously, which requires more effort to solve. When analysing a large structure composed of small sub-structures, the behaviour can be described by the degrees of freedom at the connections between sub-structures. It is possible to obtain a matrix involving the boundary only by transforming the original matrix for each sub-structure, and this process of reducing the number of degrees of freedom is called condensation. Condensation gives lower memory limitations on computing as the model size is reduced, and a condensed matrix can be used repeatedly unless there is any change on its original mesh. Condensed matrices are used for Stiffness/Housing components. Therefore, condensation is required to be performed for each Stiffness/Housing component, which can be done within the simulation software or externally by other Finite Element Analysis packages such as Nastran, Abaqus and Ansys.

For static analysis, stiffness and mass matrices are condensed by static condensation, which is also known as Guyan reduction. For dynamic analysis, the dynamic condensation solves eigenvalue problems as well as condensing stiffness and mass matrices, which is why the Craig-Bampton

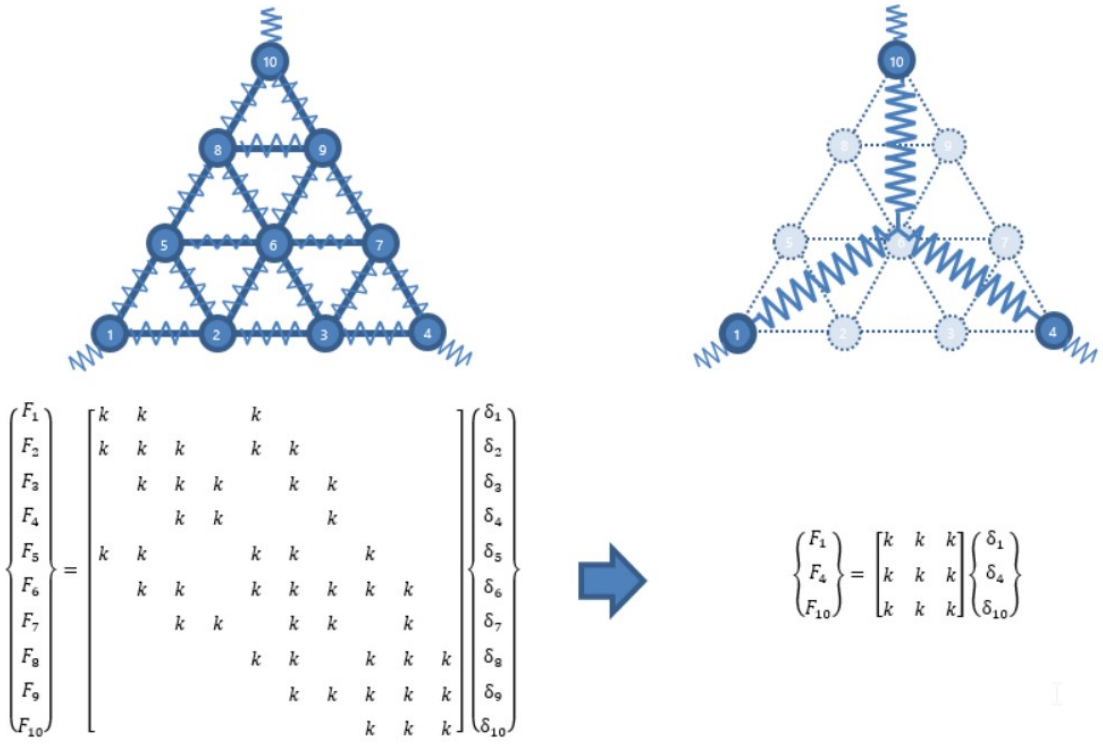

Figure 4.4: Ideal Representation of the working principle of stiffness matrix condensation: for example, when a mesh has 3 boundary nodes, its stiffness matrix will be condensed as if there are 3 nodes only and they have fully coupled each other. Image credit:[65]

method is known as Component Mode Synthesis (CMS).

4.3.3 Craig-Bampton method

In this method, the Degrees of Freedom (DoF) are partitioned into two different types, a boundary part or b as a master and an interior part or i as slave DoFs. Hence, the semi-discrete equation of motion can be formed as:

$$M\ddot{u}(t) + Ku(t) = F(t) \tag{4.6}$$

$$\begin{bmatrix} M_{ii} & M_{ib} \\ M_{bi} & M_{bb} \end{bmatrix} \begin{bmatrix} \ddot{u}_i \\ \ddot{u}_b \end{bmatrix} + \begin{bmatrix} K_{ii} & K_{ib} \\ K_{bi} & K_{bb} \end{bmatrix} \begin{bmatrix} u_i \\ u_b \end{bmatrix} = \begin{bmatrix} F_i \\ F_b \end{bmatrix} \tag{4.7}$$

In principle, this method reduces the internal degrees of freedom by defining a number of internal modes. This reduction method needs two different types of modes, the fixed-interface vibration modes (normal modes) and the constraint modes.

In order to calculate the normal modes, it is required to refer to the eigenvalue problem containing the internal mass and stiffness matrices. More specifically, as discussed earlier, the whole

system must be partitioned into internal and boundary degrees of freedom. These modes represents the information associated with the vibrations of the system and must be held fixed at its boundary DOF, i.e. ($x_b = 0$), that leads to the reduction of Equation 4.6 as:

$$[M_{ii}][u_i] + [K_{ii}][u_i] = 0 \tag{4.8}$$

And finally, in order to solve this eigenvalue problem, containing n eigenvalues (λ) and eigenvectors (Φ), the following equation can be solved:

$$(K_{ii} - \lambda_j^2 M_{ii})\Phi_{ij} = 0; where\, j = 1, 2, ...n. \tag{4.9}$$

The results are the eigen-frequencies and eigen-modes of the system and the remaining k fixed-interface vibration modes which are represent in the modal format.

$$\begin{bmatrix} \Phi_{ik} \\ 0 \end{bmatrix} = \begin{bmatrix} \Phi_{ik1} & \Phi_{ik2} & ... & \Phi_{ikk} \\ 0 & 0 & 0 & 0 \end{bmatrix} \tag{4.10}$$

The other sort of mode used in Craig-Bampton is constraint mode. This mode results from the static deformation of the system due to applying a unit displacement to one of the boundary DoF. Simultaneously, the other interface DoF must be held restrained and there is no force acting on the internal degrees of freedom. In principle, the constraint modes are the static response of the structure because of a unit deformation applied on the interface DoF. In order to calculate these modes, which is identical to calculating the normal modes, the total DoF of the system must be also divided into the internal and boundary DoF. Thus, with the assumption of the free-force internal DoF, Equation 4.6 can be summarized as:

$$[M_{ii}][\ddot{u}_i] + [M_{ib}][\ddot{u}_b] + [K_{ii}][u_i] + [K_{ib}][u_b] = 0 \tag{4.11}$$

Furthermore, in order to calculate the static response, the inertia terms can be neglected. This assumption reduces Equation 4.11 as:

$$u_{i(Static)} = -[K_{ii}]^{-1}[K_{ib}][u_b] \tag{4.12}$$

The term $-[K_{ii}]^{-1}[K_{ib}]$ is known as static mode matrix. Now, having the static mode matrix leads to writing the constraint modes matrix:

$$\begin{bmatrix} x_i \\ x_b \end{bmatrix} = [\Phi_c]x_b = \begin{bmatrix} -[K_{ii}^{-1}[K_{ib}] \\ [I] \end{bmatrix} x_b \tag{4.13}$$

where $[\Phi_C]$ is the constraint modes matrix.

As previously discussed, the aim of applying the Craig-Bampton method is to reduce the structure and total DoFs to decrease the runtime. After calculating the normal and constrained modes, it is possible to obtain the reduction matrix. The reduction matrix $[R]_{CB}$ is necessary to reduce the structure. In order to calculate the reduction matrix, the internal DoF must be described in combinations of the normal modes $[\Phi_i]$ and constraint modes $[\Phi_C]$.

$$x_i = [\Phi_i]\eta_i + [\Phi_C]x_b \tag{4.14}$$

Replacing into original the DoF leads to the reduction taking the following form:

$$\begin{bmatrix} x_i \\ x_b \end{bmatrix} = \begin{bmatrix} [\Phi_i]\eta_i + [\Phi_C]x_b \\ x_b \end{bmatrix} = \begin{bmatrix} [\Phi_i] & [\Phi_C] \\ 0 & [I] \end{bmatrix} \begin{bmatrix} \eta_i \\ x_b \end{bmatrix} = [R]_{CB} \begin{bmatrix} \eta_i \\ x_b \end{bmatrix} \tag{4.15}$$

Once the reduction matrix is available, in order to reduce the original structure, it is possible to reduce the original mass and stiffness matrices:

$$[\tilde{M}]_{CB} = [R]_{CB}[M][R]_{CB}[\tilde{K}]_{CB} = [R]_{CB}[K][R]_{CB} \tag{4.16}$$

Reduced matrices have dramatically smaller dimensions. Buckel[64] presents several useful examples when the reduction method is applied on the original matrix structure and significantly reduces the size of the matrices.

4.3.4 Considerations on RBE

When deriving the stiffness and mass properties of the components in the relevant points, that, for example, for the housing are the stiffness at the bearing races, the problem is how to create the interface between the race itself and its center point that will be the condensation node. In this kind of problem, the usual approach is to use Rigid Bar Elements (RBE). The RBE is a constraint element for the motions between nodes. Therefore, the motion of one node governs the motion of the other node, and the nodes are called the Independent node and Dependent node. There exist two kind of RBE elements in Optistruct: RBE2 and RBE3.

When RBE2 is used, the condensation node is the independent node and the connected nodes are the dependent nodes. Therefore, the displacements of all the connected nodes are the same as the condensation node. However, it is the opposite when RBE3 is used. The connected nodes are independent nodes, and the displacement of the condensation node is the average of all the connected nodes because RBE3 transmits the loads from the dependent node to the independent nodes; therefore, the displacement at each node can be different. Originally the name RBE refers to the equivalent NASTRAN element type, which stands for Rigid Body Element. However, RBE3 does not add additional stiffness to the FE component comparing to that of RBE2, which results in no relative motion between the dependent nodes as those are connected rigidly[66].

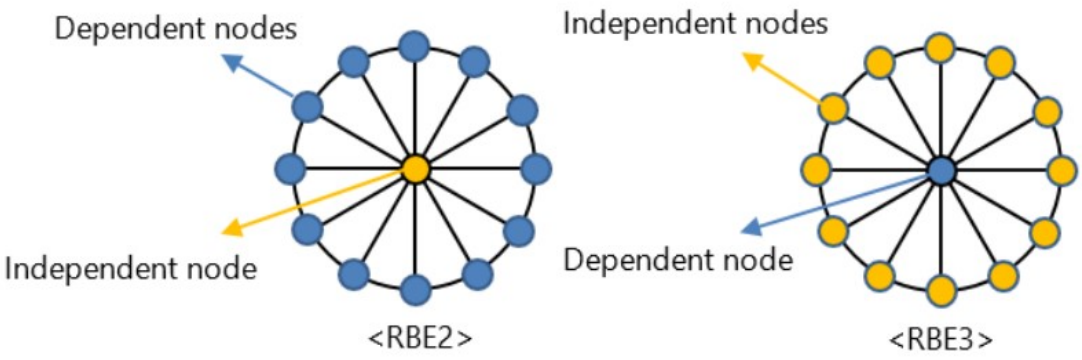

Figure 4.5: Representation of the working principle of a Rigid Bar Element (RBE). The methodology consists in deriving the stiffness and mass properties by connecting the condensation nodes in the center to the nodes of the FE unit on the circumference (that in 3D environment has typically a cylindrical shape).

4.4 Solver

Generally, an analysis model in engineering is a continuum, where the governing equation representing its phenomena involves differential relationships. Therefore, solving an engineering problem is often solving differential equations. Most of analysis models in engineering are too complex to solve and exact answers are impossible to obtain. Therefore, in practice the continuous model is discretized and replaced by a finite amount of data and approximate solution is achieved by a numerical method.

4.4.1 Linearity

When a structure is under a load, it will deflect to resist the load unless it moves. Hence the structure is stressed internally. Experimentally, it is known that the stress (intensity of force) is proportional to the strain (deformation) initially and the structure returns to its original shape once the load has been removed. The slope of the stress-strain curve in this elastic region is called the Modulus of Elasticity or also known as Young's modulus. When the structure deflects, the geometry is not identical anymore, which means its stiffness is not the same anymore. This change could be noticeable if the deflection is large, but ignorable if small. In linear analysis, the deflection is assumed as a small amount so that the relationship between load and displacement is linear (Hooke's law), and the static equilibrium with the load by internal forces generated by the deflection is defined in the un-deformed shape.

4.4.2 Iterative Method

Once a global matrix of equations is formed, the unknown nodal displacements are obtained by pre-multiplying the known, externally applied force vector with the inverse of the stiffness matrix.

$$\delta = [K]^{-1} F \tag{4.17}$$

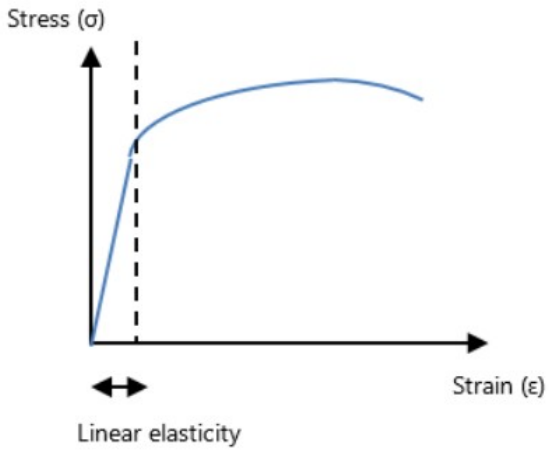

Figure 4.6: Typical Stress-Strain curve of a metallic material: focus on the linear elastic region. Credit:[65]

However, the equations cannot be solved directly, because the system model has components with non-linearity, such as bearings and gears. Therefore, it is a non-linear statically indeterminate system, which requires an iterative simultaneous solution of forces and contact deflections.

An iterative method is a mathematical procedure that starts with an initial approximation and generates sequence of improving approximate solutions. The solution iterations will follow

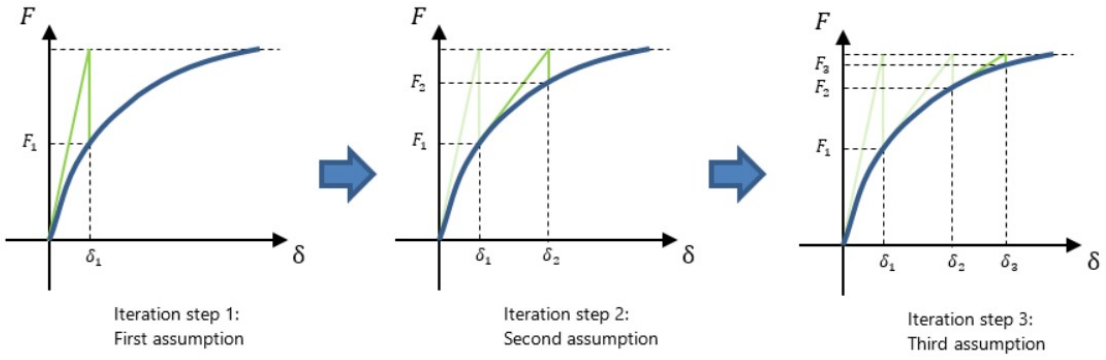

Figure 4.7: Iterative Method: In the first step, the stiffness of the components is assumed (typically designed to be way larger than the actual value), as can be seen from the figure on the left. Than, in a series of subsequent steps, the stiffness will drop and will reach a steady state value so that the system reaches an equilibrium state. Credit:[65]

Newton-Raphson type steps around the curve of load versus deflection until the systems boundary loads are satisfied and the internal component loads statically balance. The initial stiffness values are designed to be too large, which means that the initial system deflection solution will be quite small. At this small deflection, the component stiffness will suddenly drop and at the second iteration the system deflection may go quite large. The deflection will then typically drop back smoothly to the solution.

There is a smoothing between iterations of the calculated component stiffness. It controls the proportion of the old stiffness and new stiffness used for the next step by a factor, and this is called the relaxation factor.

$$k_i = rk_{i-1} + (1 - r)k_{pi} \tag{4.18}$$

Where:

- r is the relaxation factor
- k_i is the corrected stiffness term at iteration i
- k_{pi} is the predicted stiffness term at iteration i
- k_{i-1} is the corrected stiffness at iteration $i - 1$

The relaxation factor is increased when oscillation of stiffness is detected and reduced when a smooth trend is detected.

The iterative procedure is like a series of static analyses. The solution of the displacements allows a new estimate of the stiffness of the non-linear components to be made. This process is repeated until the displacement change from one iteration to the next is sufficiently small, i.e. within the convergence tolerance. However, the iteration terminates when the maximum number of iterations is exceeded. Both convergence tolerance and maximum number of iteration can be controlled in the analysis settings.

A rough flow of static analysis can be described schematically as below: If this is true for Masta and Romax, in AVL Excite it is only possible to perform dynamic analysis. It consists of a series of analyses performed in the time domain, adopting the same concept of the iterative solution, but considering also the mass and damping matrices. The solution of the simulations will not be scalar values anymore, but will be displayed as functions of time; in order to evaluate the losses the values at steady-state will be considered. The simulation time was chosen based on a trial and error procedure, and the focus was to keep it as low as possible in order to speed up the computation; however, considering the reaching of a steady-state condition. The solution at steady-state will anyway present some oscillations due to the dynamics of the system; an averaging operation was performed in order to get a scalar value useful for the computation of the efficiency.

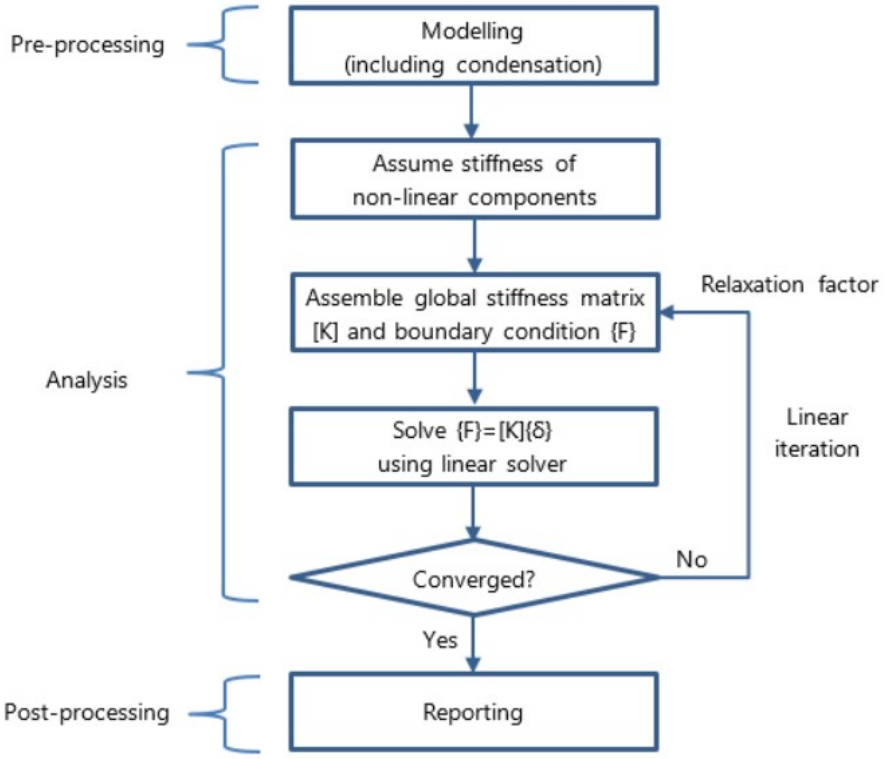

Figure 4.8: Typical Workflow of a static analysis: the pre-processing phase is comprehensive of the condensation in which the stiffness and mass properties of the components are derived, that in this work was performed in Optistruct, together with the modelling where the connection between the bodies are defined. In the Analysis phase, which is performed by Romax, Masta and Excite, the solution of the problem is found in an iterative way with the procedure described. Credit:[65]

Chapter 5

Auxiliary Reducer Unit

This chapter describes how the testing, modelling and simulation of a prototype reducer unit was performed. It will start with a description of the geometry of the unit, then the testing procedure will be explained and will end with the comparison of the results coming from the simulation with those coming from the experimental tests.

5.1 Model

The first unit analyzed is a dip lubricated single stage reducer unit. The layout is shown in

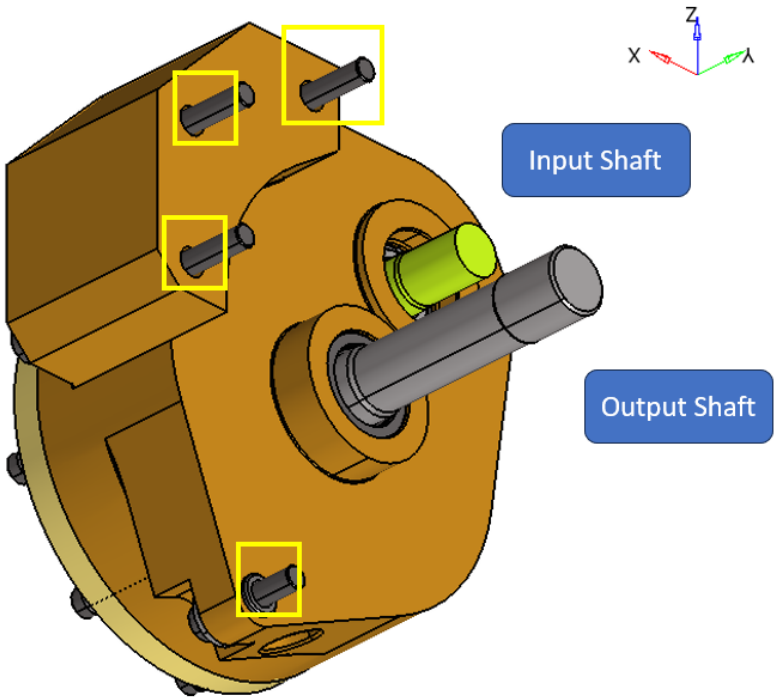

Figure 5.1: Model of the test reducer unit: note the four connection points to the test bench, highlighted with yellow squares, as well as the input shaft in yellow and the output shaft in grey.

Figure 5.1: it consists of an Input and an Output shaft, linked by a cylindrical gear pair with helical teeth.

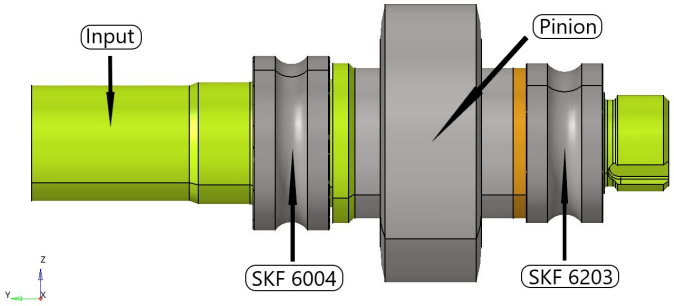

Figure 5.2: Input Shaft: note the two deep groove ball bearings' races, together with the pinion and the input to which the torque meter is applied.

The input shaft in yellow is made in a single piece, on which the 14-tooth pinion is mounted on by means of an interference fit. It is supported by two deep groove ball bearings (SKF Series 6004 and 6203, inner raceways in figure), and is linked to the test bench by means of a coupling in the input part, where the torque meter is installed, as seen in Figure 5.2.

A total of four condensation nodes are defined for this model: one for each bearing inner raceway, plus one for the pinion and one for the input boundary condition. All four nodes lie on the axis of the shaft, and their axial position is determined by the intersection with the mid-plane of each component. The output shaft is made of two components, see Figure 5.3: the first one is

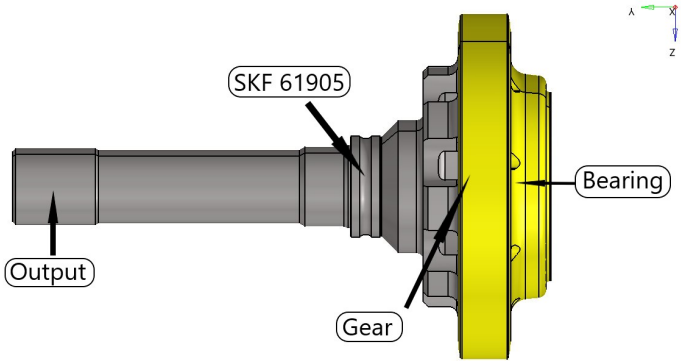

Figure 5.3: Output Shaft: on the right side is the deep groove ball bearing inner race together with the gear toothed wheel; its inner part serves as the shell of the journal bearing.

the shaft itself (grey), that is bolted to the 37-tooth wheel (yellow) by means of eight bolts. It is supported by a deep groove ball bearing (SKF 61905) and a journal bearing whose shell is fitted inside the cavity of the 37-tooth gear. Again, a total number of four nodes are defined for this component: one for the output link, one for the roller bearing, one for the gear and one for the journal bearing.

The housing is split into two main parts, see Figure 5.4, that are joined by means of ten ISO M6x1 bolts, supported by washers. The journal of the bearing is a bushing, connected to the housing by means of a M8x1.25 bolt. A total of eight condensation nodes were defined: one for each bearing outer raceway and one for the journal of the bearing. An additional four nodes were defined to simulate the links of the housing to the test bench.

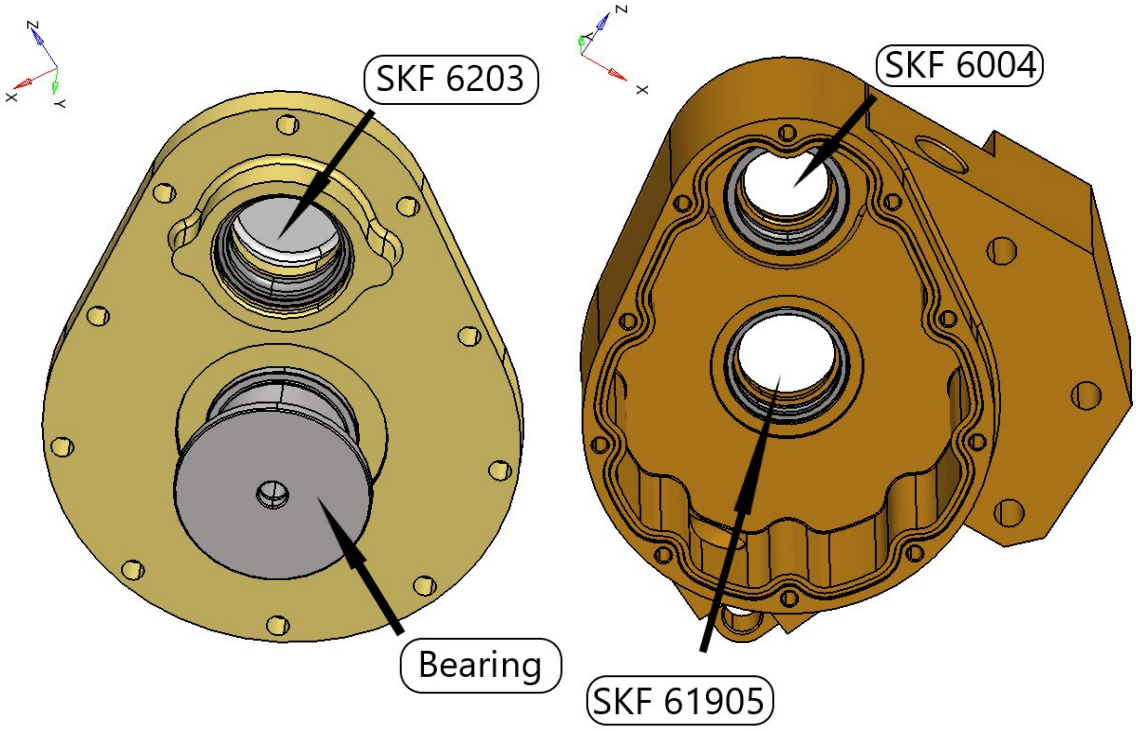

Figure 5.4: The reducer housing is split into two components that are joined together by means of bolts. The outer races of the three deep groove ball bearings are fitted to the housing, while the journal of the hydrodynamic bearing is joined by means of a bolt connection, as seen in the left part of the figure.

The housing material is aluminium, with an elastic modulus of $E = 70$ GPa, while the shafts are steel, with $E = 206$ GPa, and are linked to the test bed frame by means of four ISO M8x1.5 bolts, as shown in Figure 5.5. The macrogeometry data of the gear pair is provided in Table 5.1.

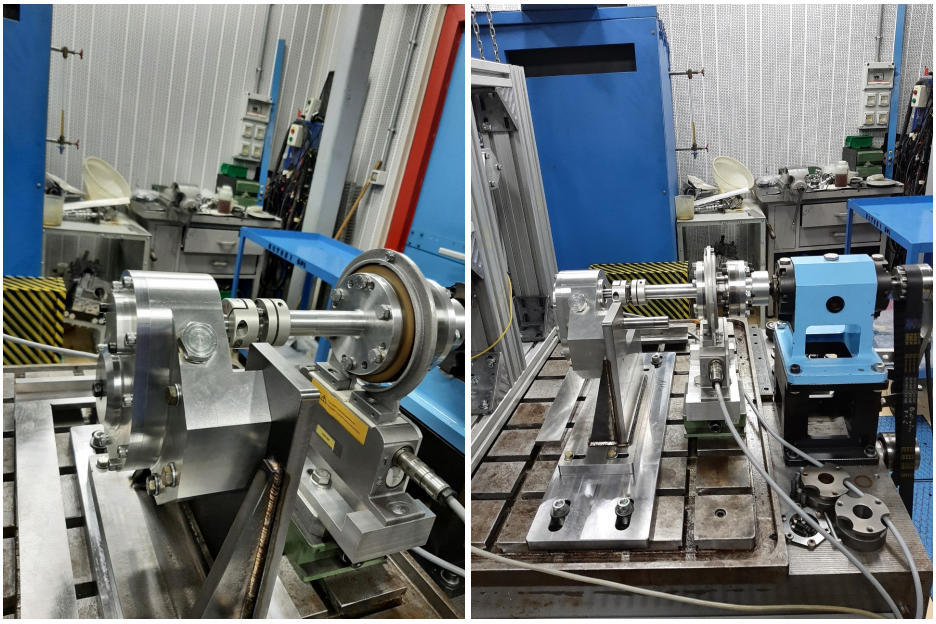

Figure 5.5: Testing Setup for the Auxiliary Reducer Unit

Table 5.1: Gear Macrogeometry Parameters for the Reducer Unit

Parameter	Symbol	Unit	Value
Ratio	τ	[-]	14/37
Normal Module	m_n	[mm]	2.65
Width	b	[mm]	14.3
Addendum	h_a	[mm]	2.65
Dedendum	h_f	[mm]	3.31
Helix Angle at pitch circle	β	[deg]	30
Normal Pressure Angle	α_n	[deg]	20

5.2 Testing

The testing of this unit was performed in order to evaluate the speed-dependent losses for two different oil levels, by keeping the temperature of the oil at the fixed value of 40°C. In order to achieve this, the test was conducted by driving the input shaft without a resistive torque applied on the output shaft. For each condition tested, the resistive torque needed to drive the unit is measured by the torque meter applied on the input shaft, while the oil temperature is monitored by means of a sensor and is actively controlled and kept at the value of 40°C. The oil properties were evaluated at 40°C, using the formulations described in Section 4.2. The oil viscosity of 24 cSt at 40°C was used to derive the density of 818.5 kg/m^3. The two calculated oil levels tested, 150 mL and 250 mL, are displayed In Figure 5.6, highlighted with a black line. It is possible to see also the inclination of the unit with respect to a horizontal plane while it was mounted on the test frame.

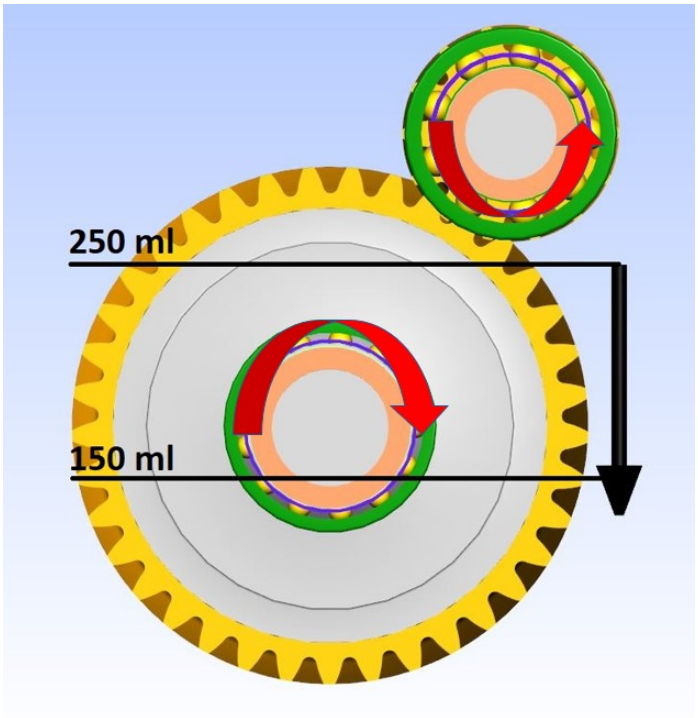

Figure 5.6: Visualization in simulation environment of the two oil level tested and the gravity vector, together with the rotation sense of the gears. Note that for both the oil levels only the gear is dipped into the oil.

5.3 Simulation

A first simulation was performed in order to understand the predicted magnitude of the various losses at high (11000 rpm) and low (500 rpm) input shaft speed. This was done in order to understand which parameters are more influential in a spin loss simulation. The system temperature was set to 40°C, since only the oil temperature is known. The results are shown in Figure 5.7. According to the loss model used, at high speeds the gear drag gives the highest loss contribution, while at low speed the oil seals are predominant. The bearing losses have a similar percentage contribution at high and low speed, while the gear mesh represents a very small percentage of the total loss.

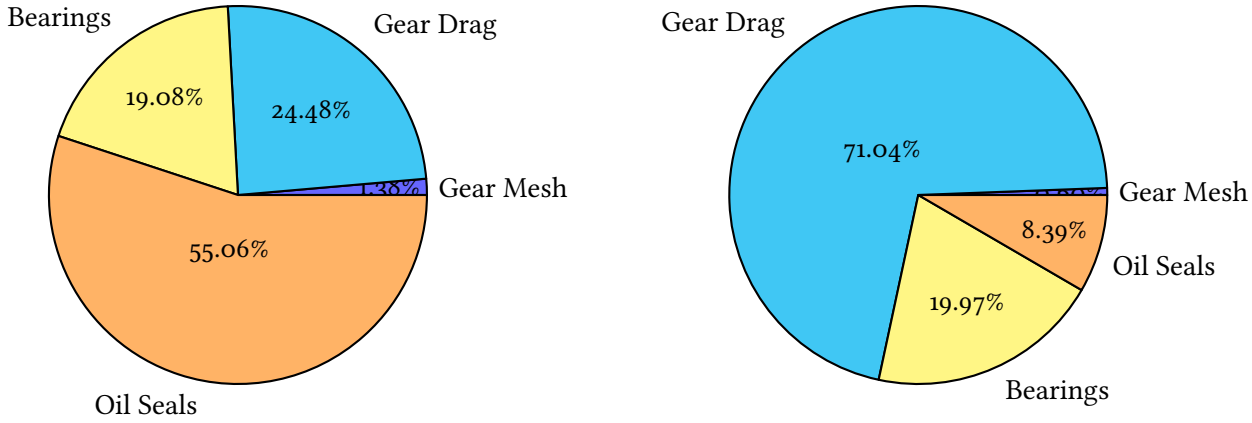

Figure 5.7: Predicted power loss contributions for the two oil level tested: the oil seals are the main contributors for the lower oil level, while the gear drag loss gives the main contribution for the higher oil level.

According to these preliminary results, a high sensitivity of the model is expected regarding torque loss prediction by changing the gear drag loss formulation. For sake of simplicity and to not complicate too much the dissertation, the influence of the gear mesh loss will be neglected in the spin tests, since it has a very low contribution relative to the other three.

By looking at the loss formulation, it is seen that the oil seals are modelled as constant torque loss objects, while for the gear drag various formulations that are functions of many parameters are used. It is expected that the latter give the 'shape' to the loss curve, while the former to give the constant part of the curve. After this first simulation, the goal was to compare the different gear and bearing churning loss models in the three simulation softwares. In the plots, the results are reported all considering the same scale for the axes for comparison purpose; however, the values were hidden in order to preserve the confidentiality of the test bench results.

For the simulation with Masta, it was used the only gear drag loss model available (ISO 14179/1), and different bearing loss model were tested. ISO 14179/1 and ISO 14179/2 gave equal results with all the other parameters unchanged, while the SKF model was giving lower torque loss values in all the speed range, as shown in Figure 5.9. In the simulations done with AVL Excite, it is possible to

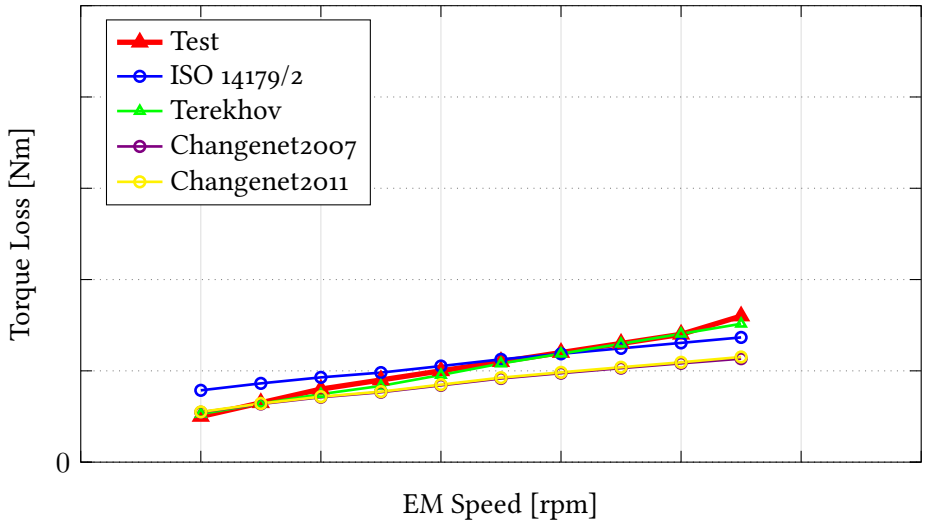

(A) 150 mL oil level

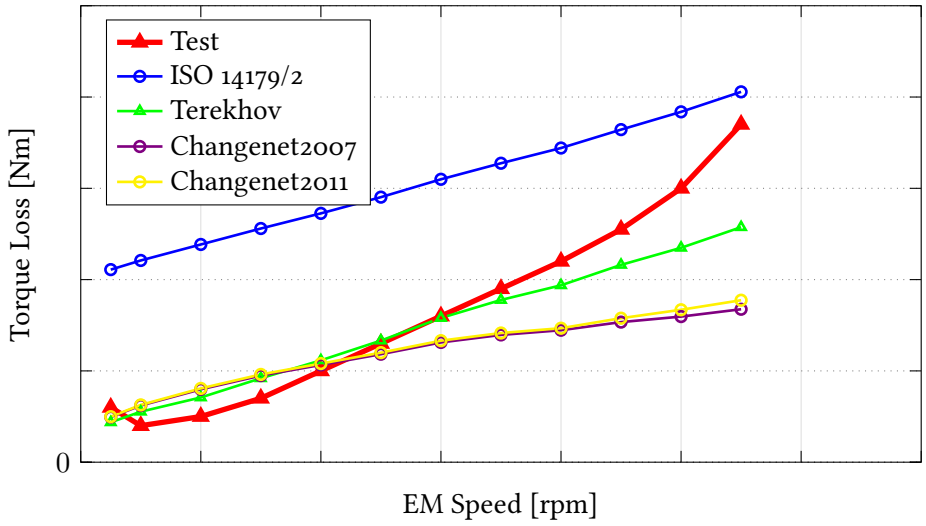

(B) 250 mL oil level

Figure 5.8: Sensitivity of the model to a change in gear drag loss formulation, with simulations performed using Romax. The ISO 14179/2 is very sensitive to a change in the oil level.

notice the great missing contribution of the gear drag torque. The only resistive torque is the one coming from the bearings; however, that is very small compared to the gear churning according to the SKF model.

In Romax the approach was to adopt the ISO 14179 formulation for bearing losses, since was providing better results as seen in Figure 5.9. All the gear drag formulations implemented were tested. As a general result, it can be seen that the ISO 14179/2 formulation is strongly influenced by the oil level (dip factors) present inside the reducer at low rotational speeds, while in the experimental tests this difference is not seen (the torque loss at 2000 rpm is similar in both cases,

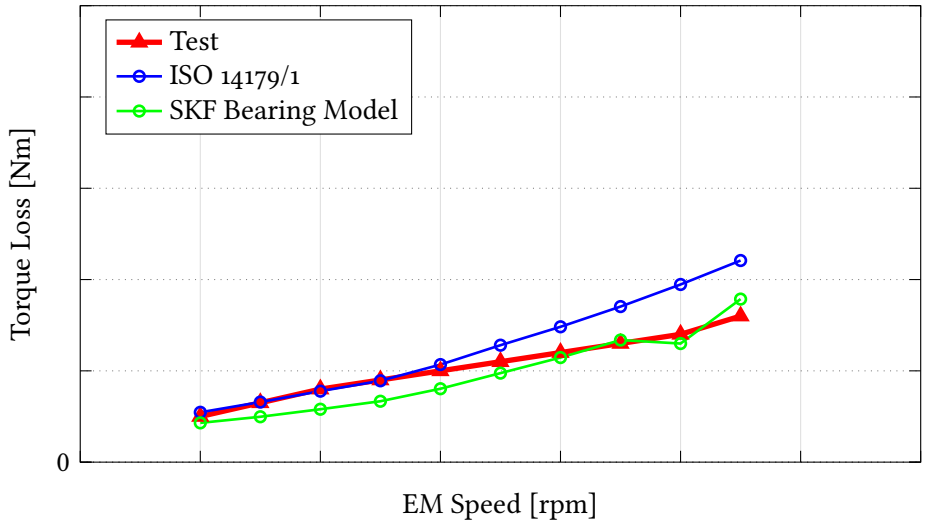

(A) 150 mL oil volume

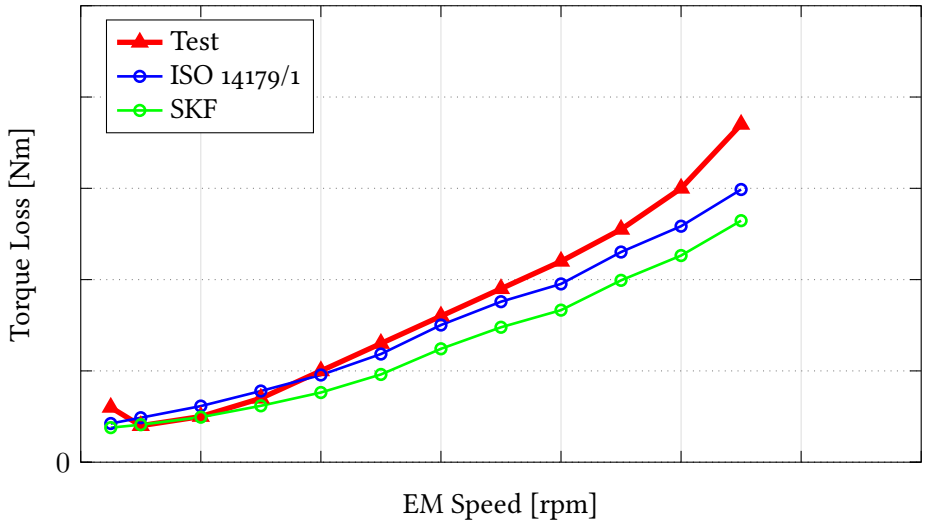

(B) 250 mL oil volume

FIGURE 5.9: Sensitivity of the model to a change in bearing loss formulation. The simulations were performed with MASTA, with ISO 14179/1 gear drag and ISO 14179/2 seal loss formulations. The simulation points replicate better the real behaviour in the low speed range, while they are overestimating the losses for the low oil level and underestimating them for the high oil level. The SKF bearing loss model predicts lower losses at high speed, indicating a lower bearing churning and windage loss prediction with respect to the ISO 14179 model

as shown in the figures looking at the test curve). The Terekhov model is the one giving a better approximation of the experimental curve, while the Changenet models are underestimating the losses in both cases.

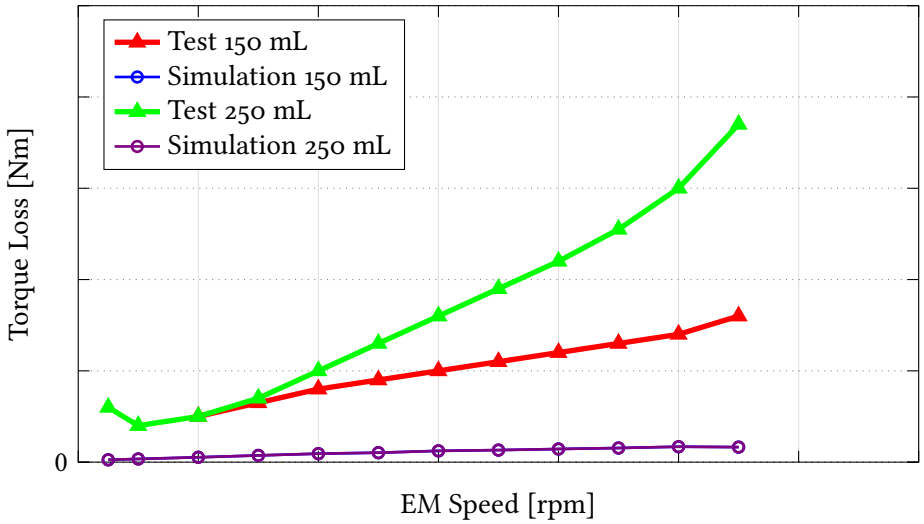

Figure 5.10: Dynamic simulation performed with AVL Excite : note the missing contribution of the gear churning and oil seal torque loss. The plot is useful to explain the relevance of considering this losses in simulation environment

5.4 Discussion

From this first set of simulation performed, it is possible to make some considerations on the results obtained, regarding the modelling and simulation of a spin test, that focus on the evaluation of the speed-dependent losses.

- The use of a 1-D or a 3-D approach has a negligible influence in the evaluation of the torque loss in a spin test. This was expected, since the forces, and so the deformations, on the components are very low, and the consideration of the housing stiffness is an additional complexity that is not required in this case.
- The SKF model for bearing losses is predicting consistently lower losses with respect to the ISO 14179 loss models. It has to be remembered that the SKF model was validated only for a certain minimum value and combination of forces acting on a bearing. In a spin test, the conditions are greatly under these thresholds, and the model is not validated here.
- The gear wheel churning losses are predicted to be the major source of loss in a test under no load, especially at high speed. At low speed, the oil seal losses are the predominant part of the losses. The gear meshing losses are predicted to be a negligible source of loss in this kind of test.
- The evaluated losses in a spin test are strongly dependent on the gear drag loss model chosen. In the simulations done, the ISO 14179/1 and Terekhov drag models were the ones performing better. The ISO 14179/2 was performing very badly especially for high dip factors: it has to be remembered that this formulation does not take into account the viscosity of the lubrication oil.

- With reference to Figures 5.9 and 5.8, it can be stated that the ISO 14179/1 gear drag loss model is the only one among the the tested that is able to fit the experimental curve for the high oil level of 250 mL, where the gear wheel has a high immersion depth, while in the low oil level of 150 mL it is overestimating the losses, with the Terekhov model being the best one.

Chapter 6

Fiat 500 EDM

This chapter describes the second unit tested, the EDM of the Fiat 500 BEV. It will start with a general description of the object, i.e., gear parameters, bearings and materials. Then it will enter into detail regarding the tailored modelling solutions adopted to represents the real behaviour of the system and all the simplifications made, and it will conclude with the description of the results of the simulations done.

6.1 Unit Description

The second unit tested is a complete EDM (Electric Drive Module), comprehensive of an Electric Machine (EM) and a Reducer Unit. The structure of the unit can be seen in Figure 6.1: on the left side of the housing, the EM can be recognized, having a nearly cylindrical shape, on the left of which there is the cover that serves as housing for the power electronics; its connector can be seen in the top left part while the double stage reducer unit is located on the right. The two sides are connected together by means of bolts, that in the figure are highlighted with blue colour. The material of the housing is aluminium. The unit is linked to the test stand at six points, as can be seen in Figure 6.1, highlighted with yellow squares; two of them belong to the reducer unit housing, while four belong to the EM housing. Those are the points that will be fully constrained while performing the housing stiffness matrix condensation.

The scheme of the internal structure of the unit is seen in Figure 6.2: the rotor shaft is supported by two deep groove ball bearings (1 and 2), that are fitted on the input shaft. On the left there is the pinion of the first reduction stage. The intermediate shaft holds the gear of the first reduction stage and the pinion of the second stage. On its extremities are located two tapered roller bearings (3 and 4).

The differential of this unit is needed in order to split the torque depending on the rotational speed of the two half-shafts. The cage is supported by two tapered roller bearings (5 and 6), an on it is mounted the gear of the second reduction stage. The internal structure consists of two planet gears fitted on the pin shaft of the differential, with the sun gears connected to the two semi-axes. The specifications of the bearings are reported in Table 6.1.

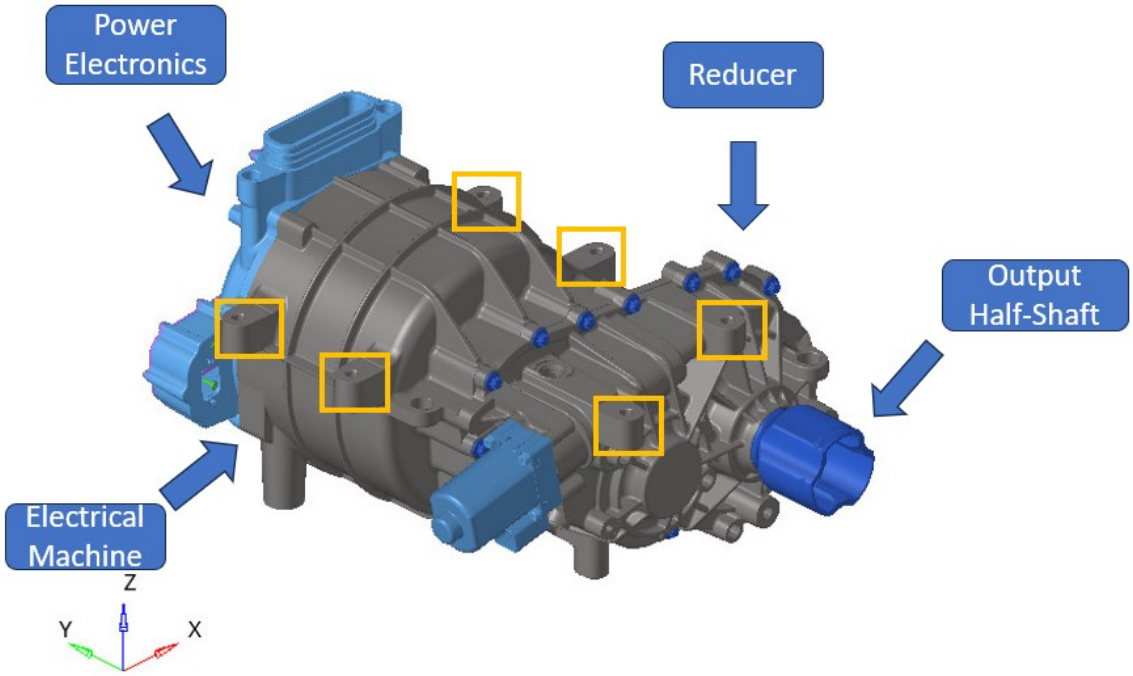

Figure 6.1: Overview of the EDM : the housing of the reducer unit containing the oil is located on the right, while on the left is located the housing of the electrical machine together with the connection for the power cables (in blue). In this view it is also possible to see the half-shaft connected to the test bench. In yellow are highlighted the holes for the connection with the frame, which have to be constrained in simulation environment.

A total number of three oil seals are present in the system: two of them are fitted on the semi-axes, while the third one on the input shafts, sealing the reducer from the EM housing just on the right of bearing number 1.

The EM is a 3-phase IPM syncronous machine: the rotor is fitted to the input shaft by mean of two keys placed on opposite sides, while the stator is fitted on its housing, which is bolt connected to the EM housing. The machine is water-cooled between the housing of the EM and the stator housing. The gear macrogeometry parameters are reported in Table 6.2. Both gear pairs are helical.

Table 6.1: EDM Bearings

N	Bearing	Type	Code
1	EM Front	Ball Bearing	6211
2	EM Rear	Ball Bearing	61909 2RZ
3 and 4	Interim Shaft	Tapered Roller Bearing	K1988/K1922
5 and 6	Differential	Tapered Roller Bearing	32009 X

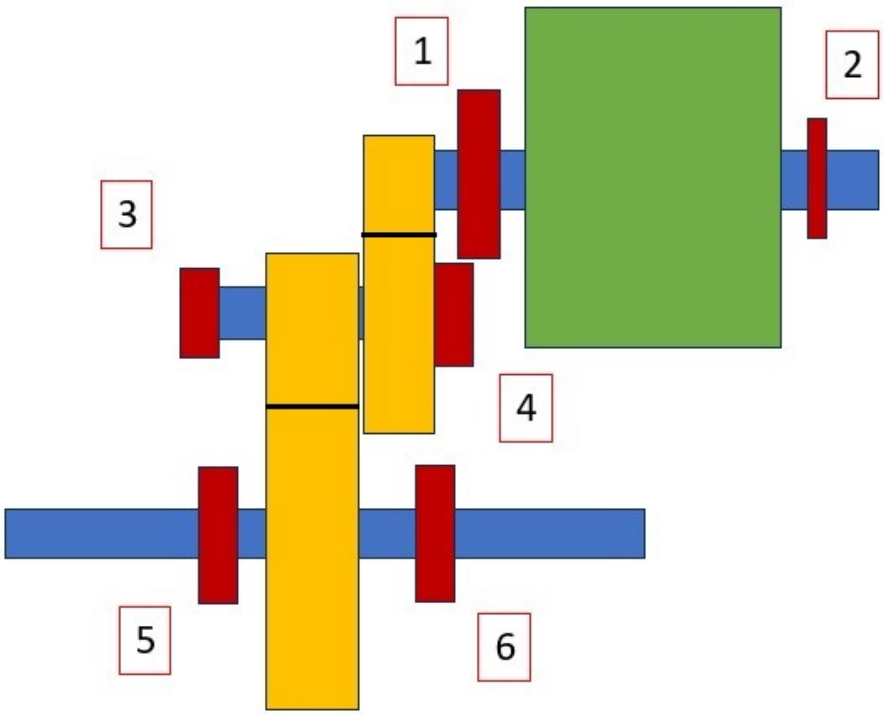

Figure 6.2: Schematic representation of a cross-section of the Electric Drive Module : the shafts are depicted in blue, with the rotor of the EM in green. The bearings, in red, are numbered according to Table 6.1.

Table 6.2: EDM Gear Macrogeometry

Parameter	Symbol	Unit	Stage 1		Stage 2	
Normal Module	m_n	[mm]	1.555		2.347	
Normal Pressure Angle	α_n	[deg]	19		20	
Nominal Operating Center Distance	a	[mm]	87		118	
Normal Backlash	j_n	[mm]	0.107		0.119	
Helix Angle at pitch circle	β	[deg]	20		25	
			Pinion	Gear	Pinion	Gear
Number of teeth	z	[-]	29	77	20	72
Tip Diameter	d_a	[mm]	52.65	128.75	59.35	188.45
Root Diameter	d_f	[m]	43.189	120.338	44.977	175.393

6.2 Testing

According to the ISO 14179/2 and the EHL Theory gear mesh loss formulations, the friction coefficient in the gear meshing is also a function of the roughness of the gear teeth. In order to accomplish a deeper analysis of the loss models, it was necessary to measure the roughness of the gear teeth. A measurement was performed on the two toothed wheels of the intermediate shaft, which are the gear of the first reduction stage and the pinion of the second reduction stage, as shown in Figure 6.3.

The roughness was measured in a section perpendicular to the axis of the two wheels along a line; the measure of one tooth flank was considered. In order to simplify the measurement procedure, the approach was to impose in the simulation the same roughness values for the two pinions and the two gears. The results of the roughness test are shown in Table 6.3 and Figure 6.4.

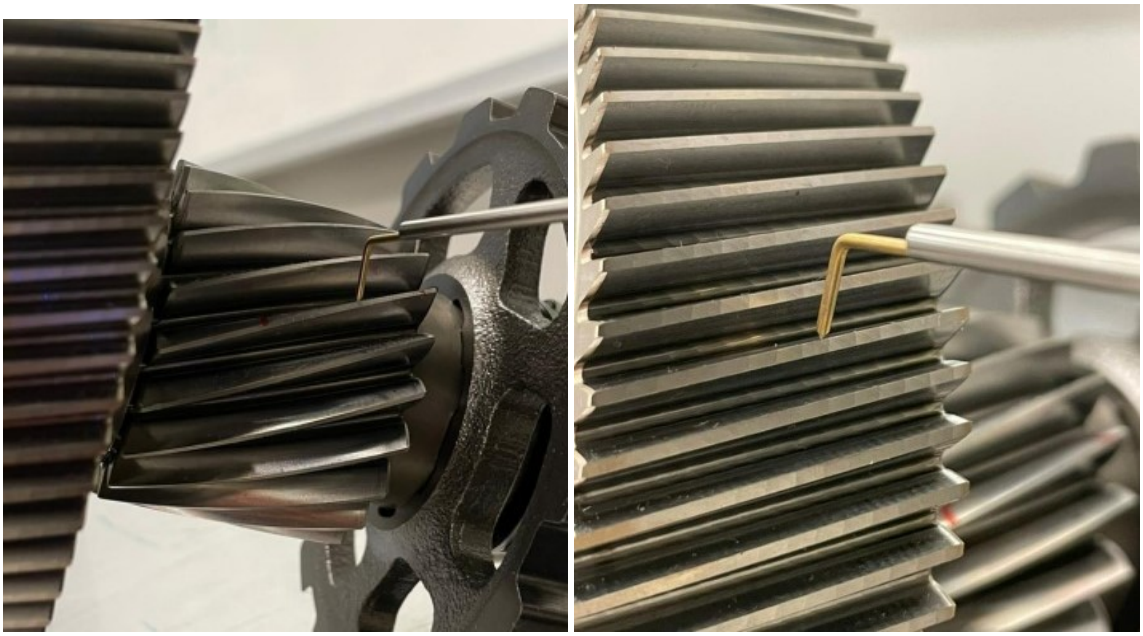

Figure 6.3: Roughness Test Methodology: The roughness was measured with a Zeiss Surfcom 1500 SD instrument, at an ambient temperature of 21°C, according to the ISO'97/'09 standard. The measuring speed was 0.3 mm/s, with a normal movement with respect to the axis of the gear in the positions shown.

The reducer unit was tested in order to evaluate the efficiency in a wide set of working conditions. The schematic setup of the test rig is shown in Figure 6.5. The EDM is connected on the EM side to the Inverter Module, which converts the DC current coming from the Battery Emulator into the AC current needed from the motor. The output half-shaft is connected to the torque-meter by means of an additional reduction stage.

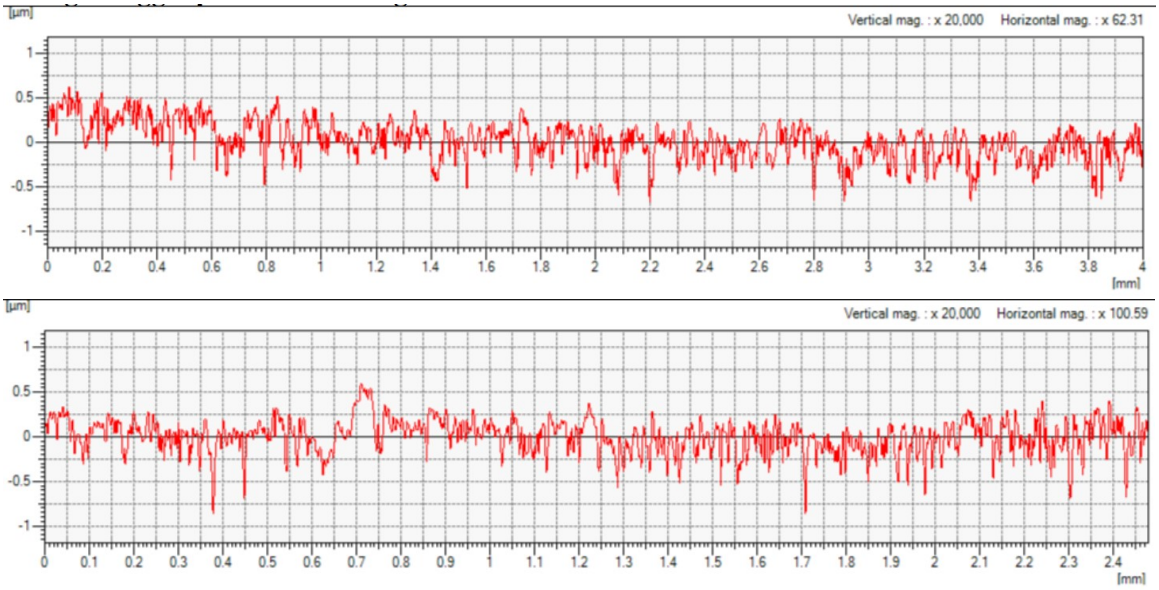

Figure 6.4: Roughness Test Results : the test was performed on the intermediate shaft of the reducer unit. In the top figure is displayed the measured profile of the pinion of the second stage, while in the bottom figure is displayed the result of the gear of the first stage.

The torque meter on the output shaft is mounted between the EDM and the reduction stage, while the one for the EM torque is mounted on the input shaft. Both of them are HBM T12, and the given accuracy is in the range of ±0.01%. The oil sump and cooling water temperature are measured by means of two thermocouples K, with an accuracy of ±0.1°C.

In all the tests performed, the differential is kept locked, meaning that the speed of the left and right half-shafts are always equal, regardless of the torque applied on them. In this condition, the overall reduction ratio becomes:

$$\tau = \left(\frac{77}{29}\right)\left(\frac{72}{20}\right) = 9.553 \tag{6.1}$$

A first test was performed in order to evaluate the speed dependent losses, so consisted in varying the speed of the input shaft without applying a resistive torque on the output, and measuring the torque needed to drive the system, for two oil temperatures of 40°C and 80°C, to study also the

Table 6.3: Roughness Values: the pinions and the gears of the two reduction stages have the same roughness values in simulation.

	Pinions	Gears
Ra(μm)	0.173	0.148
Rz(μm)	1.018	1.232
Rt(μm)	1.311	1.462

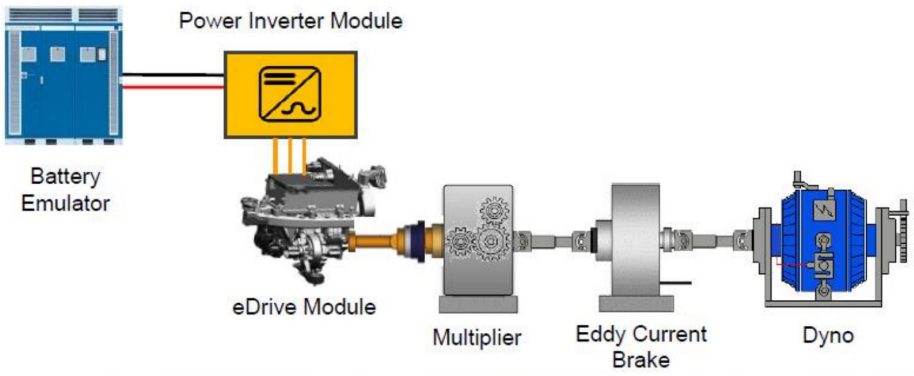

Figure 6.5: EDM Test Bench Schematic Representation: the torque meter is represented with the violet item between the eDrive Module and the Torque Multiplier

effect of the oil temperature on this kind of losses. These temperatures were chosen because they are representative of the working conditions during the actual functioning of the unit. A low temperature was used to understand the losses during the first part of driving when the oil sump temperature is still low, followed by a high temperature that is close to the one at steady state during driving. The result of this test is a torque loss curve as a function of the speed of the EM.

The second test performed is a test under load. The differential is still kept locked, while a resistive torque is imposed at the output half-shaft by means of the Eddy Current Brake, with the speed of the system being controlled by the EM. The results of this test are efficiency curves as function of the speed of the EM.

The oil level, whose properties are displayed in Figure 6.6, was checked by a pipe mounted on the housing, as shown in Figure 6.7. It was measured to be approximately 11 mm under the differential shaft axis in a vertical way.

Figure 6.8 shows how the unit was oriented on the test bench, an important parameter to be set in each of the simulation codes, in order to evaluate the dip factors in all the bearings and the gear wheels, that is provided as input in the loss models analytical formulations. The unit was

Table 6.4: Test Matrix for the EDM

		EM Speed [rpm]										
		500	1000	1500	2000	3000	4000	5000	6000	8000	10000	12000
EM Torque [Nm]	150	X	X	X	X	X						
	80	X	X	X	X	X	X	X				
	40	X	X	X	X	X	X	X	X	X	X	X
	20	X	X	X	X	X	X	X	X	X	X	X
	10	X	X	X	X	X	X	X	X	X	X	X
	5	X	X	X	X	X	X	X	X	X	X	X
	-5	X	X	X	X	X	X	X	X	X	X	X
	-10	X	X	X	X	X	X	X	X	X	X	X
	-20	X	X	X	X	X	X	X	X	X	X	X
	-50	X	X	X	X	X	X					
	-100	X	X	X	X	X						

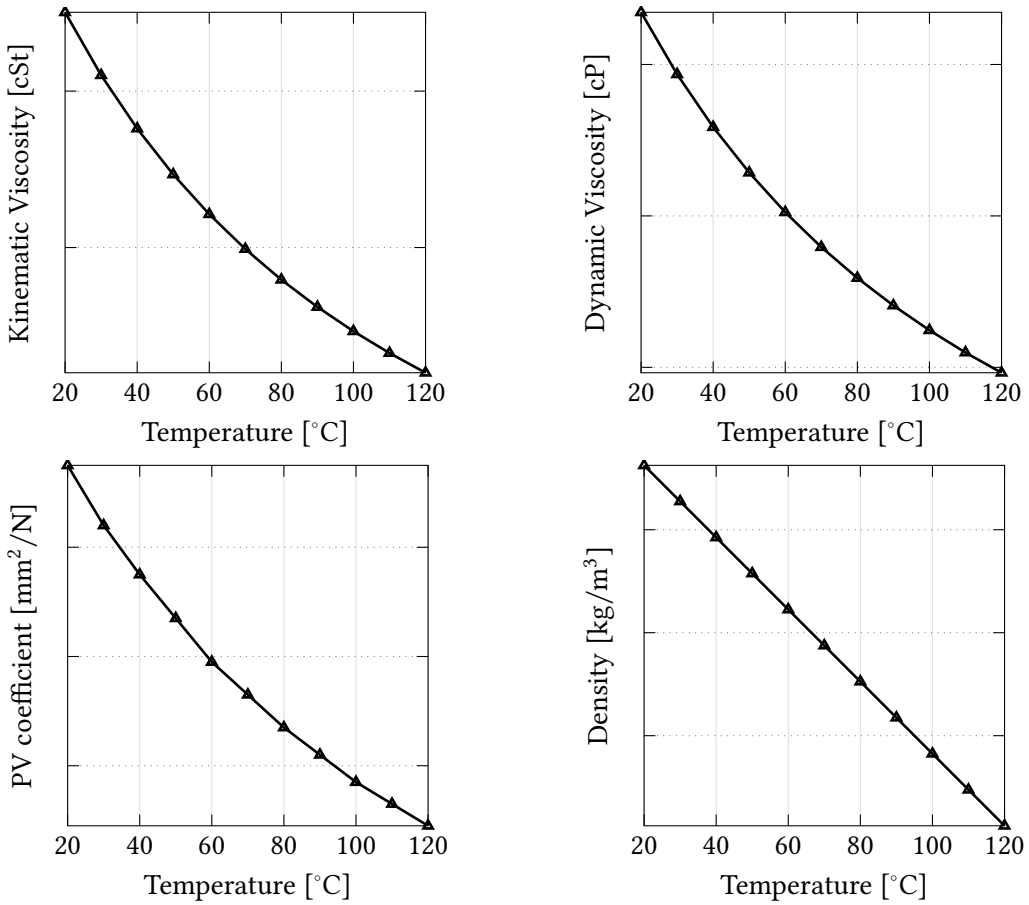

Figure 6.6: Relevant oil properties for the Petronas TDS217006. The kinematic viscosity at 40°C and 80°C and the density at 15°C are provided by the manufacturer, while all the other parameters are derived.

tested for a wide range of working conditions, as can be seen in Table 6.4. The maximum tested power in driving mode delivered by the EM was 50.26kW reached for a driving torque of 40 N m at 12000 rpm, while the maximum in regenerative mode was -31.41 kW, reached at -100 N m at 3000 rpm. It is useful to report the Pitch Line Velocity (PLV) of the two mating gear pairs, as a function of the speed of the EM. This because most of the standards were validated for a precise range of these values.

Figure 6.7: EDM oil level measure : It is performed by means of a pipe connected to the housing, that allow the visualization of the oil level and permits the measure of it.

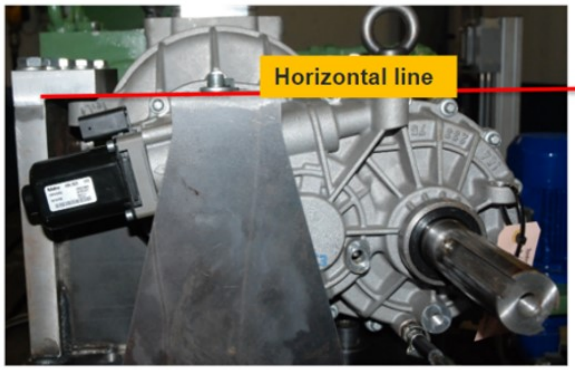

Figure 6.8: Inclination of the EDM while mounted on the test rig : an important parameter to be known to evaluate the level of immersion of each gear in the oil.

It is necessary to focus on the limitations of the gear mesh loss models present. The ISO 14179/1 model was validated for PLV ranging from 2–25 m/s, where the ISO 14179/2 has an higher limit of 50 m/s. The Anderson model was firstly adopted for spur gears, and in Romax is present a correction to adapt it to helical gearsets, but apparently has not been validated yet. In Table 6.5 is reported the trend of the Pitch Line Velocity of the two gear pairs as a function of the speed of the EM. The minimum is reached for the second reduction stage at the lowest speed, with a value of PLV=0.463 m/s, while the maximum is reached by the first gear stage at the highest speed of 12000 rpm, with a value of PLV=28.333 m/s.

Table 6.5: Evaluated Pitch Line Velocity (PLV) for the two gear stages (1 is the first and 2 is the second) for rotational speed of the EM ranging from 500–12000 rpm. It is useful to compare these values with the validation ranges in the standards.

Speed [rpm]	PLV1	PLV2
500	1.181	0.463
1000	2.361	0.926
1500	3.542	1.388
2000	4.722	1.851
3000	7.083	2.777
4000	9.444	3.702
5000	11.805	4.628
6000	14.167	5.554
8000	18.889	7.405
10000	23.611	9.256
12000	28.333	11.107

Unlike the PLV, which is a well-defined parameter knowing the macrogeometry of the gear pairs, the contact force has a strong dependence of the gear flank microgeometry and the force exchanged in the meshing, the latter being also a function of the loss model adopted. As an approximation, however, it is possible to evaluate the loading parameters considering an ideal situation, such that with no losses in the components.

It is possible to evaluate the load intensity for the two gear pairs following the ISO 14179 standard. In Table 6.6, the calculated values for the two meshing gears are reported for the motoring test conditions. It is possible to see that for low loads (5,10,20 N m), the load intensity K is lower than the recommended limit of 1.4 N/mm^2 for which the ISO 14179/1 model was validated. This is true also for the lower limiting values of tooth normal force over tooth face width highlighted in the ISO 14179/2 formulation: a lower accuracy of the ISO models is expected in this zone.

Table 6.6: Evaluated load intensity values according to ISO 14179 formulation, for values from 5–150 N m of input torque. It is useful to compare these values with the one of the validation ranges present in the standards.

Torque	K1	K2	F1	F2
5	0.195	0.374	14.385	32.241
10	0.390	0.747	28.770	64.483
20	0.780	1.495	57.540	128.967
40	1.561	2.990	115.081	257.933
80	3.121	5.980	230.162	515.866
150	5.853	11.212	431.553	967.249

Regarding the gear drag loss models, obviously the most logical zone to have a comparison is in the spin tests, as was done for the reducer unit. Here the main difference is that there are two gear pairs in one housing, both having helical gear teeth. It is, however, useful to evaluate the dip factors for all the components present in the system. A schematic visualization of the oil level distribution inside the reducer unit is reported in Figure 6.9, and the corresponding dip factors in Table 6.7.

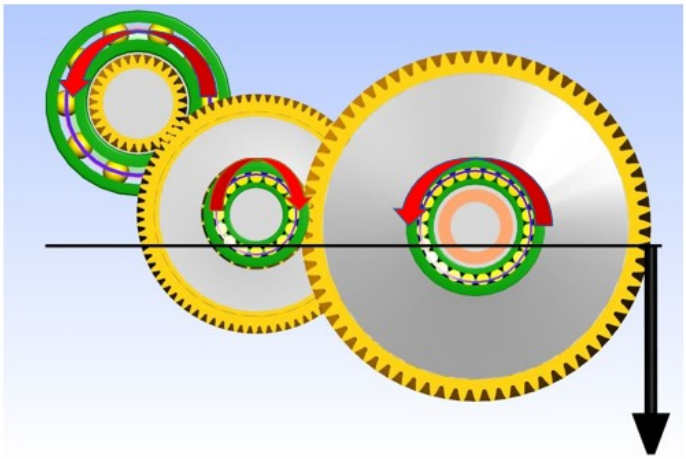

Figure 6.9: Visualization of the oil level in simulation environment, in front view, together with the rotation sense of the gears during forward driving: note the clockwise sense of the second reduction stage while the counter-clockwise sense of the first reduction stage, according to Changenet

Table 6.7: Evaluated Dip Factors for the Fiat 500 BEV EDM

Component	Bearing 5 and 6	Bearings 3 and 4	Gear 2	Pinion 2	Gear 1
Dip Factor	0.3445	0.1671	0.4416	0.2037	0.3634

6.3 Modelling

Regarding the modelling of the unit in simulation environment, it is possible to distinguish between two approaches:

- Static Model (Masta and Romax): it is necessary to know the stiffness of the components, in order to derive the deflections and so the forces acting on the system.
- Dynamic Model (AVL Excite) : it is necessary to know also the mass and damping properties of the components, since now the simulation is performed in time domain.

Despite the many differences that are present between the two models, it is possible to identify a common point, that is how the boundary conditions were applied to the model: the methodology consisted in replicating the way in which the two experimental tests, spin losses and efficiency curves, were performed. With reference to Figure 6.10:

- For the spin loss test, a speed is imposed to the output half-shaft, with a null torque imposed to the EM rotor shaft. By applying the loss formulations in each component, the required torque to have equilibrium at the output will represent the torque loss in the system due to speed-dependent losses.
- For the efficiency tests under load, a speed is imposed as well, but this time a torque is imposed at the EM rotor shaft, and the required torque to have equilibrium at the output is derived. The efficiency will then be calculated considering the input to output power ratio.

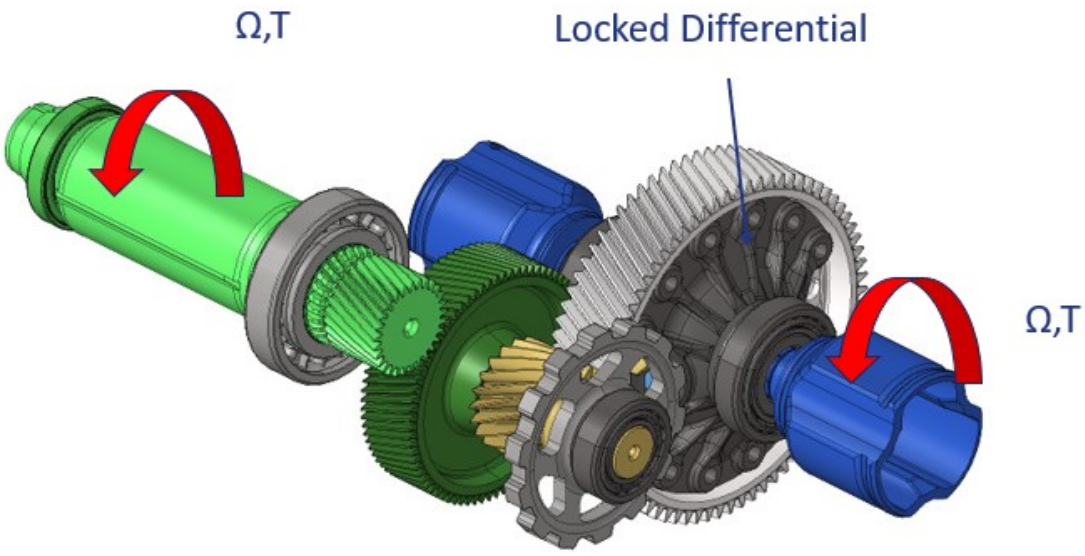

Figure 6.10: Boundary Conditions: the rotational speed of the system has to be specified, as well as the torque acting on one end. The system will then be solved taking into account the losses in the components by either a static or a dynamic simulation.

In any case, the differential is considered as a single flexible body, since it was kept locked during the testing. The stiffness of the bearing joints is a common point as well, and is derived according to the methods in Chapter 4.1.3., according to Harris theory.

In the following will be described the main differences between the static model of Masta and Romax and the dynamic Model of AVL Excite.

6.3.1 Masta and Romax Static Model

In the static models built with Masta and Romax, the stiffness of the shafts, as well as the one of the gear bodies, is derived according to the Timoshenko beam theory, while the gear mesh stiffness is calculated according to the ISO 6336 standard. In Figure 6.11 is possible to see the two models in simulation environment.

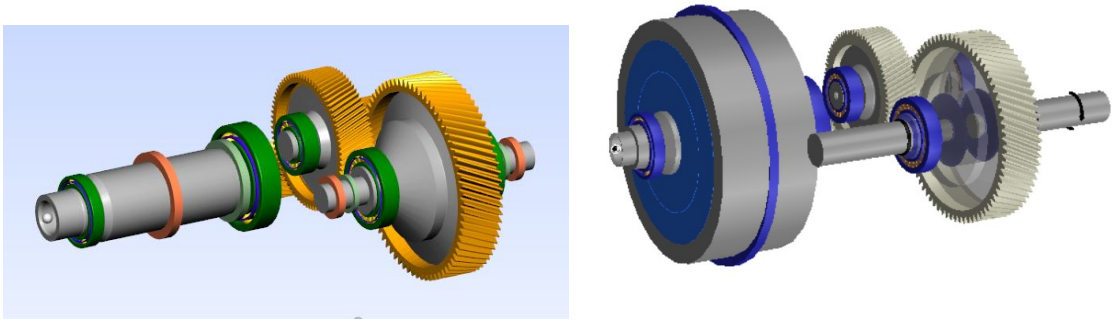

Figure 6.11: Masta and Romax models, as they appear in the simulation environment

6.3.2 Excite Dynamic Model

Unit Modelling

In the Excite Dynamic Model, the gear contact was simulated by means of the Advanced Cylindrical Gear Joint (ACYG): it is able to provide an appropriate level of detail in the model, especially when the contact of flank surfaces plays a major role, as it is the case in the coefficient of friction evaluation using EHL theory.

In this joint, the flank contact stiffness is evaluated according to Hertz-Petersen theory, while the tooth bending stiffness according to Weber/Babascheck theory. Regarding the damping in the two contacts, it is evaluated according to Peeken empirical methodology. This empirical method is base on the theory of elasto-hydrodynamic lubrication of rigid running surfaces. It is evaluated according to:

$$d = 13.7 \frac{\eta_0 R_{eqv}^{1.5}}{x_n^{1.5}} b_w \tag{6.2}$$

where η_0 is the fluid dynamic viscosity, R is the equivalent radius at curvature at pitch circles $R = \frac{1}{\frac{1}{R_1}+\frac{1}{R_2}}$, x_n is the current position in backlash (approach distance along the pressure line), b_w is the common face width of pinion/gear. The evaluated values are reported in Figure 6.12 for the two gear pairs.

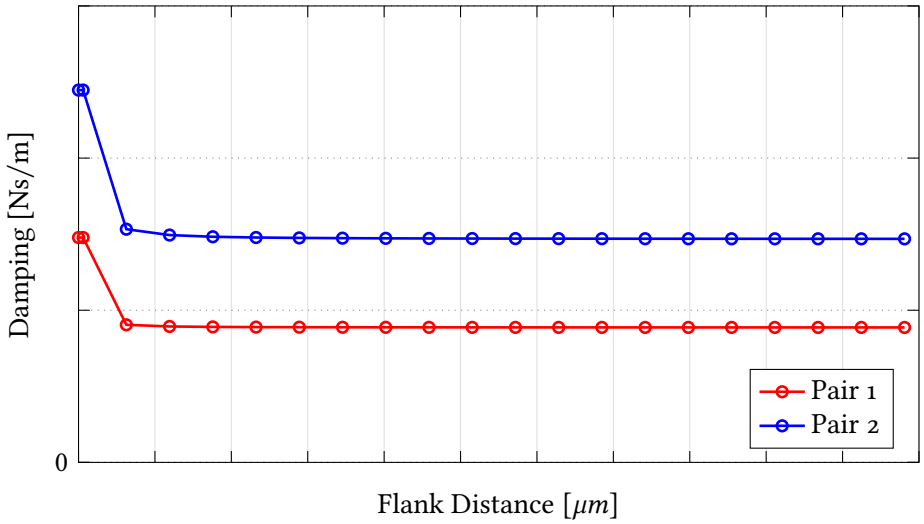

Figure 6.12: Evaluated damping values as a function of the gear flank distance in normal direction, to be used as input for the ACYG joint in the AVL Excite Dynamic simulation.

In order to impose a constant rotation to the differential shaft, it is necessary to connect a rigid body to the differential by means of a rotational joint: this is because, due to dynamics, every shaft will not have a perfectly constant rotational speed but will display an oscillatory behaviour. This

was also used to simulate the torque meter present at the output shaft, and was modelled with high enough torsional stiffness and low damping in order to simulate a rigid connection.

Bodies in AVL Excite can be defined as rigid or flexible depending on the consideration of their stiffness: the elastic components like shafts and housing must be defined as flexible; however, there are some components like the test rig platform that due to the very high mass and stiffness can be defined as rigid bodies. The stiffness and mass properties of the shafts and housing was derived using the previously mentioned Craig-Bampton matrix reduction method, in order to get stiffness and mass matrices.

Efficiency Evaluation

In order to get usable results from a dynamic simulation, an averaging operation was performed on the relevant characteristics in order to extract usable parameters. The obvious choice was to average the torque seen by the rotational joint at the output, and by knowing the torque provided by the electric motor and the transmission ratio it was possible to derive the efficiency of the system.

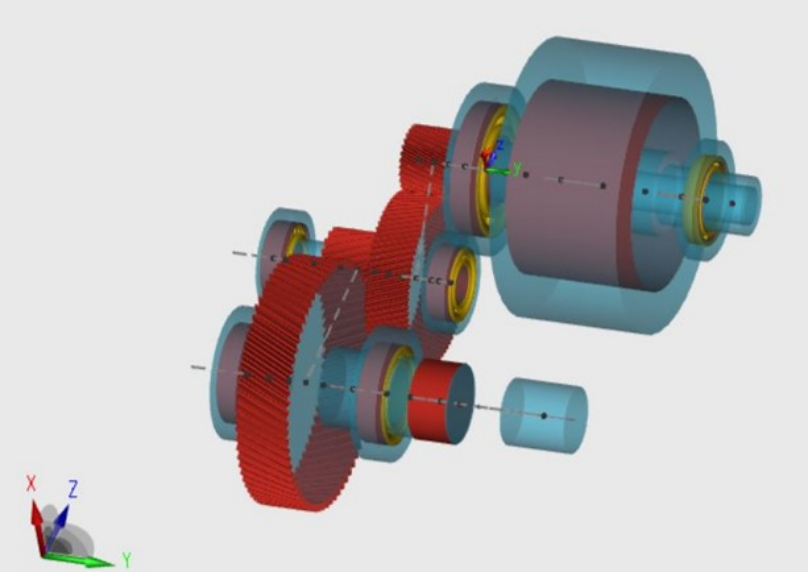

Figure 6.13: Schematic representation of the AVL Excite Dynamic model: Note the condensation nodes present for each shaft, representing the stiffness and mass properties in those points. The nodes representing the bearing races are superimposed in the model, and are connected by means of bearing joints. The nodes of the gears (three for each toothed wheel) are connected by means of two ACYG joints. The differential body is connected to the cylinder, that imposes a constant rotation to the system, by means of a ROTX joint. The electrical machine is simulated by applying its torque signal to five pairs of nodes, describing the stator and rotor stiffness and mass properties, taking into account the skewing of the machine by an angular shift of the simulated torque signal along the nodes.

Some time was spent in order to understand the length of simulation time needed to stabilize the system and to reach steady-state. An example of dynamic simulation output is provided in Figure 6.14. The torque ripple coming from the dynamic behaviour of the driveline is clearly visible, but also due to the harmonic excitation from the electric motor.

For this application, the simulation time was chosen to be 2 seconds, and the results were averaged in the last 0.2 seconds of simulation. It was chosen based on the experience coming from many simulations done.

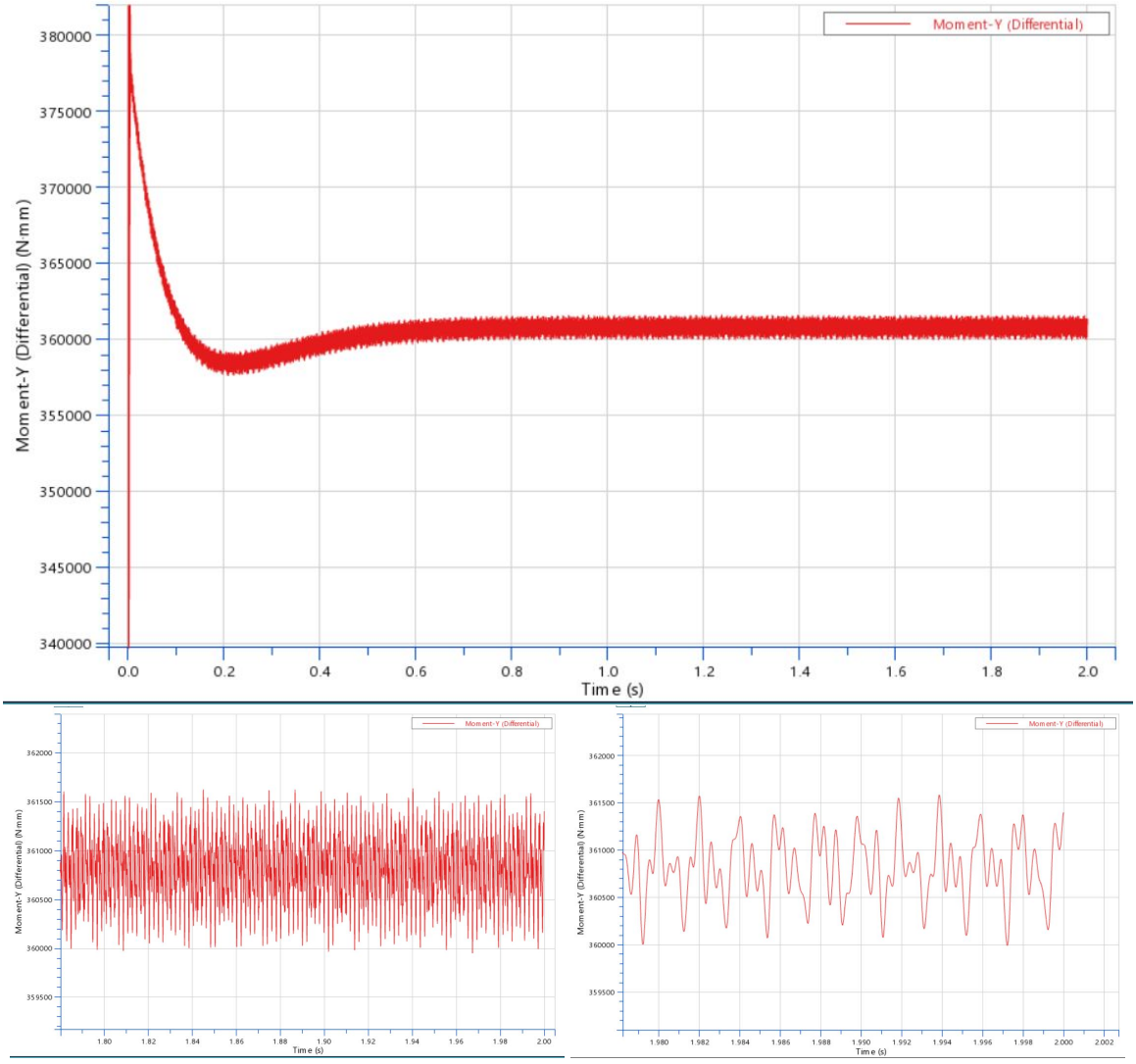

Figure 6.14: Dynamic Simulation Example: Motoring test at 40°C oil sump temperature, 40 N m EM torque and 4000 rpm EM speed. In figures, evaluated torque at the output measured with the rotational joint. In top figure, note the transient behaviour starting from the first integration step, that turns in an oscillatory steady state condition afterwards. In bottom figures, detail of the torque signal with two different levels of magnification are shown.

6.4 Results

In this section, the results coming from the simulation will be compared with the one coming from experiments.

6.4.1 Spin Losses

The first simulations performed were the test without load applied at the output half-shaft, in order to assess the accuracy of the speed-dependent loss models. As was seen in Figure 6.19, at low loads the oil seal losses are predicted to be the main loss contributors, while at high speed the gear drag becomes the main source of loss considering just the reducer unit. A first set of simulations was performed with Romax, Figure 6.15 and 6.16, to asses the accuracy of the gear drag loss models. In Figure 6.15, the gear drag model was varied by keeping constant the bearing loss model. The ISO 14179/2 model is overestimating the losses with respect to the test simulation, in particular with an upper shift of the constant part of the curve. The Terekhov model seems to be the one providing the better results, while the Changenet models seem to provide inconsistent results with respect to the unit tested. In the reducer they were both underestimating the losses, while in the EDM they are both overestimating; however, the 2011 model is providing better results with respect to the 2007 model, which shows a big increase of resistive torque at high speed.

In a further comparison, the sensitivity of the bearing loss model chosen was studied by fixing the gear drag loss model, reported in Figure 6.15. The ISO and Palmgren models are providing very similar results, with the 14179/1 norm providing the lower loss values in the high speed range. The SKF model is consistently underestimating the losses and confirms the trend seen in the reducer unit. In the simulations done with Masta, the ISO 14179/1 gear drag loss model is tested, the only one present in the software. As can be seen in Figure 6.17, this model is able to approximate quite well the losses in the test at high temperature (80°C), while in the low temperature test, the model is underestimating the losses at low speed while it is greatly overestimating at high speed; more over, the concavity of the curve is opposite with respect to the one from the experimental test. The same conclusions are derived for the ISO and SKF bearing loss models in a spin test. In AVL Excite, the spin loss contribution is not present. It is only possible to study the influence of the SKF model to the oil temperature (viscosity): a higher temperature gives lower losses as is expected due to the lower churning losses in the bearings for lower oil viscosity, as seen in Figure 6.18. Before performing the motoring tests, the model was calibrated regarding the gear drag loss model, by choosing the one that was approximating in a better way the experimental curve. In Excite and Masta there is not a choice possibility regarding the gear drag loss model, while in Romax the Terekhov loss model was chosen due to its better capability to approximate the loss curve.

By looking at the results of the spin tests, it is expected to have an overestimation of the efficiency in Excite in all the torque range, and especially at low loads where the speed-dependent losses are predominant.

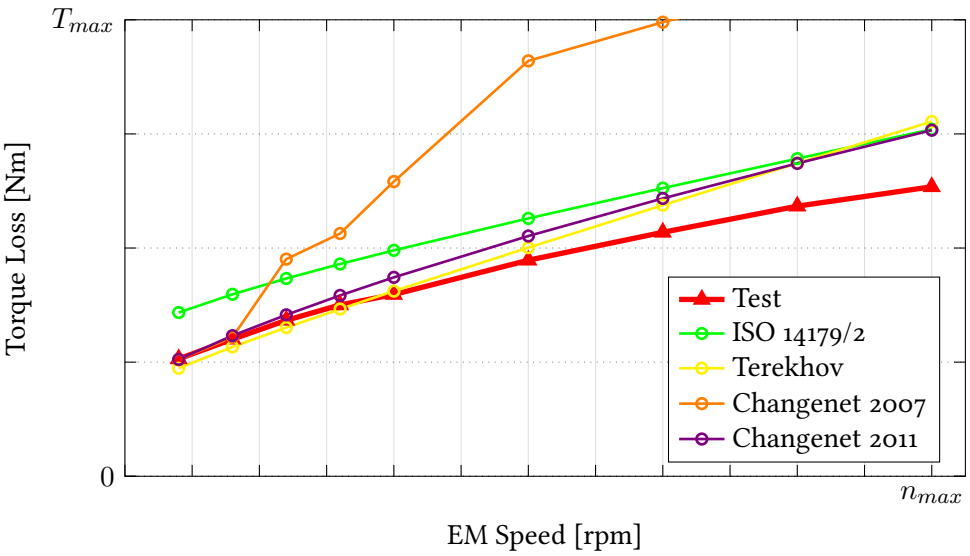

(A) 40°C

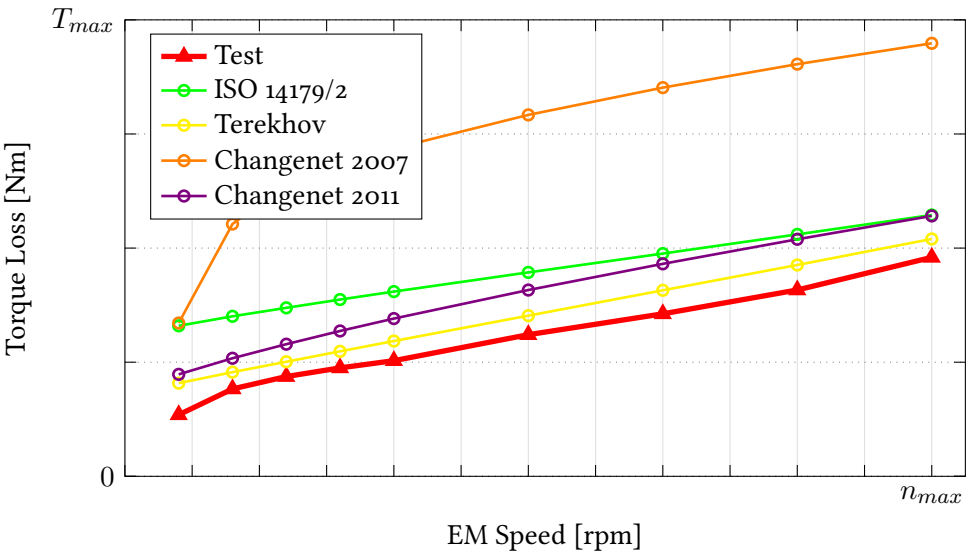

(B) 80°C

Figure 6.15: Sensitivity of the model to a change in gear drag loss model, the greatest speed dependent loss according to the simulations. ISO 14179/2 bearing, gear mesh and seals loss model. The model by Terekhov is approximating better the experimental curve, while the Changenet 2007 model greatly overestimate the losses. Simulation performed with Romax

In Masta, a worse correlation with the experimental efficiency is expected at 40°C rather than at 80°C, where the ISO 14179/1 gear drag loss model was approximating well the experimental curve. In particular, it is expected an underestimation of the efficiency at high speeds and a slight overestimation at low speeds, in the low torque range.

In Romax, by using the Terekhov model, a good correlation in the low torque range is expected.

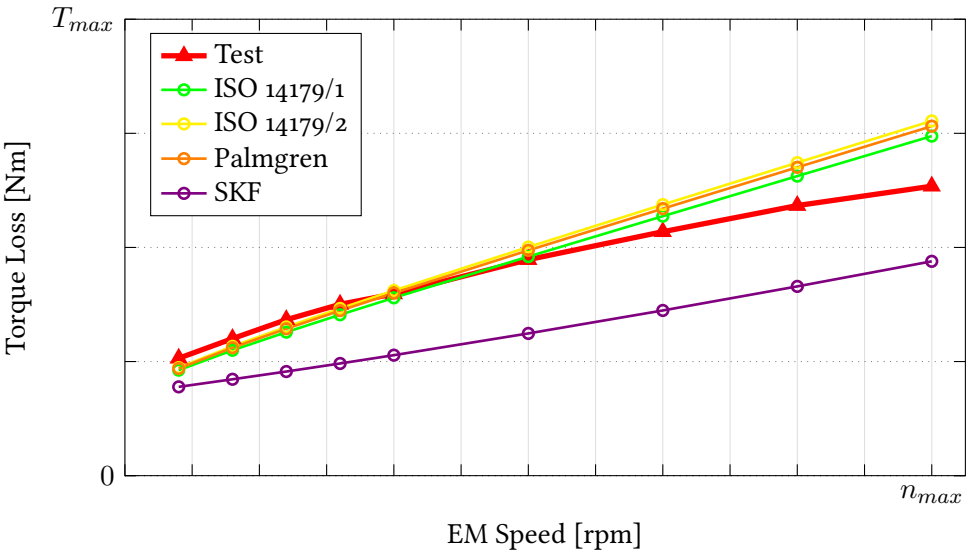

(A) 40°C

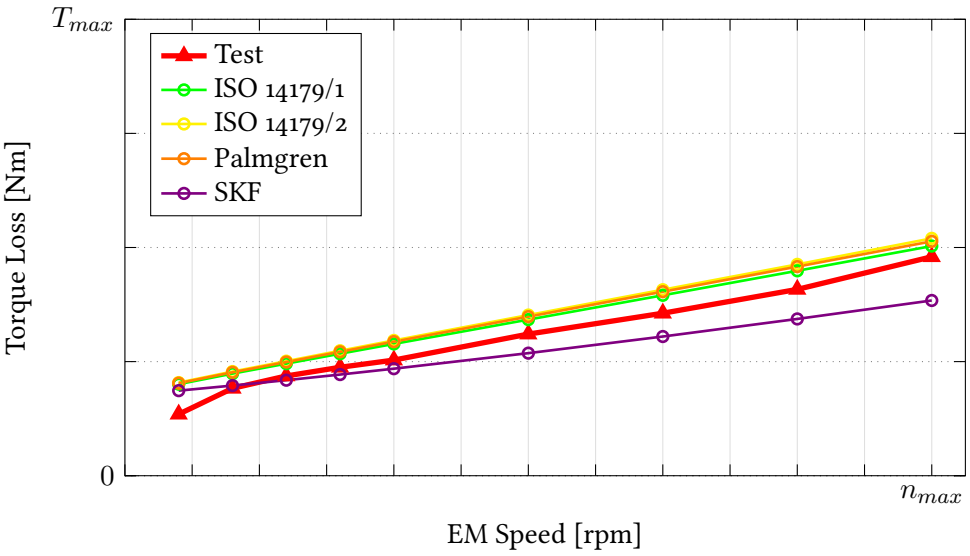

(B) 80°C

Figure 6.16: Predicted Torque Loss for different bearing loss models: Terekhov gear drag model and ISO 14179/2 gear mesh and seals loss model. In this plot it is possible to understand how the different models predict churning losses in the bearing. As seen in the standard, the ISO 14179/1 and ISO 14179/2 have different factors for bearing churning loss formulation, with the latter predicting slightly higher losses. The SKF model is predicting much lower speed dependent losses with respect to the other formulations. Simulation performed with Romax.

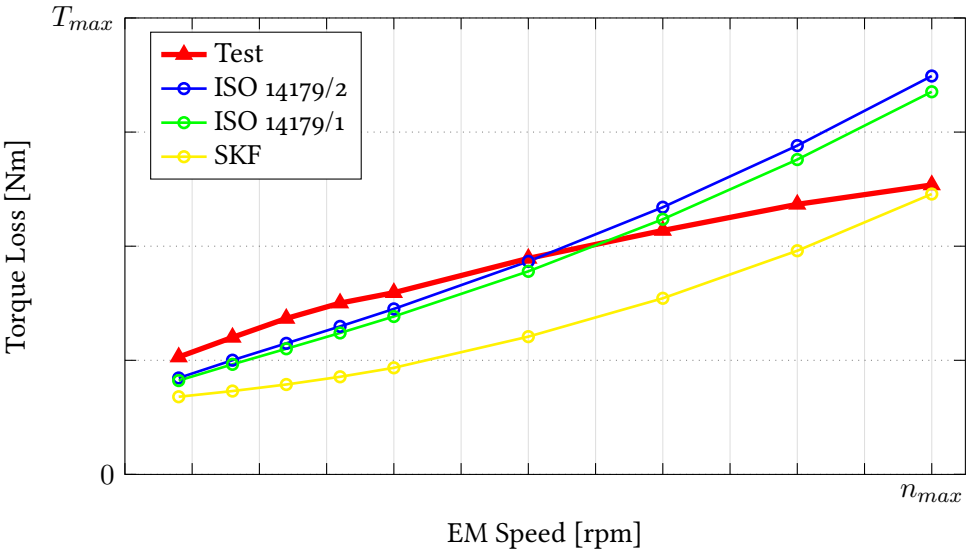

(A) 40°C

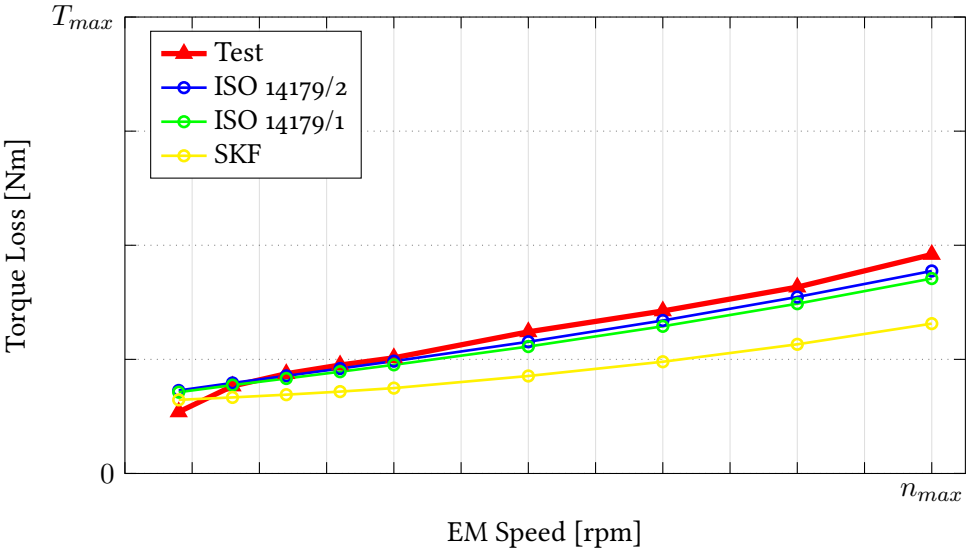

(B) 80°C

FIGURE 6.17: Sensitivity of the MASTA model to a change in Bearing loss formulation regarding speed-dependent losses. The gear drag model is the only one available, ISO 14179/1, with gear mesh and seal loss models being the ISO 14179/2.

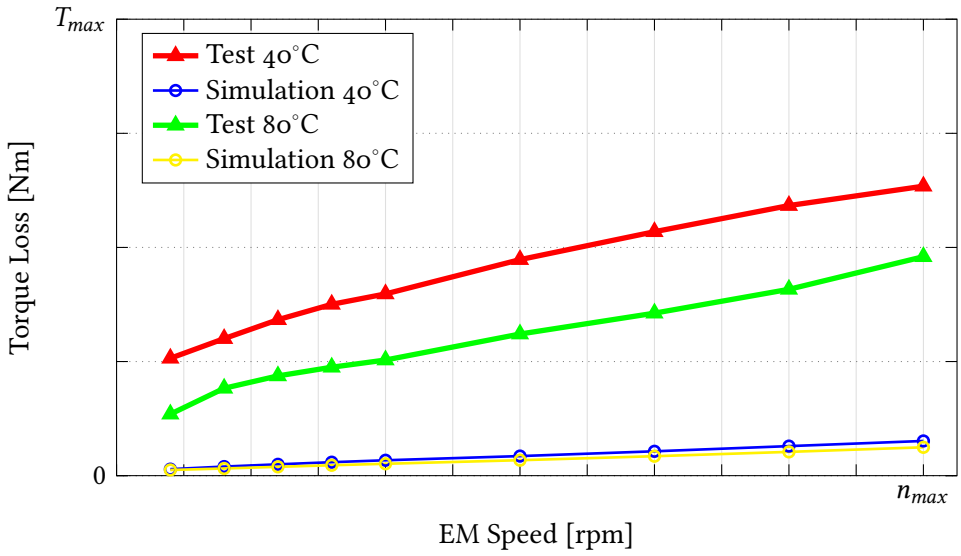

Figure 6.18: Speed-dependent loss simulation performed in AVL Excite: note the missing contribution of the gear drag and seal losses.

6.4.2 Load Test

The second kind of test performed are the tests under load. As was seen in Figure 6.19, at high loads the main source of predicted mechanical loss becomes the gear meshing, while at low loads, the oil seals at low speed and the gear drag at high speed are the main contributors. In the simulations performed with Masta, the influence of the gear mesh loss and bearing loss model was studied at high and low torques (5Nm and 150Nm) for both high and low temperatures (40°C and 80°C). The results of the simulations are shown in Figure6.20. It is possible to state that at low loads (5 N m), the oil seals and the gear drag still gives the highest contribution to the total power loss. The situation is different at the highest torque tested: at both high and low speeds, the gear mesh is the greatest contributor, followed by the bearing losses and the oil seals: the gear drag gives still a very low contribution to the torque loss at 3000 rpm. At low loads, the ISO 14179/1 gear mesh loss model is greatly overestimating the losses with respect to the ISO 14179/2. At high loads, the ISO 14179/2 model performs better regarding both the shape of the efficiency curve and the error. The SKF model was also compared with respect to the ISO 14179 bearing loss model under load. For the same gear mesh loss model, the SKF bearing loss model is predicting higher efficiency at light loads, confirming the trend seen in the spin losses. At high loads it is predicting higher losses, and is the one that better approximates the experimental trend. In Romax is it possible to consider loss models that account for the microgeometry of the gear teeth. In this case, the friction coefficient is derived according to the gear geometrical parameters and operating conditions, but the force acting along the contact line is not constant, resulting in a non-constant friction force along the contact patch. It is also possible to exploit a formulation in which the friction coefficient is not constant, but is evaluated according to the position along the contact line according to EHL theories (VFC (Variable Friction Coefficient)) in the plots.

The results of the simulations done with this methodology are shown in Figure 6.21. The ISO 14179/2 is approximating the losses at low loads in a better way with respect to the ISO 14179/1 model, confirming what was seen in the simulations done with Masta. The VFC model performs similar to the Anderson and ISO 14179/2 models at light loads, while overestimating the losses at high loads like the Anderson Model. In the simulations done with AVL Excite, Figure 6.22, in order to have comparable results, the bearing losses from the SKF model and the gear mesh loss by EHL theory were summed with the churning losses provided by the Terekhov model and the seal losses by the ISO 14179/2 model.

At light load of 5 N m, the simulation is still overestimating the efficiency. This result is in line with what was seen in bearing churning loss prediction with the SKF model, as was seen in the comparison done in MASTA for the bearing loss models, in Figure 6.20.

Comparing the high and low oil temperatures, the simulation is overestimating the losses at low temperature while it shows a good correlation at high temperature. The same result was obtained in Romax in Figure 6.21, with the ISO 14179/2 gear mesh loss model.

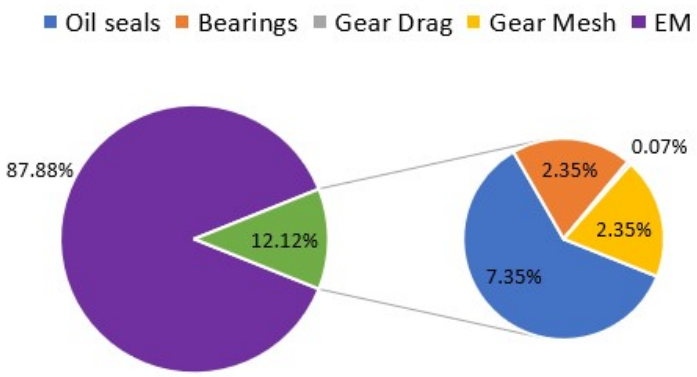

(A) 5 N m 12000 rpm

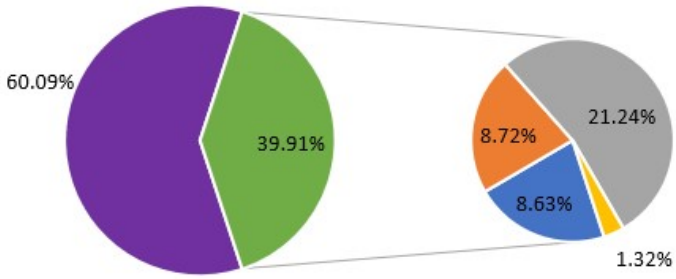

(B) 5 N m 500 rpm

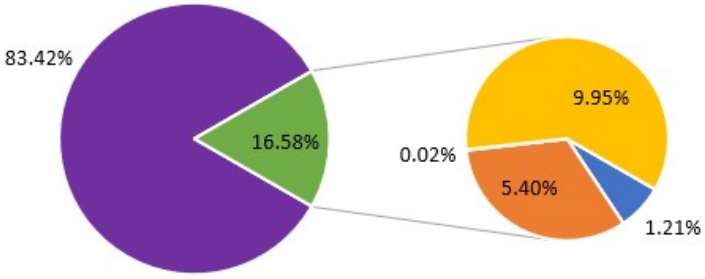

(C) 150 N m 3000 rpm

FIGURE 6.19: Total Power Loss predicted contributions at 80°C sump temperature for different speeds and loads: simulation performed with Romax (ISO 14179/2 formulation for gear mesh and seal losses, the Terekhov model for gear drag and the SKF model for bearing losses). In the top side of the figure, contributions at 5 N m EM torque at 500 rpm where the seal losses are predominant and 12000 rpm where the gear drag gives the highest power loss. In the bottom part, simulation performed at 150 N m EM torque where the gear mesh power loss gives the highest contribution. Also reported is the contribution of the EM losses for the considered operation point, as a percentage of the total loss. Note that for the considered points, the EM is the highest loss contributor considering the entire EDM.

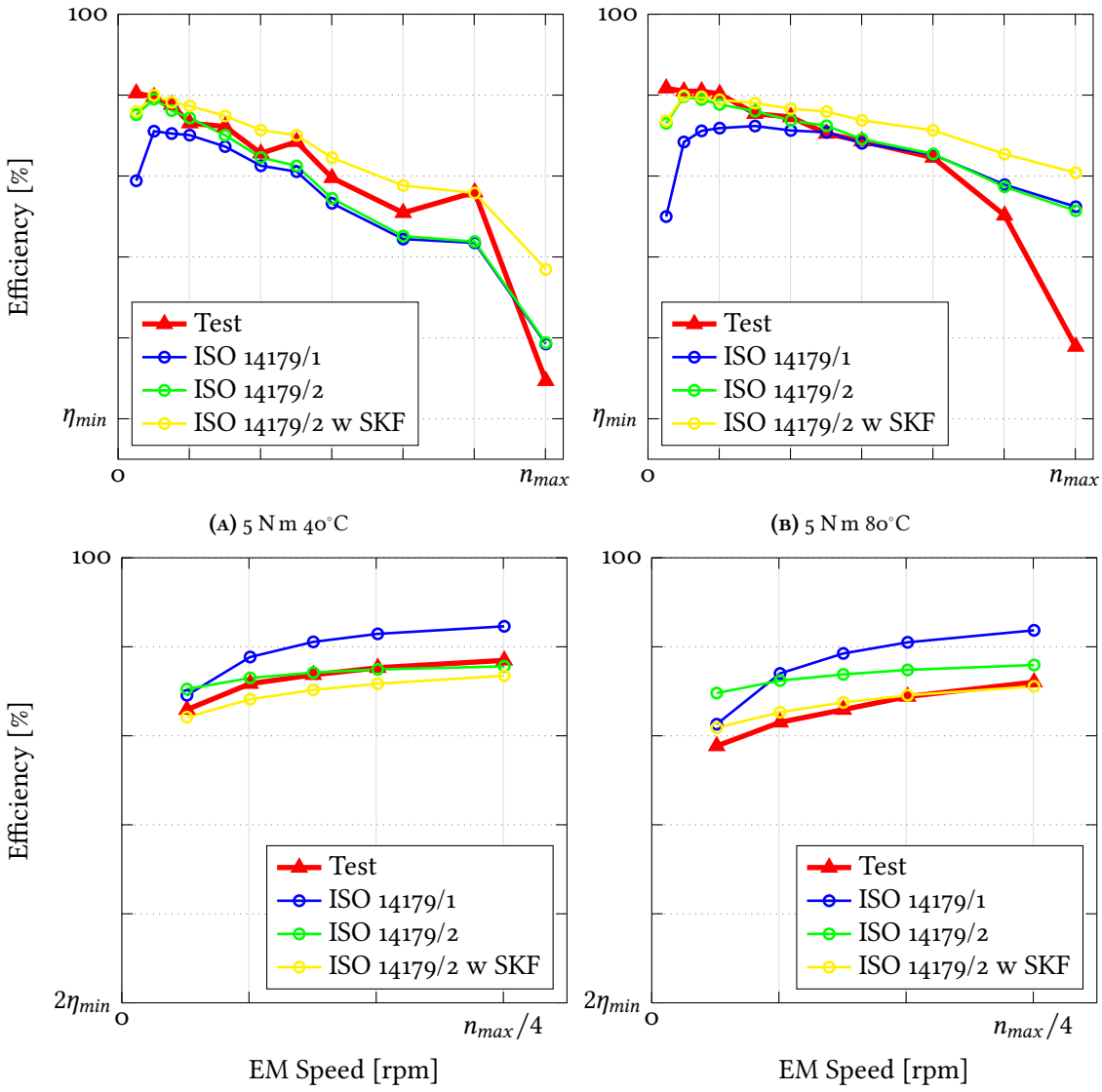

(A) 5 N m 40°C

(B) 5 N m 80°C

(C) 150 N m 40°C

(D) 150 N m 80°C

FIGURE 6.20: Sensitivity of the model to a change in gear mesh and bearing loss model, simulations performed with MASTA. Note that the ISO 14179/1 gear mesh loss model greatly underestimates the efficiency at low input torque and speeds. It has to be noted that this model does not take into account the roughness of the gear teeth. The ISO 14179/2 gear mesh loss model approximates in a better way the shape of the experimental curve. The SKF model predicts higher losses at high torques while lower losses at low torques, with the main difference being at high rotational speeds due to a lower churning loss prediction, as was seen in the spin tests. The seal loss model is the ISO 14179/2.

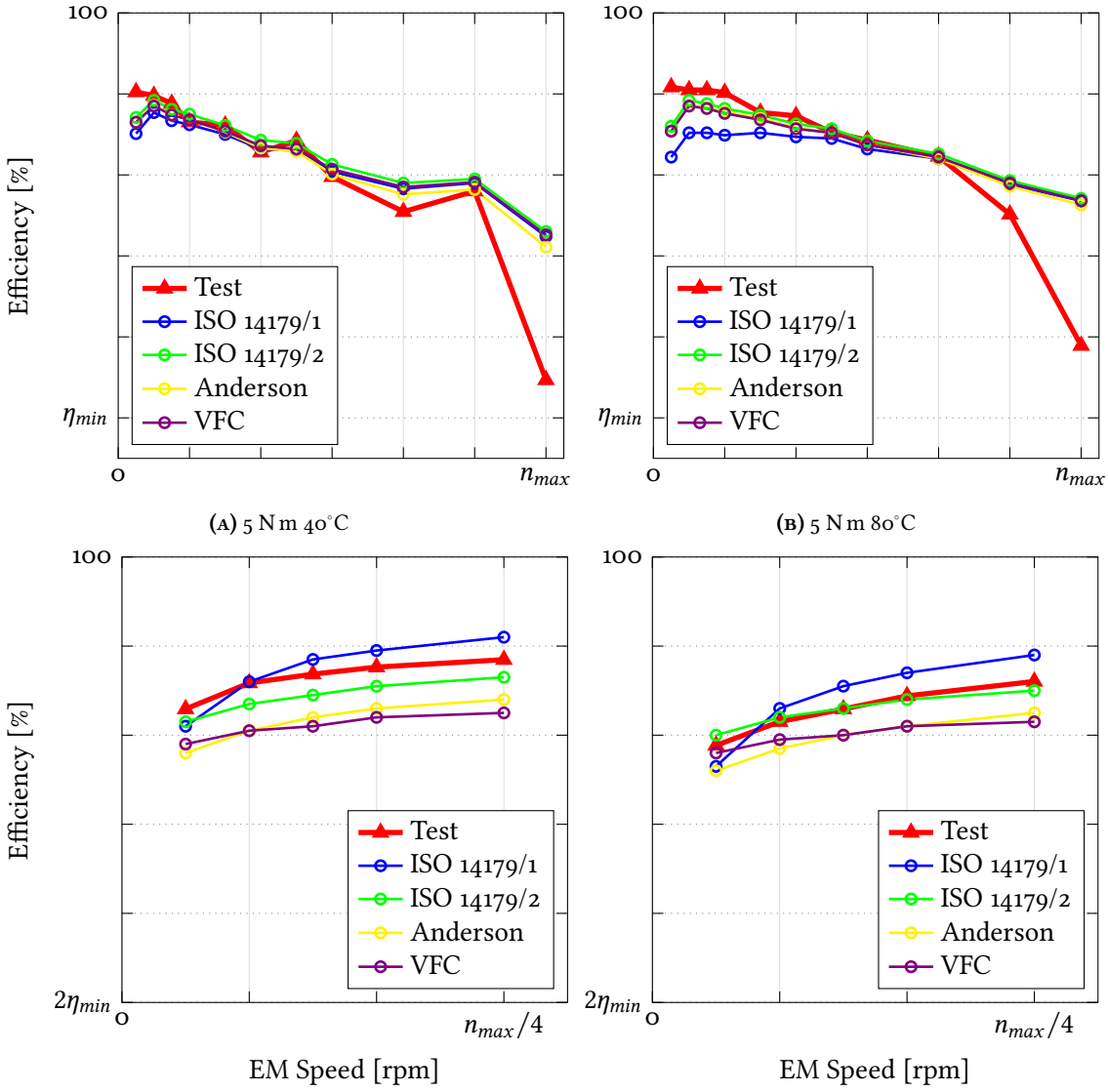

(A) 5 N m 40°C

(B) 5 N m 80°C

(C) 150 N m 40°C

(D) 150 N m 80°C

FIGURE 6.21: Sensitivity of the model to a change in gear mesh loss model, simulations performed with Romax. The model that better approximates the experimental curve is the ISO 14179/2. However, none of the models is able to predict an efficiency drop at 12000 rpm happening at light load.

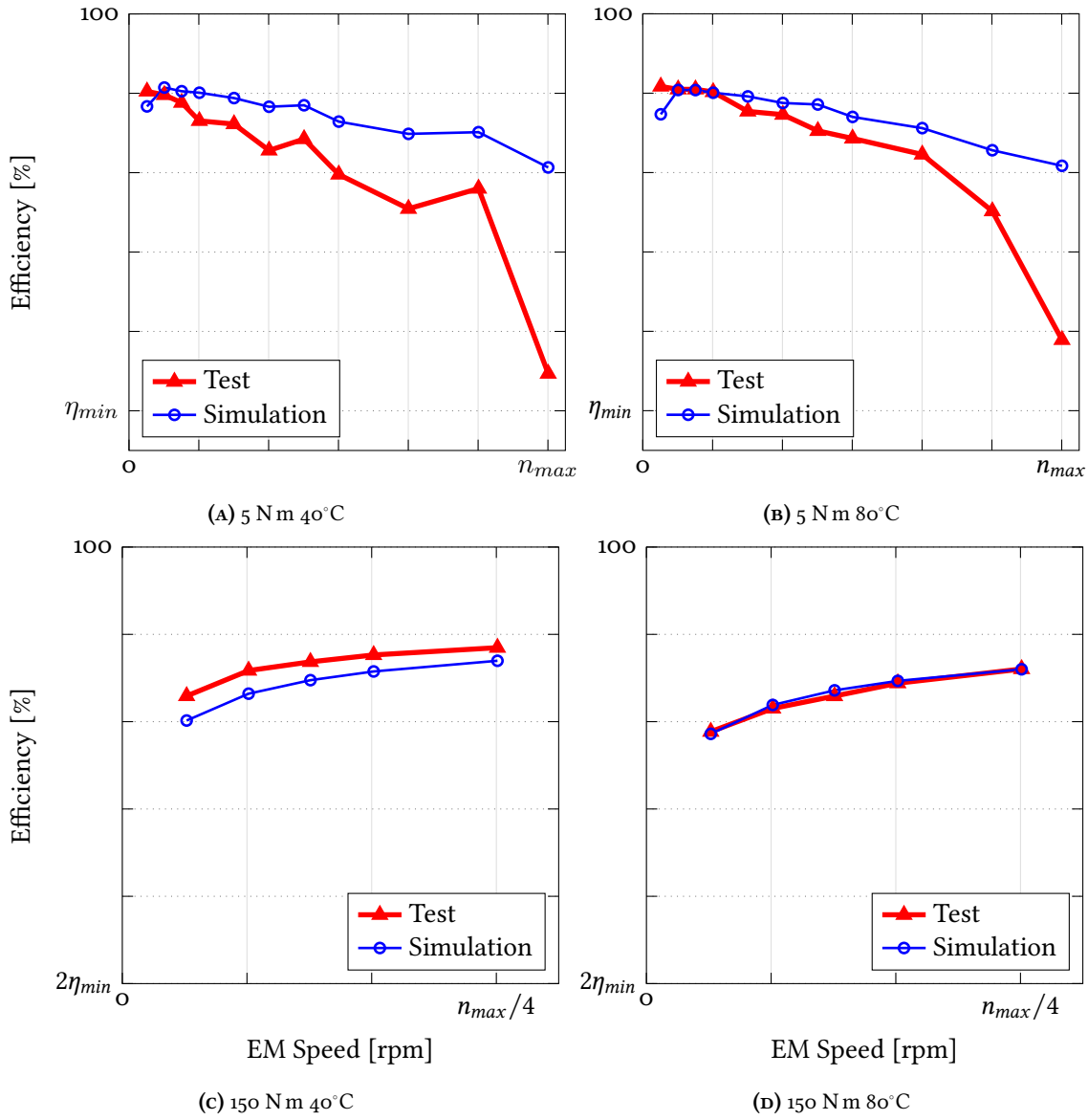

(A) 5 N m 40°C

(B) 5 N m 80°C

(C) 150 N m 40°C

(D) 150 N m 80°C

FIGURE 6.22: Simulation performed with AVL Excite: at light load of 5 N m, the efficiency is overestimated: this can be attributed to the underestimation of the bearing churning losses of the SKF model. More over, an efficiency drop is predicted at 500 rpm, that does not appear in the experimental test performed. They dynamic simulation is still not able to predict the large efficiency drop happening at 10000 rpm and more significantly at 12000 rpm. At high load of 150 N m, the losses are overestimated at 40°C while are in line with the tests at 80°C oil sump temperature.

6.4.3 Final Software Comparison

To conclude this chapter, the full efficiency map of the Electric Drive Module was reported, and the best results coming from each simulation software were compared with the experiments, in a trade-off study that reports the percentage error for each operating point. The error is evaluated as:

$$e = 100 \left| \frac{\eta_{\text{test}} - \eta_{\text{sim}}}{\eta_{\text{test}}} \right| \tag{6.3}$$

where η_{test} is the efficiency of the results coming from the experiments while η_{sim} is the simulated efficiency. The loss formulations that were fitting the experimental data with the least error are reported in Table 6.8.

Table 6.8: Loss Formulations for final comparison.
*The loss model is applied in the data post-processing, being unavailable in the software, for comparison purposes.

	AVL Excite	Masta	Romax
Gear Mesh	EHL Theory	ISO 14179/2	ISO 14179/2
Gear Drag	Terekhov*	ISO 14179/1	Terekhov
Bearings	SKF	ISO 14179/2	SKF
Oil Seals	ISO 14179/2*	ISO 14179/2	ISO 14179/2

In Table 6.9, a final comparison of the three softwares is provided, based on experience accumulated over the past few months of work.

Table 6.9: Software Evaluation

	AVL Excite	Masta	Romax
User-Friendliness	+	+++	++
Loss Models	+	++	+++
Simulation Time	+	+++	+++
Modelling Time	+	+++	++
Flexibility	+++	++	++

With Masta and Romax being special purpose software for driveline analysis, AVL Excite was born as a multibody modelling of Power Units. This difference was noted in the user interface, with the latter being much more tangled to learn and use. On the contrary, it was noted that Excite allows one to model and simulate the driveline in a more flexible way, also regarding the post-processing of the data, that balance is user-unfriendliness.

Regarding the loss models availability, Romax is by far the the most complete, followed by Masta. However, the possibility to rely on the EHL theory formulation for friction coefficient evaluation in the gear mesh of AVL Excite is a big plus, and as was seen in the final result comparison of Tables 6.11 and 6.12, it showed a better accuracy in the high torque range.

Table 6.10 summarizes the average percentage errors for the three simulation software, at low and high temperature and low and high torque range tested, and is build averaging the average error for Low Torques (5, 10, 20 N m) and High Torques (40, 80, 150 N m) in the speed range up to 10000 rpm, to exclude the big error seen at the 12000 rpm working condition. AVL Excite shows the lowest error considering high torque operating points, while it lacks in accuracy in the low torque range. At low torques, Romax is performing the best, in this case due to the better accuracy of the Terekhov gear drag loss model.

Table 6.10: Software Evaluation: average percentage error for low and high EM torque

	40°C			80°C		
	AVL Excite	Masta	Romax	AVL Excite	Masta	Romax
High Torque	0.49	0.48	0.59	0.23	0.25	0.35
Low Torque	2.54	0.95	1.06	1.30	1.34	1.25

Regarding simulation and modelling time, AVL Excite is the slowest due to the only possibility of a time-domain dynamic simulation, with Masta and Romax being much faster due to the possibility of a static simulation.

Table 6.11: Percentage Error Map, for an oil temperature of 40°C. The commonality is the higher error from the experimental data obtained at low torques and high rotational speeds. AVL Excite, with the EHL theory for gear contact friction coefficient evaluation, provides better results at high torques as average.

EM Torque [Nm]												
	150	0,58	0,55	0,43	0,39	0,31						
	80	0,82	0,72	0,68	0,64	0,46	0,22	0,17				
	40	0,94	0,86	0,86	0,52	0,15	0,09	0,12	0,19	0,57	0,58	2,35
	20	0,87	0,84	0,61	0,04	0,57	0,65	0,50	0,86	1,83	1,37	5,23
	10	0,14	0,49	0,73	0,57	0,51	1,53	1,28	2,04	2,96	3,55	10,29
	5	2,09	1,04	1,63	4,10	3,80	6,64	5,05	8,35	12,50	9,11	47,50
		500	**1000**	**1500**	**2000**	**3000**	**4000**	**5000**	**6000**	**8000**	**10000**	**12000**
		EM Speed [rpm]										

(A) AVL Excite

EM Torque [Nm]												
	150	0.18	0.36	0.35	0.37	0.36						
	80	0.29	0.48	0.56	0.61	0.53	0.39	0.45				
	40	0.48	0.72	0.89	0.64	0.43	0.49	0.45	0.47	0.35	0.68	0.58
	20	0.67	1.05	1.03	0.60	0.22	0.36	0.78	0.57	0.07	1.11	1.63
	10	0.10	0.81	0.16	0.17	0.54	0.14	0.60	0.05	0.06	0.35	4.06
	5	2.53	0.20	0.33	2.47	1.51	3.46	0.94	3.12	4.46	0.13	25.19
		500	**1000**	**1500**	**2000**	**3000**	**4000**	**5000**	**6000**	**8000**	**10000**	**12000**
		EM Speed [rpm]										

(B) Masta

EM Torque [Nm]												
	150	0,30	0,48	0,48	0,44	0,40						
	80	0,39	0,58	0,63	0,68	0,61	0,51	0,54				
	40	0,66	0,93	1,09	0,80	0,61	0,72	0,57	0,62	0,39	0,49	1,08
	20	0,86	1,24	1,34	0,90	0,58	0,65	1,05	0,79	0,04	0,68	2,79
	10	0,60	1,23	0,36	0,69	1,22	0,52	1,19	0,56	0,05	0,54	6,49
	5	3,47	0,66	0,81	1,12	0,02	1,81	0,40	1,92	4,70	1,92	33,49
		500	**1000**	**1500**	**2000**	**3000**	**4000**	**5000**	**6000**	**8000**	**10000**	**12000**
		EM Speed [rpm]										

(C) Romax

Table 6.12: Percentage Error Map, for an oil temperature of 80°C. As average, the three softwares are approximating better the test behaviour in the whole efficiency map, especially at high torques, while at low torque the error is still high.

EM Torque [Nm]	500	1000	1500	2000	3000	4000	5000	6000	8000	10000	12000
150	0,05	0,08	0,14	0,05	0,01						
80	0,35	0,11	0,16	0,14	0,32	0,24	0,27				
40	0,39	0,29	0,28	0,41	0,54	0,28	0,24	0,44	0,15	0,04	1,71
20	0,73	0,07	0,13	0,36	0,28	0,26	0,45	0,04	0,03	0,10	4,36
10	0,71	0,96	0,81	0,22	0,97	1,14	0,34	0,73	0,60	0,72	9,85
5	3,86	0,09	0,10	0,10	2,16	1,68	3,90	3,22	4,03	10,21	37,22

EM Speed [rpm]

(a) AVL Excite

EM Torque [Nm]	500	1000	1500	2000	3000	4000	5000	6000	8000	10000	12000
150	0,42	0,24	0,17	0,03	0,10						
80	0,33	0,21	0,01	0,06	0,33	0,27	0,35				
40	0,29	0,00	0,15	0,37	0,59	0,36	0,38	0,52	0,25	0,08	1,68
20	0,17	0,09	0,11	0,47	0,46	0,47	0,71	0,20	0,07	0,08	4,38
10	0,45	1,02	1,04	0,06	1,30	0,84	0,72	0,84	0,55	0,88	10,04
5	4,44	0,62	0,78	0,81	1,49	1,16	3,19	3,05	4,10	10,08	36,47

EM Speed [rpm]

(b) Masta

EM Torque [Nm]	500	1000	1500	2000	3000	4000	5000	6000	8000	10000	12000
150	0,24	0,10	0,01	0,08	0,21						
80	0,19	0,09	0,07	0,17	0,48	0,43	0,57				
40	0,09	0,11	0,29	0,59	0,80	0,63	0,67	0,88	0,58	0,48	1,28
20	0,40	0,20	0,14	0,76	0,86	0,92	1,25	0,81	0,72	0,64	3,55
10	0,87	1,48	1,59	0,66	2,02	0,11	1,74	2,03	0,76	0,63	8,30
5	5,33	1,42	1,86	2,17	0,34	1,14	0,53	0,12	0,39	5,54	30,85

EM Speed [rpm]

(c) Romax

Chapter 7

Conclusions and recommendations

The final chapter of this dissertation has the aim to provide the reader with the conclusions of this research, also clarifying its limitations and analyzing possible future work.

7.1 Summary

The proposed virtual methodology for the evaluation of the EDM (Electric Drive Module) efficiency takes into account the power loss sources arising in the reducer unit and analyzes them in detail, by considering the forces and torques coming from the electric machine and the resistive torque coming from the half-shafts.

The laboratory testing phase consisted of the evaluation of the speed-dependent losses, by performing the so called 'spin tests', in which the gearbox is operated without a resistive load, meaning only its rotational speed is varied. The speed dependent losses (mainly due to oil churning) were predicted by using empirical formulations coming from the literature.

The second kind of test performed was the test under load, in which the gearbox is operated with a resistive torque applied at the output. The load dependent losses (mainly due to gear meshing friction) were predicted both considering empirical formulations coming from tests and from theoretical formulations such as EHL (Elasto-Hydrodynamic Lubrication) theory.

Two units were tested, the first one being a simple reducer in which only speed-dependent losses were evaluated and simulated for two oil volumes inside the housing, and the second one being the EDM of the Fiat 500 BEV for which both speed-dependent and load-dependent losses were simulated and compared with experimental tests, done in a wide range of operating conditions and for two oil temperatures.

The two units were modelled by considering both a simplified approach that neglects the housing flexibility and treats the shafts as Timoshenko beams, and a more complete approach that takes into account the flexibility of the housing and the shafts by performing a condensation to obtain mass and stiffness matrices performed with Altair Optistruct.

The simulations were performed both in a static domain (Masta and Romax softwares) and in a dynamic domain (AVL Excite software), always considering steady state operating points.

7.2 Conclusions

The following conclusions can be drawn at the end of this research activity:

- The consideration of a more advanced approach that includes housing flexibility has a very low influence on the simulated efficiency result. It can be stated that the adoption of a simple approach considering the shafts as beam elements and a rigid housing is adequate to derive an efficiency map of this kind of units. This is a remarkable result since the condensation operation often requires the use of an external tool/software to be performed, but more importantly is time-consuming.
- Regarding the prediction of the speed-dependent losses, which arise mainly due to oil churning of the gear wheel, the outcome was that among the different formulations tested, different ones were performing the best when it came to compare them to the experimental results. It is expected that applying them to other reducer units could lead to even different outcomes. In this framework, if a precise prediction of the speed-dependent losses has to be achieved, it is suggested to consider a simulation relying on Computational Fluid Dynamics, in which all the loss mechanisms, and more importantly, the actual shape and arrangement of the housing is taken into account.
- Regarding the prediction of the load-dependent losses, it was observed that knowledge of the gear teeth roughness played an important role in the prediction of the power losses, since the models that were considering this parameter provided a better fitting of the experimental curve, especially in the high load-low speed condition where a mixed lubrication regime is most likely to be happening.
- Some words have to be spent on the time-domain simulation performed with AVL Excite, where the dynamic excitation coming from the electrical machine was considered. As was seen in literature and in simulation, at high loads the main contributor to the power loss is the gear meshing friction. As discussed in the previous chapter and in the appendices, the dynamic simulation performed with AVL Excite (that relies on an EHL theory formulation for the gear meshing friction evaluation) is the one approximating better the experimental curve. It can be said that if one considers dynamic effects at the gear meshing, deviation in the efficiency calculation with respect to a static simulation can be observed.

7.3 Limitations and recommendations

Although the modelling of the two units was good enough to approximate the experimental curves and to achieve a reasonably small error on the efficiency curves prediction, still some

limitations are present:

- First of all, the microgeometry (excluding the roughness) of the gear pairs was not considered, due to the lack of available measurements. This was proven to be not influential if one considers the analytical loss formulations for the gear meshing coefficient of friction evaluation, but is expected to be relevant when using more advanced approaches that compute a non-constant coefficient of friction along the gear tooth by relying on EHL theories that evaluate the oil distribution and properties at the gear meshing.
- Secondly, the bearings were considered to operate in a range of not too high misalignment, where the loss formulations were validated, and with normal operating clearances. It is obvious that these parameters could have an effect especially in non-ideal operating conditions, but it is not possible to capture these behaviours in these models.
- The test temperatures were imposed on all the components present in the units. Even if the temperature of the oil in the sump is measured and controlled in an active way, this is the only one known, meaning that all the other components in the unit could have different values of temperature. This could be a problem when there is a need to evaluate the viscosity of the oil inside each of the bearings and in the gear pair meshing, that as seen in the loss formulations, affect the magnitude of the power losses.
- The gear churning losses were evaluated relying on analytical formulations that do not take into account the internal arrangement of the gearbox and the housing shape, that as was seen in the literature could have an influence on the speed-dependent losses prediction.

7.4 Research contributions

The present thesis focused on the development of a methodology to evaluate the efficiency of an Electric Drive Module (EDM). One contribution of the work is that no previous studies that consider the effect of the dynamic excitation from the electric motor on the efficiency of the system were found in the literature. Most of these works considered only the dynamic effects that arise in the gearbox, mainly at the gear teeth contact. There are no studies in the literature that consider this wide a range of operating points coming from an extensive testing campaign, studying the influence of torque, speed and oil temperature at the same time, and validating them with experimental results in a double stage reducer unit. In this field, since in the literature only single gear pairs were tested, it is important to understand if the loss formulations are reliable when considering multiple stages of reduction in the same housing, and where the main differences can be observed. Lastly, the main novelty of this work is the study of the cross-interaction between the losses that arise in a drive module, in a simulation environment; that is something that was not studied before.

References

[1] Romeo Danielis, Mariangela Scorrano, and Marco Giansoldati. “Decarbonising transport in Europe: Trends, goals, policies and passenger car scenarios”. In: *Research in Transportation Economics* 91 (2022), p. 101068.

[2] “Selected Impacts of Regulation (EU) 2019/631 On Value Creation in the Automative Industry”. In: *Financial Internet Quarterly* 17.3 (2021), pp. 76–87.

[3] Florian Kellner, Bernhard Lienland, and Sebastian Utz. “A multi-criteria decision-making approach for assembling optimal powertrain technology portfolios in low GHG emission environments”. In: *Journal of Industrial Ecology* 25.6 (2021), pp. 1412–1429.

[4] `https://khkgears.net/new/gear_knowledge/`, *Accessed April 2023*.

[5] `https://www.intechopen.com/`, *Accessed April 2023*.

[6] HM Martin. “Lubrication of gear teeth”. In: *Engineering* 102 (1916), p. 119.

[7] DGRAV Dowson, GR Higginson, and AV Whitaker. “Elasto-hydrodynamic lubrication: a survey of isothermal solutions”. In: *Journal of Mechanical Engineering Science* 4.2 (1962), pp. 121–126.

[8] A Gu. “Elastohydrodynamic lubrication of involute gears”. In: (1973).

[9] KL Wang and HS Cheng. “A numerical solution to the dynamic load, film thickness, and surface temperatures in spur gears, part I: analysis”. In: (1981).

[10] D Zhu and HS Cheng. “A Comprehensive Analysis for Contact Geometry, Kinematics, Lubrication Performance, Bulk”. In: *Vehicle Tribology* 18 (1991), p. 383.

[11] Dong Zhu and Yuan-Zhong Hu. “The study of transition from elastohydrodynamic to mixed and boundary lubrication”. In: *The advancing frontier of engineering tribology, Proceedings of the 1999 STLE/ASME HS Cheng Tribology Surveillance* (1999), pp. 150–156.

[12] Yuan-Zhong Hu and Dong Zhu. “A full numerical solution to the mixed lubrication in point contacts”. In: *J. Trib.* 122.1 (2000), pp. 1–9.

[13] MJA Holmes, HP Evans, and RW Snidle. “Analysis of mixed lubrication effects in simulated gear tooth contacts”. In: *J. Trib.* 127.1 (2005), pp. 61–69.

[14] Ning Ren et al. “A three-dimensional deterministic model for rough surface line-contact EHL problems”. In: (2009).

[15] Ashlie Martini, Dong Zhu, and Qian Wang. “Friction reduction in mixed lubrication”. In: *Tribology Letters* 28 (2007), pp. 139–147.

[16] Klaus Michaelis, Bernd-Robert Hohn, and Michael Hinterstoißer. “Influence factors on gearbox power loss”. In: *Industrial lubrication and tribology* (2011).

[17] Bernd-Robert Höhn, Klaus Michaelis, and Michael Hinterstoißer. "Optimization of gearbox efficiency". In: *Goriva i maziva: časopis za tribologiju, tehniku podmazivanja i primjenu tekućih i plinovitih goriva i inžinjerstvo izgaranja* 48.4 (2009), pp. 441–461.

[18] GH Benedict and BW Kelley. "Instantaneous coefficients of gear tooth friction". In: *ASLE transactions* 4.1 (1961), pp. 59–70.

[19] JP O'donoghue and A Cameron. "Friction and temperature in rolling sliding contacts". In: *ASLE TRANSACTIONS* 9.2 (1966), pp. 186–194.

[20] Yu N Drozdov and Yu A Gavrikov. "Friction and scoring under the conditions of simultaneous rolling and sliding of bodies". In: *Wear* 11.4 (1968), pp. 291–302.

[21] Ju A Misharin. "Influence of the Friction Conditions on the Magnitude of the Friction Coefficient in the Case of Rolling with Sliding". In: *Instn. Mech. Engrs., Proc. Int. Comf. Gearing, 1958* 159 (1958).

[22] Caleb Gurd et al. "Computing Gear Sliding Losses". In: (2020).

[23] Neil E Anderson and Stuart H Loewenthal. "Efficiency of nonstandard and high contact ratio involute spur gears". In: (1986).

[24] David Roger Chase. "Development of an efficiency test methodology for high-speed gearboxes". PhD thesis. The Ohio State University, 2005.

[25] Yong Yang et al. "On the mixed EHL characteristics, friction and flash temperature in helical gears with consideration of 3D surface roughness". In: *Industrial Lubrication and Tribology* 71.1 (2019), pp. 10–21.

[26] Alastair Clarke et al. "Effects of profile errors on lubrication performance of helical gears". In: *Tribology International* 111 (2017), pp. 184–191.

[27] Lin Han, Da-Wei Zhang, and Fu-Jun Wang. "Predicting film parameter and friction coefficient for helical gears considering surface roughness and load variation". In: *Tribology Transactions* 56.1 (2013), pp. 49–57.

[28] Bernd-Robert Höhn, Klaus Michaelis, and Hans-Philipp Otto. "Influence of immersion depth of dip lubricated gears on power loss, bulk temperature and scuffing load carrying capacity". In: *International Journal of Mechanics and Materials in Design* 4 (2008), pp. 145–156.

[29] Hua Liu et al. "Detailed investigations on the oil flow in dip-lubricated gearboxes by the finite volume CFD method". In: *Lubricants* 6.2 (2018), p. 47.

[30] AS Terekhov. "Hydraulic losses in gearboxes with oil immersion". In: *Russian Engineering Journal* 55.5 (1975), pp. 7–11.

[31] Christophe Changenet et al. "A note on flow regimes and churning loss modeling". In: *Journal of Mechanical Design* 133.12 (2011).

[32] Yu Dai et al. "Numerical simulation investigation on the windage power loss of a high-speed face gear drive". In: *Energies* 12.11 (2019), p. 2093.

[33] Dong Guo et al. "Numerical modeling of churning power loss of gear system based on moving particle method". In: *Tribology Transactions* 63.1 (2020), pp. 182–193.

[34] Christophe Changenet and Philippe Velex. "Housing influence on churning losses in geared transmissions". In: *Journal of Mechanical Design* 130.6 (2008).

[35] Petra Heingartner and David Mba. "Determining power losses in helical gear mesh: case study". In: *International Design Engineering Technical Conferences and Computers and Information in Engineering Conference*. Vol. 37025. 2003, pp. 965–970.

[36] Michal Ruzek et al. "On windage losses in high-speed pinion-gear pairs". In: *Mechanism and Machine Theory* 132 (2019), pp. 123–132.

[37] Y Dai et al. "Application of an unstructured overset method for predicting the gear windage power losses". In: *Engineering Applications of Computational Fluid Mechanics* 15.1 (2021), pp. 130–141.

[38] Wenjun Gao. "Modelling of windage and churning losses in high speed rolling element bearings". PhD thesis. Lyon, 2018.

[39] J Croes and S Iqbal. "D2. 1 document 3: Literature survey: seal losses". In: *Technical Report* (2009).

[40] Dr. Frank Bauer and Prof. Dr.-Ing. habil. Werner Hass. "The tribology of elastomeric lip seals - reducing emissions, preventing leakage, saving the ecology". In: *World Tribology Congress, Torino, Italy* (2013).

[41] Jing Li, Chang-Chun Li, and Jing Huang. "Transmission efficiency analysis and experiment research of gear box". In: *3rd Annual International Conference on Mechanics and Mechanical Engineering (MME 2016)*. Atlantis Press. 2016, pp. 298–303.

[42] Wang Wei et al. "Automotive traction drive speed reducer efficiency testing-the importance of low power efficiency for a typical drive cycle". In: ().

[43] Carlos H Wink, Luigi Marson, and Sweety Goyal. "Hybrid analytical-experimental method to map power losses of automotive transmissions over their operating range". In: *Tribology International* 143 (2020), p. 106070.

[44] Tiantang Duan et al. "Transmission error investigation of gearbox using rigid-flexible coupling dynamic model: Theoretical analysis and experiments". In: *Mechanism and Machine Theory* 157 (2021), p. 104213.

[45] Sinisa Draca. "Finite element model of a double-stage helical gear reduction." In: (2006).

[46] Pedro Miguel Teixeira Marques. "Power Loss in Planetary Gearboxes Including the Influence of Gear Elastic and Dynamic Effects". PhD thesis. Universidade do Porto (Portugal), 2017.

[47] Stephen A Hambric, Micah R Shepherd, and Robert L Campbell. "Effects of gears, bearings, and housings on gearbox transmission shafting resonances". In: *ASME International Mechanical Engineering Congress and Exposition*. Vol. 44502. 2010, pp. 229–238.

[48] "Development of a Practical Thermal Rating Method for Enclosed Gear Drives". In: *AGMA 96FTM9* (October 1996).

[49] Ludwig Schlenk. "Untersuchungen zur freßtragfähigkeit von großzahnrädern". PhD thesis. Technische Universität München, 1994.

[50] NE Anderson and SH Loewenthal. "Selecting Spur-Gear Geometry for Greater Efficiency". In: *MACHINE DESIGN* 55.10 (1983), pp. 101–105.

[51] Neil E Anderson, Stuart H Loewenthal, and Joseph D Black. "An analytical method to predict efficiency of aircraft gearboxes". In: *J. Mech., Trans., and Automation* 108(3) (1986), pp. 424–432.

[52] Markus Klein. "Zur fresstragfhigkeit von kegelrad-und hypoidgetrieben". PhD thesis. Technische Universität München, 2012.

[53] AM Ertel et al. "Hydrodynamic lubrication based on new principles". In: *Akad. Nauk SSSR Prikadnaya Mathematica i Mekhanika* 3.2 (1939), pp. 41–52.

[54] AN Grubin. "Fundamentals of the hydrodynamic theory of lubrication of heavily loaded cylindrical surfaces". In: *Investigation of the Contact Machine Componets* 2 (1949).

[55] Christophe Changenet and Philippe Velex. "A model for the prediction of churning losses in geared transmissions—preliminary results". In: (2007).

[56] E Lauster and M Boos. "Zum wärmehaushalt mechanischer schaltgetriebe für nutzfahrzeuge". In: *VDI-Berichte* 488 (1983), pp. 45–55.

[57] RJ Boness. "Churning losses of discs and gears running partially submerged in oil". In: *Proceedings of the ASME International Power Transmission and Gearing Conference*. Vol. 1. Chicago. 1989, pp. 355–359.

[58] P Dennis, Darle W Dudley, and Gear Handbook. *Dudley's gear handbook*. McGraw-Hill, 1992.

[59] W Mauz. "Zahnradschmierung—Leerlaufverluste". In: *FVA-Forschungsheft* 185 (1985).

[60] https://www.skf.com/binaries/pub12/Images/0901d1968065e9e7-The-SKF-model-for-calculating-the-frictional-moment_tcm_12-299767.pdf, *Accessed December 2022*.

[61] Tedric A Harris. "Rolling Bearing Analysis, John Willey & Sons". In: *Inc., New York* 753 (1991).

[62] "Calculation of micropitting load capacity of cylindrical spur and helical gears — Part 1: Introduction and basic principles". In: *ISO/TR 15144-1:2014* (2014).

[63] Roy R Craig Jr and Andrew J Kurdila. *Fundamentals of structural dynamics*. John Wiley & Sons, 2006.

[64] Sebastian Buckel. "Dynamic Substructuring using the Finite Cell Method". In: (2014).

[65] https://help.hexagonmi.com/bundle/romax_knowledge_base/page/Knowledge-Base_43024727.html, *Accessed January 2023*.

[66] Gert HK Heirman and Wim Desmet. "Interface reduction of flexible bodies for efficient modeling of body flexibility in multibody dynamics". In: *Multibody System Dynamics* 24.2 (2010), pp. 219–234.

Appendix A

Equations for the gear mesh losses

A.1 ISO 14179/1

For spur and helical gears, mesh efficiency is a function of sliding ratios and the coefficient of friction:

$$P_{Mi} = \frac{f_m T_1 n_1 \cos^2(\beta_w)}{9549 M} \tag{A.1}$$

where:

- f_m is the mesh coefficient of friction
- T_1 is the pinion torque
- n_1 is the pinion rotational speed
- β_w is the operating helix angle
- M is the mesh mechanical advantage

A.1.1 Mesh Coefficient of Friction

$$f_m = \frac{v^j K^g}{C_1 V^h} \tag{A.2}$$

where:

  - v is the kinematic oil viscosity
  - $j = -0.223$
  - K is the load intensity
  - V is the tangential pitch line velocity
  - $g = -0.4$

- $h = 0.7$
- $C_1 = 3.239$

Load Intensity

It is dependent on the gear geometry and the calculated torque and for external gears is calculated as:

$$K = \frac{1000T_1(z_1 + z_2)}{2b_w(r_{w1})^2 z_2} \tag{A.3}$$

where:

- T_1 is the pinion torque
- z_1 and z_2 are the number of teeth of the pinion and wheel respectively
- r_{w1} is the pinion operating pitch radius
- b_w is the engaged face width

A.1.2 Mesh Mechanical Advantage

It is calculated from:

$$M = \frac{2cos\alpha_W(H_s + H_t)}{H_s^2 + H_t^2} \tag{A.4}$$

where:

- α_W is the transverse operating pressure angle
- H_s is the sliding ratio at start of approach
- H_t is the sliding ratio at end of recess

Therefore, M is totally dependent on the gear geometry

A.2 ISO 14179/2

The ISO 14179/2 norm estimates the gear mesh power loss based on the Coulomb law, which is given by:

$$P_{M_i} = F_n v_{gm} \mu_{mz} \tag{A.5}$$

where:

- F_n is the normal force at the gear tooth contact
- v_{gm} is the mean sliding speed

- μ_{mz} is the mean coefficient of friction of the gear mesh

The average sliding speed is calculated as:

$$v_{gm} = v_{gs} + \frac{(v_{g\gamma 1} - v_{gs})^2 + (v_{g\gamma 2} - v_{gs})^2}{2(v_{g\gamma 1} + v_{g\gamma 2} - 2v_{gs})} \tag{A.6}$$

where:

- v_{gm} is the mean sliding speed
- v_{gs} is the helical speed
- $v_{g\gamma 1,2}$ are the total surface speed at tooth tip of pinion and gear respectively

And the coefficient of friction is evaluated according to:

$$\mu_{mz} = 0.048 \left(\frac{F/b}{v_{\sum} \rho} \right) \eta_{oil}^{-0.05} R_a^{0.25} X_L \tag{A.7}$$

where:

- b is the gear face width
- η_{oil} is the oil dynamic viscosity
- X_L is the oil lubricant factor

Appendix B

Equations for Gear Churning and Windage Losses

B.1 ISO 14179/1

For cylindrical gears, the churning loss has two contributions, one from the smooth sides of the gear blank and one from the tooth surfaces:

$$P_{GW} = \frac{1.474 f_g \nu n^3 D^{5.7}}{A_g 10^{26}} \tag{B.1}$$

$$P_{GW} = \frac{7.37 f_g \nu n^3 D_t^{4.7} F(\frac{R_f}{\sqrt{\tan\beta}})}{A_g 10^{26}} \tag{B.2}$$

where:

- f_g is the dip factor
- D_t is the tip diameter of the gear
- D_r is the root diameter of the gear
- $A_g = 0$ is the arrangement constant
- F is the total face width
- β is the helix angle
- ν is the kinematic oil viscosity
- n is the rotational shaft speed
- R_f is the roughness factor for the gear teeth

B.2 ISO 14179/2

The total hydraulic loss torque, T_H of a gear stage system loss are determined according to Mauz:

$$T_H = C_{Sp} C_1 e^{C_2 \frac{v_t}{v_{t0}}} \tag{B.3}$$

The factors C_1 and C_2 state the effect of the tooth width and the immersion depth and are determined according to:

$$C_1 = 0.063 \frac{h_{e1} + h_{e2}}{h_{e0}} + 0.0128 \left(\frac{b}{b_0} \right)^3 \tag{B.4}$$

$$C_2 = \frac{h_{e1} + h_{e2}}{80 h_{e0}} + 0.2 \tag{B.5}$$

The splash oil factor, C_{sp}, considers the effect of the splash oil supply, dependent on the immersion depth:

$$C_{Sp} = \left(\frac{4 h_{e,max}}{3 h_c} \right)^{1.5} \frac{2 h_c}{l_h} \tag{B.6}$$

B.3 Changenet

In Changenet's gear churning loss models, the torque loss is given by:

$$C_{ch} = \frac{1}{2} \rho_{oil} \omega^2 r_p^3 S_m C_m \tag{B.7}$$

where:

- C_m is the drag dimensionless group
- S_m the immersed surface of the pinion/wheel (flank and teeth)
- r_p the pinion reference radius
- ω is the angular frequency
- ρ oil the bulk density of the lubricant at the working temperature.

The dimensionless drag group, derived by dimensional analysis, is expressed according to:

$$C_m = \phi_1 \left(\frac{h}{d_p} \right)^{\phi_2} \left(\frac{V_0}{d_p^3} \right) Fr^{\phi_4} Re_c^{\phi_5} \left(\frac{b}{r_p} \right)^{\phi_6} \tag{B.8}$$

The ϕ_i coefficients are derived from experimental results. The ϕ_i numerical values depend on the working conditions, and four sets of coefficients (dpending on the nature of the flow regime), are used depending on the value of the centrifugal acceleration parameter:

$$\gamma = \omega^2 (r_p b m)^{1/3} \tag{B.9}$$

The Froude (Fr) and critical Reynolds (Re_c) numbers are defined according to:

$$Fr = \frac{r_p \omega^2}{g} \tag{B.10}$$

$$Re_c = \frac{r_p b \omega}{\nu_0} \tag{B.11}$$

The C_m parameter used for each flow conditions depends not only on the centrifugal acceleration γ, but also on the critical Reynolds number Re_c, as it follows:

- if $\gamma < 750 m/s^2$ and $Re_c < 4000$

$$C_m = 1.366 \left(\frac{h}{d_p}\right)^{0.45} \left(\frac{V_0}{d_p^3}\right)^{0.1} Fr^{-0.6} Re_c^{-0.21} \left(\frac{b}{r_p}\right)^{0.21} \tag{B.12}$$

- if $\gamma < 750 m/s^2$ and $Re_c > 4000$

$$C_m = 0.239 \left(\frac{h}{d_p}\right)^{0.45} \left(\frac{V_0}{d_p^3}\right)^{0.1} Fr^{-0.6} \left(\frac{b}{r_p}\right)^{0.21} \tag{B.13}$$

- if $\gamma > 1250 m/s^2$ and $Re_c < 4000$

$$C_m = 20.797 \left(\frac{h}{d_p}\right)^{0.1} \left(\frac{V_0}{d_p^3}\right)^{-0.35} Fr^{-0.88} Re_c^{-0.21} \left(\frac{b}{d_p}\right)^{0.85} \tag{B.14}$$

- if $\gamma > 750 m/s^2$ and $Re_c > 4000$

$$C_m = 3.644 \left(\frac{h}{d_p}\right)^{0.85} \left(\frac{V_0}{d_p^3}\right)^{-0.35} Fr^{-0.88} \left(\frac{b}{d_p}\right)^{0.85} \tag{B.15}$$

An interpolation between the equations should be performed when $750 m/s^2 < \gamma < 1250 m/s^2$.
This model is usually applied to spur gears, but it can be extended to helical gears. In this way the geometrical parameter that accounts for the immersed surface of the pinion (S_m) is defined according to:

$$S_m = r_p^2(2\theta - \sin 2\theta) + d_b\theta + 2\frac{z\theta H_{tooth} b}{\pi \cos\alpha \cos\beta} \tag{B.16}$$

Finally, to obtain the churning power loss on a single pinion the churning torque loss, (C_{ch}) is multiplied by the angular speed ω, resulting in:

$$P_{VZ0} = C_{ch}\omega \tag{B.17}$$

Table B.1: Dimensionless parameters for Terekhov model for differents flow regimes

Flow regime	Coefficient						
	ψ_1	ψ_2	ψ_3	ψ_4	ψ_5	ψ_6	ψ_7
$10 < Re < 2250$ $Re^{-0.6}Fr^{-0.75} < 8.7e-3$	4.57	1.5	-0.3	-0.2	-0.4	-0.6	-0.25
$10 < Re < 2250$ $Re^{-0.6}Fr^{-0.75} >= 8.7e-3$	2.63	1.5	-0.53	-0.2	-0.4	-0.6	-0.25
$2250 < Re < 360000$	0.97	0.37	-0.376	-0.2	-0.124	-0.3	-0.064-0.037(R_o/h)

B.4 Terekhov

The churning torque C_{ch} is defined as:

$$C_{ch} = \rho \left(\frac{\pi N_s}{30} \right)^2 R_o^4 b C_m = \rho \omega^2 R_o^4 b C_m \tag{B.18}$$

with the dimensionless torque C_m given by:

$$C_m = \psi_1 \left(\frac{h}{R_o} \right)^{\psi_2} \left(\frac{V_l}{V_m} \right)^{\psi_3} \left(\frac{V_g}{V_m} \right)^{\psi_4} \left(\frac{b}{R_o} \right)^{\psi_5} Re^{\psi_6} Fr^{\psi_7} \tag{B.19}$$

Table B.1 shows the values of the dimensionless quantities ψ_i for different flow regimes.

Appendix C

Equations for Bearing Losses

C.1 ISO 14179

The total power loss from a bearing is a combination of load dependent friction losses and speed dependent windage losses.

C.1.1 Speed Dependant Losses

Bearing churning losses can be evaluated as:

$$P_{WB} = \frac{(M_0 + M_3)n}{9549} \tag{C.1}$$

Where:
M_0 is the no-load torque of the bearing

- If $vn < 2000$ $M_0 = 1.6 \times 10^{-8} f_0 d_m^3$
- If $vn >= 2000$ $M_0 = 10^{-10} f_0 (vn)^{2/3} d_m^3$

where:

- v is the kinematic viscosity at oil temperature
- n is the rotational shaft speed
- d_m is the mean diameter given by the bearing geometry
- f_0 is the bearing dip factor

The bearing dip factor adjusts the torque based on the amount the bearing dips into the oil.

According to ISO 14179, f_0 is calculated from:

$$f_0 = f_{0(min)} + (f_{0(max)} - f_{0(min)}) \frac{H}{D_{OR}} \tag{C.2}$$

Where:

- $f_{0(min)}$ and ($f_{0(max)}$ are obtained from Table 5 of ISO/TR 14179-1:2001. They are dependant on the bearing type, number of rows and series.
- H/D_{OR} is a measure of how much the bearing is immersed in the oil.

M_3 is the frictional moment of the bearing seal
M_3 is included only if the bearing is sealed. It is calculated from:

$$M_3 = \frac{\left(\frac{d_m}{f_3}\right)^2 + f_4}{1000} \tag{C.3}$$

Where:

- d_m is the mean diameter given by the bearing geometry
- f_3 and f_4 are bearing seal factors given by Table 6 of ISO/TR 14179-1:2001. They are dependant on the bearing type.

C.1.2 Load Dependant Losses

The Bearing Friction losses are evaluated as:

$$P_{Bi} = \frac{(M_1 + M_2)n}{9549} \tag{C.4}$$

where:

- M_1 is the load dependant torque It is calculated by:

$$M_1 = \frac{f_1(P_1)^a(d_m)^b}{1000} \tag{C.5}$$

  where:

  - f_1 is the coefficient of friction, which can depend on:
    - Series-From the bearing designation
    - P_0 The equivalent static bearing load
    - C_0 The basic static load rating (From bearing catalogue)
    - F_a The axial component of the dynamic bearing load.
  - P_1 is the dynamic load, which can depend on:
    - Series-From the bearing designation

    - F_a The axial component of the dynamic bearing load.
    - F_r The radial component of the dynamic bearing load.
    - F_a The axial component of the dynamic bearinAxial load factors which can be found in ISO 281
  - d_m is the mean diameter given by bearing geometry
  - a and b are exponents whose values are 1 except for spherical roller bearings where they are dependent on the series and are given by Table 3 in the standard.
- M_2 is the frictional moment It is calculated by:
  - f_2 is a factor which depends on the bearing design and lubrication
  - F_a is the axial component of the dynamic bearing load
  - d_m is the mean diameter given by bearing geometry
- n is the rotational shaft speed

C.2 SKF Method

The SKF model for calculating the frictional moment uses:

$$M = M_{rr} + M_{sl} + M_{seal} + M_{drag} \tag{C.6}$$

C.2.1 Rolling frictional moment

The rolling frictional torque is calculated according to Equation (1.3.10). G_{rr} depends on the loading conditions, bearing type and mean diameter. The kinematic viscosity of the lubricant ($\nu 0$) and the angular speed (n) are also important parameters.

$$M_{rr} = \Phi_{ish}\Phi_{rs}G_{rr}(\nu n)^{0.6} \tag{C.7}$$

Furthermore, in order to more closely follow the real behaviour of the rolling bearing, additional effects should be considered. Among these effects, the considered ones are:

- Inlet shear heating reduction;
- Replenishment/starvation speed effects for oil-spot, oil jet, grease and low level oil bath lubrication;
- Mixed lubrication for low speeds and/or low viscosities.

In order to account for the aforementioned effects the rolling frictional torque should be multiplied by two correction factors, the inlet shear heating reduction factor Φ_{ish}, and the kinematic

replenishment/starvation reduction factor Φ_{rs}. When sufficient lubricant is available in the rolling bearing, not all of it can go through the contacts since only a tiny amount of lubricant is used to build up the film thickness. The excess lubricant will form a separated reverse flow bubble that by shearing effects will produce heat and by consequence will lower the viscosity of the lubricant entering the contact. For the effect described above, the inlet shear heating reduction factor can be obtained approximately from:

$$\Phi_{ish} = \frac{1}{1 + 1.84e^{-9}(nd_m)^{1.28}\nu_0^{0.64}} \tag{C.8}$$

Due to the rolling bearing speed or high viscosity, the lubricant at the edges of the contacts might not have enough time to replenish the raceways, this effect is called kinetic starvation and causes a drop in the film thickness and in the rolling frictional torque. For the conditions described above the kinematic replenishment/starvation reduction factor can be obtained approximately from equation . It depends on the kinematic replenishment/starvation constant (K_rs) and the on rolling bearing and geometry (KZ, D, d).

$$\Phi_{rs} = \frac{1}{e^{k_{rs}\nu_0 n(d+D)\sqrt{\frac{k_z}{2(D-d)}}}} \tag{C.9}$$

C.2.2 Sliding frictional moment

The sliding frictional torque is calculated according to. G_{sl} depends on the loading conditions, rolling bearing type and mean diameter. The sliding coefficient of friction (μ_{sl}) is also a very important factor.

$$M_{sl} = G_{sl}\mu_{sl}^{SKF} \tag{C.10}$$

The sliding friction coefficient μ_{sl} can be calculated according to eqn.μ_{sl}^{SKF} is the full film coefficient of friction and μ_{bl} is the boundary coefficient of friction. Φ_{bl} is the weighting factor for the sliding coefficient of friction and can be calculated according the equation. μ_{EHD}^{SKF} and μ_{bl}^{SKF} have reference values that are recommended by SKF.

$$\mu_{sl}^{SKF} = \Phi_{bl}\mu_{bl}^{SKF} + (1 - \Phi_{bl})\mu_{EHD}^{SKF} \tag{C.11}$$

$$\Phi_{rs} = \frac{1}{e^{2.6e^{-8}(n\nu_0)^{1.4d_m}}} \tag{C.12}$$

C.2.3 Drag Loss

In oil bath lubrication, the rolling bearing is partially, or in special situations, completely submerged. Under these conditions the size and geometry of the oil reservoir together with the oil level used can have a substantial impact on the bearing friction torque. Depending on the rolling

bearing type, SKF suggests equations and for the drag losses in ball and roller bearings respectively.

$$M_{drag}^{ball} = 0.4 V_M K_{ball} d_m^5 n^2 + 1.09310 e^{-7} n^2 d_m^3 \left(\frac{n d_m^2 f_t}{\nu} \right)^{-1.379} R_s \tag{C.13}$$

$$M_{drag}^{roll} = 4 V_M K_{roll} C_W B d_m^4 n^2 + 1.09310 e^{-7} n^2 d_m^3 \left(\frac{n d_m^2 f_t}{\nu} \right)^{-1.379} R_s \tag{C.14}$$

V_M is a variable that is a function of the oil level and K_{ball} and K_{roll} depend on the roller bearing type (ball or roller).

C.2.4 Seal Loss

The rolling bearing seal losses are defined according to Equation C.15 . The constants $K_{S1,2}$ and β_r depend on the geometry and rolling bearing seal type.

$$M_{seal} = K_{S1} d_s^{\beta_r} + K_{S2} \tag{C.15}$$

Appendix D

Simulation Results

In the following, the results of the simulations performed with the three softwares are displayed. In table are reported the loss formulations that were fitting in the best way the experimental data for the three simulation softwares.

Table D.1: Loss Formulations

	AVL Excite	Masta	Romax
Gear Mesh	EHL Theory	ISO 14179/2	ISO 14179/2
Gear Drag	Terekhov*	ISO 14179/1	Terekhov
Bearings	SKF	ISO 14179/2	SKF
Oil Seals	ISO 14179/2*	ISO 14179/2	ISO 14179/2

* the loss model is applied in the data post-processing, being unavailable in the software, for comparison purpose.

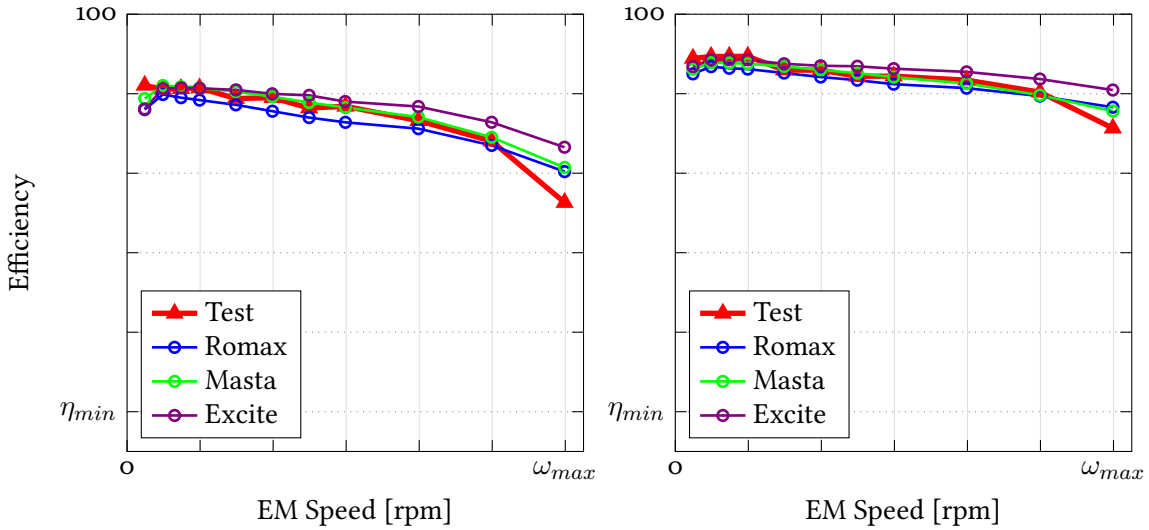

(A) 5 Nm

(B) 10 Nm

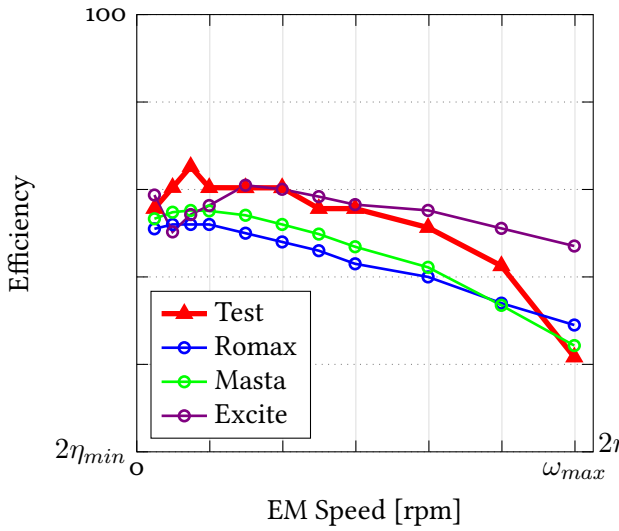

(C) 20 Nm

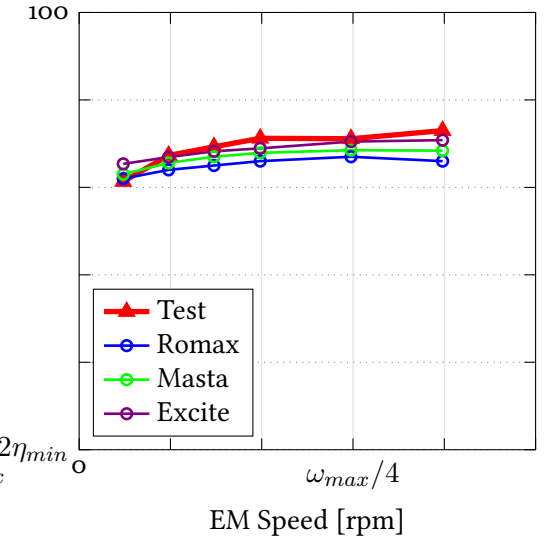

(D) 50 Nm

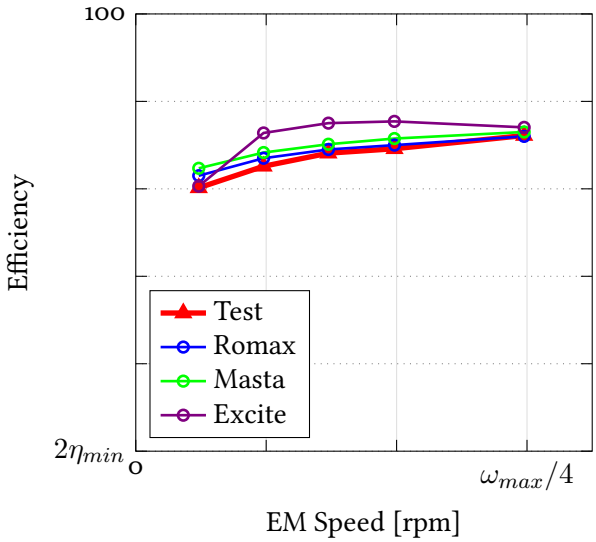

(E) 100 Nm

Figure D.1: Regenerative 40 °C

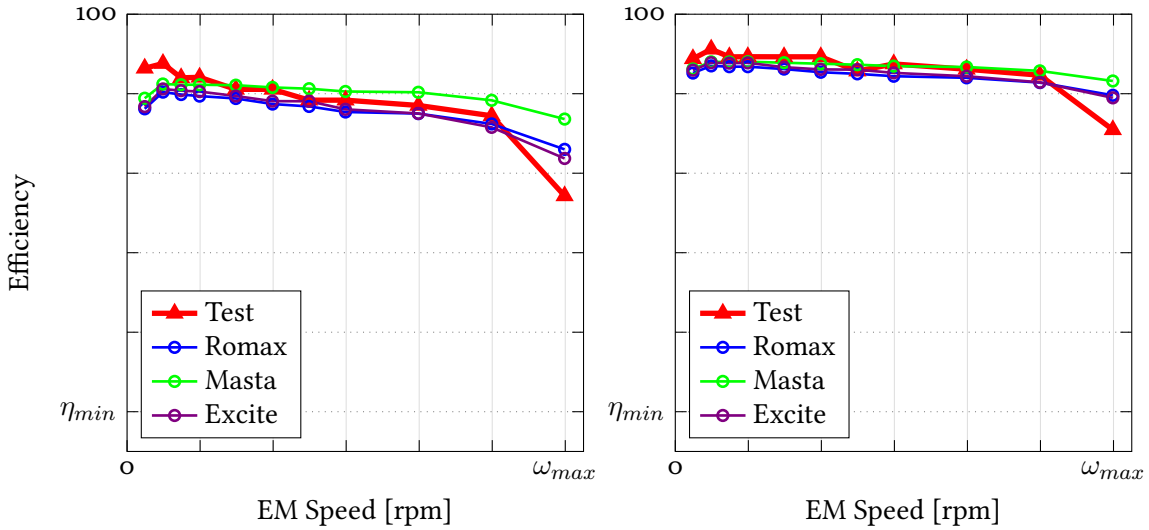

(A) 5 Nm

(B) 10 Nm

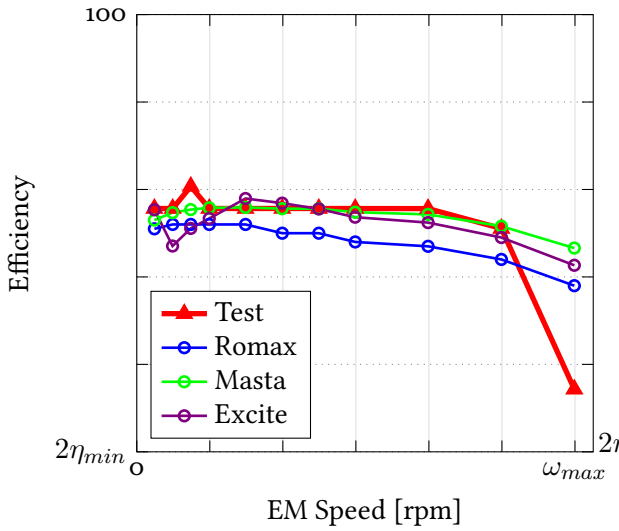

(C) 20 Nm

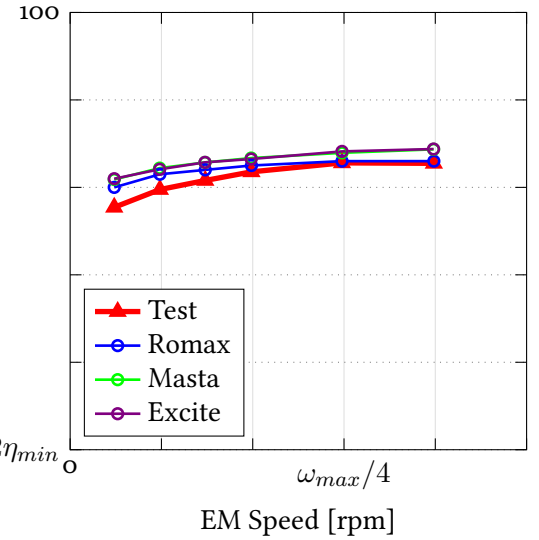

(D) 50 Nm

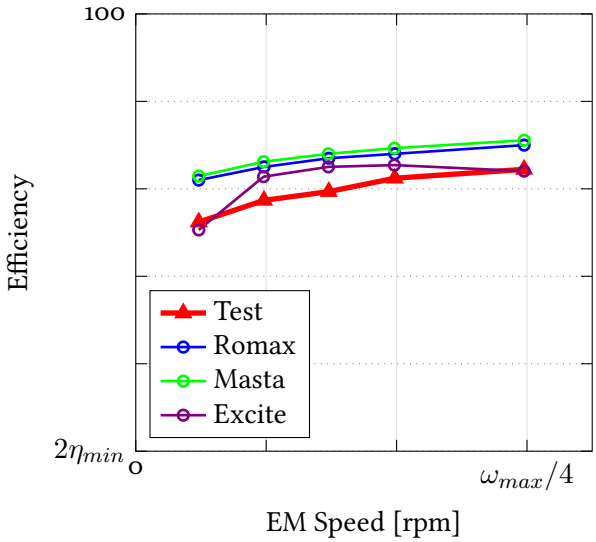

(E) 100 Nm

Figure D.2: Regenerative 80 °C

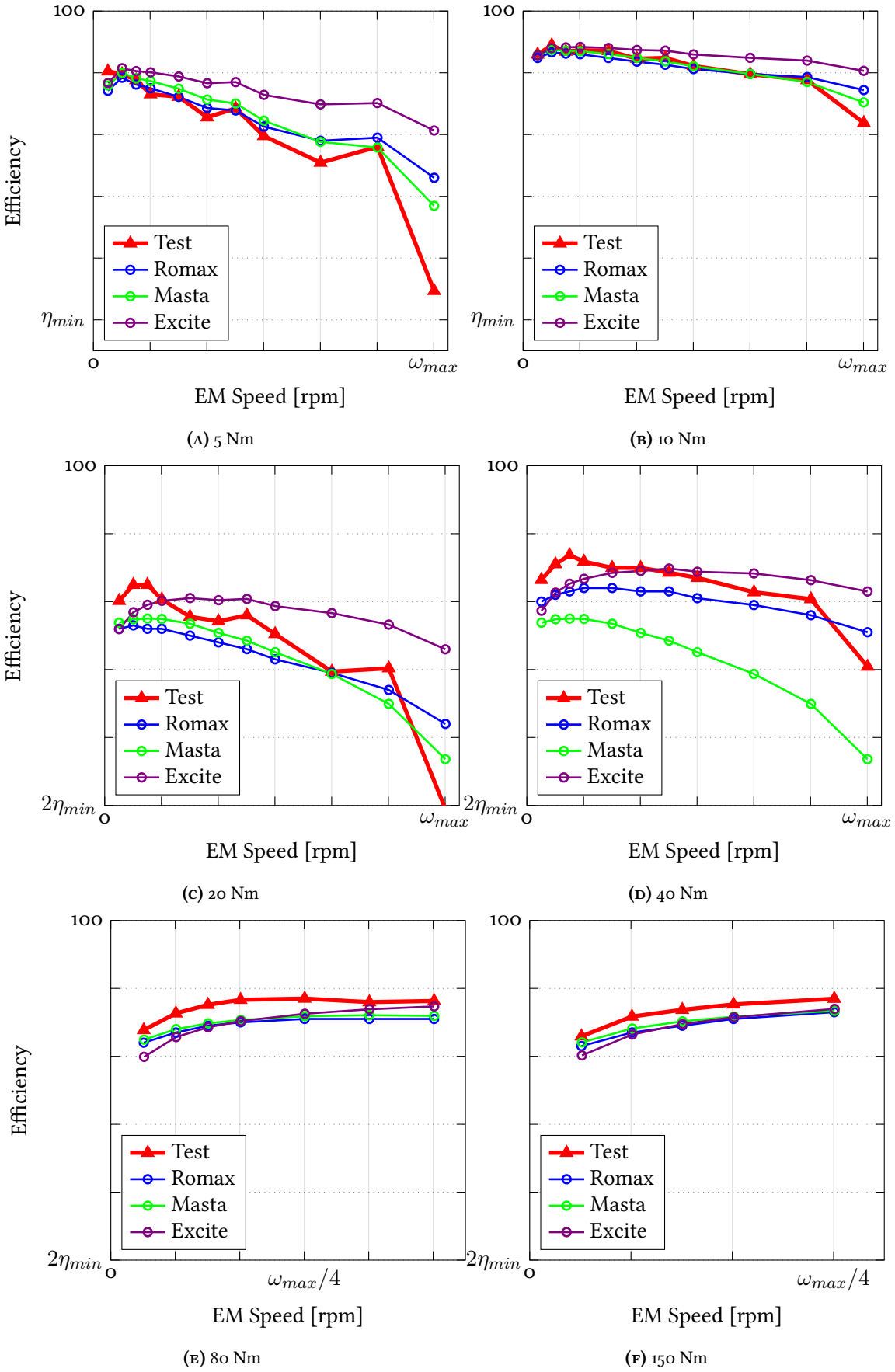

(A) 5 Nm

(B) 10 Nm

(C) 20 Nm

(D) 40 Nm

(E) 80 Nm

(F) 150 Nm

FIGURE D.3: Motoring 40 °C

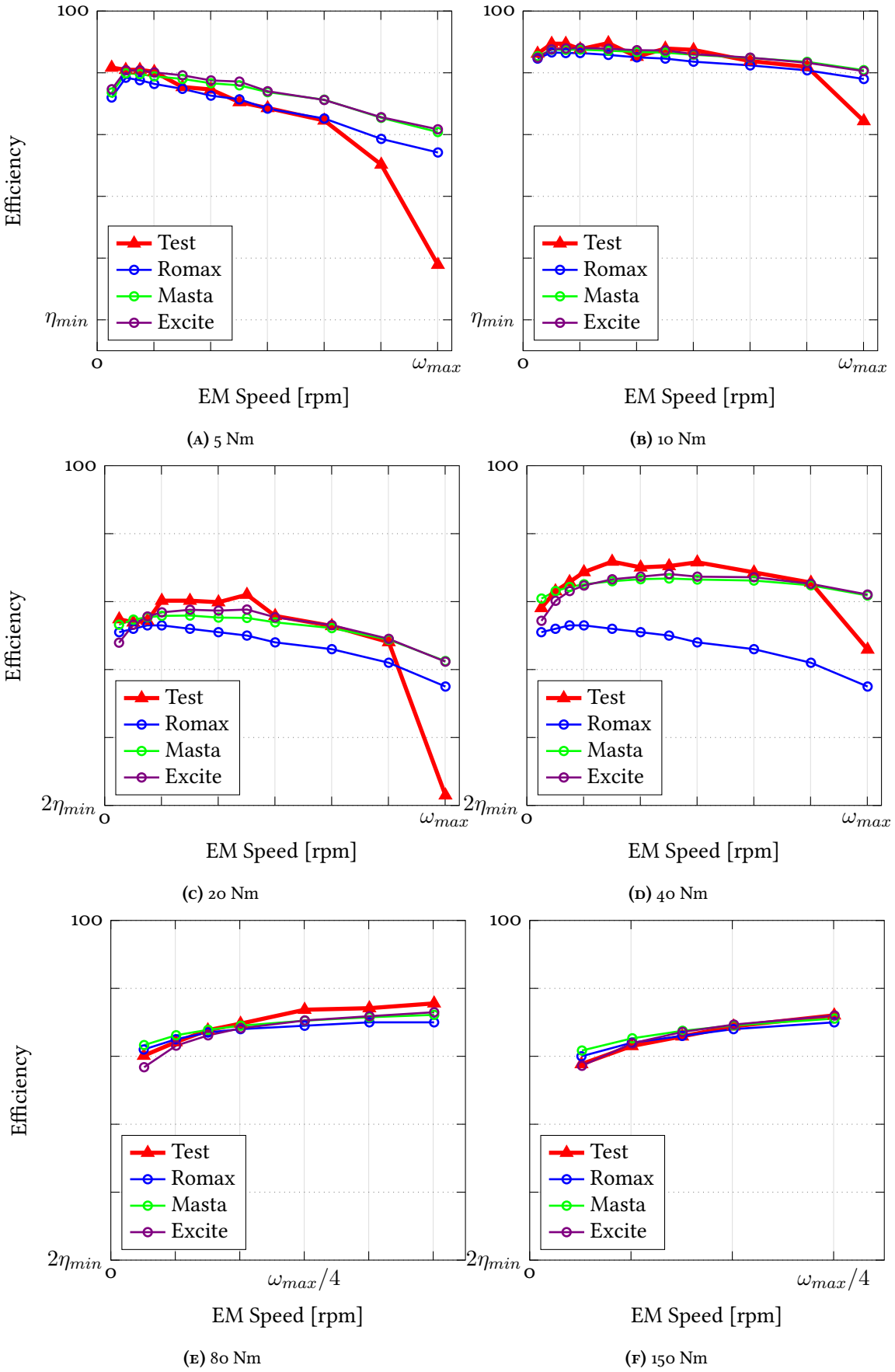

(A) 5 Nm

(B) 10 Nm

(C) 20 Nm

(D) 40 Nm

(E) 80 Nm

(F) 150 Nm

FIGURE D.4: Motoring 80 °C

Vita Auctoris

Luca Gonella was born in 1999 in Nizza Monferrato, Piemonte, Italy. He graduated from Nicola Pellati high school in Nizza Monferrato in 2018. He moved to Torino the following year to study Automotive Engineering at the Politecnico di Torino. He completed his Bachelor's Degree in 2021, with a thesis focused on internal combustion engine modelling, titled 'Performance Analysis of a Split Cycle Engine by means of 1D simulation'. After the Bachelor's degree, he continued his studies at Politecnico di Torino at the Master's level, and is currently enrolled in the Dual International Master's Degree program between the Politecnico di Torino and the University of Windsor in Ontario, Canada. He is expected to graduate from the University of Windsor in August 2023 and from Politecnico di Torino in October 2023.